

1 **Antarctic sedimentary basins and their influence on ice-sheet dynamics**

2 A.R.A. Aitken^{1,2}, L. Li¹, B. Kulesa^{3,4}, D. Schroeder^{5,6}, T.A. Jordan⁷, J.M. Whittaker⁸, S. Anandakrishnan⁹, E.J.
3 Dawson⁵, D. A. Wiens¹⁰, O. Eisen^{11,12}, M.J. Siegert^{13,14}

- 4 1. School of Earth Sciences, The University of Western Australia, Perth, Western Australia, Australia
- 5 2. Australian Centre of Excellence for Antarctic Science, The University of Western Australia, Perth,
6 Western Australia, Australia
- 7 3. School of Biosciences, Geography and Physics, Swansea University, Wales, UK
- 8 4. School of Geography, Planning and Spatial Sciences, The University of Tasmania, Hobart Tasmania,
9 Australia
- 10 5. Department of Geophysics, Stanford University, Stanford, California, USA
- 11 6. Department of Electrical Engineering, Stanford University, Stanford, California, USA
- 12 7. British Antarctic Survey, Cambridgeshire, UK
- 13 8. Institute for Marine and Antarctic Studies, University of Tasmania, Hobart, Tasmania, Australia
- 14 9. College of Earth and Mineral Sciences, Pennsylvania State University, Pennsylvania, USA
- 15 10. Department of Earth & Planetary Sciences, Washington University, St. Louis, Missouri, USA
- 16 11. Glaciology, Alfred Wegener Institute, Helmholtz Centre for Polar and Marine Research,
17 Bremerhaven, Germany
- 18 12. Department of Geosciences, University of Bremen, Bremen, Germany
- 19 13. Grantham Institute and Department of Earth Science and Engineering, Imperial College London,
20 London, UK
- 21 14. Tremough House, University of Exeter, Penryn, Cornwall, UK

22
23 Corresponding author: Alan Aitken (alan.aitken@uwa.edu.au)
24

25 **Key Points**

- 26 • Recent advances in detection and characterization of subglacial sedimentary basins are
27 reviewed
- 28 • A new map of Antarctic sedimentary basins is presented and implications for glacial
29 processes are discussed
- 30 • Some future directions in Antarctic subglacial sedimentary basins research are explored

31

32 **Abstract**

33 Knowledge of Antarctica's sedimentary basins builds our understanding of the coupled evolution of
34 tectonics, ice, ocean, and climate. Sedimentary basins have properties distinct from basement-dominated
35 regions that impact ice-sheet dynamics, potentially influencing future ice-sheet change. Despite
36 their importance, our knowledge of Antarctic sedimentary basins is restricted. Remoteness, the harsh
37 environment, the overlying ice sheet, ice shelves and sea ice all make fieldwork challenging. Nonetheless, in
38 the past decade the geophysics community has made great progress in internationally coordinated data
39 collection and compilation with parallel advances in data processing and analysis supporting a new insight
40 into Antarctica's subglacial environment. Here, we summarize recent progress in understanding Antarctica's
41 sedimentary basins. We review advances in the technical capability of radar, potential fields, seismic and
42 electromagnetic techniques to detect and characterize basins beneath ice and advances in integrated multi-
43 data interpretation including machine-learning approaches. These new capabilities permit a continent-wide
44 mapping of Antarctica's sedimentary basins and their characteristics, aiding definition of the tectonic
45 development of the continent. Crucially, Antarctica's sedimentary basins interact with the overlying ice sheet
46 through dynamic feedbacks that have the potential to contribute to rapid ice-sheet change. Looking ahead,
47 future research directions include techniques to increase data coverage within logistical constraints, and
48 resolving major knowledge gaps, including insufficient sampling of the ice-sheet bed and poor definition of
49 subglacial basin structure and stratigraphy. Translating the knowledge of sedimentary basin processes into
50 ice-sheet modelling studies is critical to underpin better capacity to predict future change.

51 **Plain Language Summary**

52 Antarctica is the keystone to the former supercontinent Gondwana and, because of its unique isolated
53 location at the South Pole, it has important consequences for understanding changing global climate and
54 ocean change. In several ways, sedimentary basins beneath the ice sheet interact with the ice sheet above
55 and can potentially contribute to rapid ice-sheet changes that impact global sea level and climate. These
56 sedimentary basins have not all been systematically mapped due to the challenge of studying them beneath
57 thick ice. In this work we review technical progress towards the understanding of sedimentary basins in the
58 subglacial environment, and we map out the sedimentary basins beneath Antarctica's ice. We explore how
59 improved knowledge of Antarctica's basins helps to (1) understand important tectonic events in the
60 continent, (2) unravel the evolution of the landscape and the ice sheet, and (3) contribute to improved
61 predictions of future ice-sheet change. Remaining challenges to advance Antarctic sedimentary basins
62 research are identified and some future directions for study are discussed.

63 1 Introduction

64 Sedimentary basins are widely preserved on all of Earth's continents and provide distinct environments for
65 physical, chemical and biological processes (Evenick, 2021). Antarctica is no exception and possesses several
66 major sedimentary basins and many smaller ones distributed across the continent. Seasonally ice-free
67 marine regions, including the Ross, Weddell, and Amundsen seas, and much of the East Antarctic continental
68 margin are relatively well surveyed (Fig 1). However, the unique challenge of ice-covered inland Antarctica,
69 with very limited and spatially clustered outcrops (Fig 1), a kilometers-thick ice sheet and severe
70 environmental and logistical challenges has meant that the distribution and nature of sedimentary basins is
71 poorly known inland. On the continental shelf, ice shelves and perennial sea ice limit access to both marine
72 and terrestrial techniques. Sedimentary basins are important not just for the understanding of Antarctic
73 geology, but also because they provide key boundary conditions for glacial processes, with major impacts on
74 the dynamics of the overlying ice sheet (Bell et al., 1998; Gooch et al., 2016; Kulesa et al., 2019; Li et al.,
75 2022; Person et al., 2012; M. J. Siegert et al., 2018; M. Studinger et al., 2001; Tankersley et al., 2022; Zhang
76 et al., 2018).

77 The discovery of sedimentary basins in Antarctica has been a continuing theme since the earliest Antarctic
78 expeditions. The earliest explorations captured both the existence of extensive sedimentary rocks in outcrop
79 (Ferrar, 1907; Mawson, 1940) and speculated on the presence of major sedimentary basins in the marine
80 regions, especially the Ross, Weddell and Scotia Seas (Mawson, 1928). A more comprehensive record
81 emerged in the second half of the 20th Century, in particular the period following the 1957/8 International
82 Geophysical Year (IGY) (Naylor et al., 2008), when geophysical mapping of subglacial geology became a
83 consistent feature of Antarctic exploration (Bailey et al., 1964; Bentley et al., 1960; S. Evans & Robin, 1966).
84 Key techniques were developed and adapted to Antarctic requirements, including radio-echo sounding
85 (RES), since the 1960s (R. G. Bingham & M. J. Siegert, 2007; Dustin M. Schroeder et al., 2020; Turchetti et al.,
86 2008), active- and passive-seismic surveying, since the 1950s and 1990s respectively (Anandakrishnan et al.,
87 2000; Bentley et al., 1960; Lawrence et al., 2006; Robin, 1958) and airborne magnetic and gravity surveys,
88 since the 1960s and 1990s respectively (Behrendt et al., 1966; R. E. Bell et al., 1999). The data collected led
89 to the first continent-scale compilations, including for ice thickness and bed elevation (BEDMAP; Lythe &
90 Vaughan, 2001), magnetic data (ADMAP; A. Golynsky et al., 2001; A. Golynsky et al., 2006) and gravity data
91 (ADGRAV; R. Bell et al., 1999).

92 The 21st Century has seen continued development and refinement of these approaches, and of course the
93 broadening of coverage over the continent, and the last decade has seen the development of much more
94 detailed and comprehensive compilations (Frémand, Fretwell, et al., 2022; Fretwell et al., 2013; A. V.
95 Golynsky et al., 2018; Scheinert et al., 2016). New techniques for compilation have emerged including the
96 integration of satellite gravity and magnetic data (Ebbing et al., 2021; Ebbing et al., 2018; Scheinert et al.,

97 2016), and for topography the inclusion of mass-conservation techniques (Mathieu Morlighem et al., 2020)
98 and geostatistical approaches (Emma J. MacKie et al., 2021).

99 These advances in the coverage and quality of key geophysical datasets, coupled with the development of
100 new data processing and analysis techniques, mean it is now feasible to map with some confidence the
101 sedimentary basins of the Antarctic continent (Li et al., 2022). In this review, we explore the state of the art
102 with respect to defining the subglacial sedimentary basins of Antarctica, and we summarize the extent and
103 nature of these across the continent. The evolving tectonic setting of basin formation since Pangea is
104 discussed. We explore the interactions of sedimentary basins with glacial processes and consider
105 implications for ice sheet dynamics. Finally, we look ahead to the next set of challenges in defining the
106 extent, characteristics and importance of sedimentary basins in Antarctica.

107 2 Defining Subglacial Sedimentary Basins

108 2.1 What is a sedimentary basin?

109 A sedimentary basin is defined by the development of accommodation space into which sediments have
110 been deposited. This definition needs several concepts to align: first, the development of a topographic
111 depression or shallow-sloped platform is required; second, there must be a source of sediment derived from
112 mechanical erosion, or from chemical or biological processes; third the deposition and accumulation of
113 sediments must occur and fourth, these must be preserved to the present day. The most common situation
114 on continents is that sediments eroded from highlands are deposited and preserved in a topographic
115 depression, forming a sedimentary basin (Allen et al., 2015).

116 Sedimentary and metasedimentary rocks are commonly interpreted to represent their sedimentary basin,
117 potentially defining such properties as extent and thickness of fill and the depositional environment. Later
118 uplift, erosion, deformation, intrusion by magmatic rocks, or other events may make the original
119 depositional basin hard to define. Furthermore, in metamorphic rocks, physical properties may become
120 dominated by crystal structures rather than fluid-filled pore networks, and this affects both the geophysical
121 expression (Enkin et al., 2020) and the nature of their interaction with glacial processes (Krabbendam &
122 Glasser, 2011). For these reasons we exclude exposed metasedimentary rocks of greenschist facies or above
123 from consideration in this study. Recent sediment deposits are widely exposed in ice-free regions (Cox et al.,
124 2023) and subglacial sediments are a prominent feature of the ice sheet bed across all environments. While
125 these sediments are an important facet of subglacial geology, their presence does not intrinsically define a
126 sedimentary basin in line with the definition above and so they are excluded from consideration in our
127 classification.

128 We define two major classes of sedimentary basin. Type 1 basins exist where a substantial amount of basin-
129 fill, including sediments and sedimentary rocks, is preserved in the original depositional basin, with no

130 evidence for substantial uplift, major deformation or metamorphism. A certain degree of compaction,
131 diagenesis and deformation are expected in all basins. In contrast, Type 2 basins exist where exposures or
132 other evidence indicate the presence of sedimentary rocks for which the original depositional basin is not
133 preserved.

134 2.2 Recent progress in characterization of subglacial sedimentary basins

135 Globally, the analysis of sedimentary basins is commonly achieved through extensive use of outcrops, where
136 available, supported by drill-core and high-resolution active seismic reflection studies allowing detailed basin
137 characterization. In Antarctica these key data are available only in selected areas (Fig 1) and, in the general
138 case, the major challenge is to define and characterize basins in the subglacial environment, for which
139 specialized techniques are needed.

140 2.2.1 Direct geological characterization

141 Direct access to rocks through outcrop, detrital samples or drill core is fundamental to sedimentary basin
142 analysis, permitting a full assessment of sedimentary characteristics and enabling application of detrital
143 geochronology, thermochronology and other key analysis techniques. In marine and some sub-ice-shelf
144 settings of Antarctica (Fig 1), drilling programs with linked seismic surveys have revealed many key features
145 of sedimentary basins on the continental shelf, in particular in the Ross Sea, Prydz Bay and Amundsen Sea (K.
146 Gohl et al., 2017; Marschalek et al., 2021; R. M. McKay et al., 2016; Whitehead et al., 2006). Ice-shelf and
147 sea-ice cover is a major limitation for offshore studies, leading to a substantial data gap on the inner
148 continental shelf (Fig 1). Developing offshore exploration technologies including autonomous underwater
149 vehicles (Batchelor et al., 2020; Davies et al., 2017; Dowdeswell et al., 2008), seafloor drilling (K. Gohl et al.,
150 2017) and sub-ice shelf drilling (Gong et al., 2019) are enabling these data gaps to be filled.

151 For onshore regions, Antarctica possesses high-quality sedimentary rock outcrops in numerous areas, and
152 these can provide the key knowledge for basin studies in those regions. The collation of Antarctic geological
153 data has progressed significantly, with continent-scale compilations of key data now accessible (Cox et al.,
154 2023; Sanchez et al., 2021). While a great deal of knowledge has been gained by these approaches, a severe
155 limitation is the tendency for outcrops to occur only on major highlands, isolated nunataks and coastal
156 islands, leaving unsampled the low-lying regions that contain the bulk of sedimentary rocks. This leads to
157 some undesirable bias towards older and/or uplifted sedimentary rocks and, therefore, the utility of
158 outcrop-based data to infer subglacial geology is limited. Outcrop data are focused in spaced clusters (Fig 1),
159 often with a high degree of internal complexity, meaning that interpolation between these clusters carries
160 high uncertainty.

161 Detrital samples from much younger sediments can mitigate exposure bias (Maritati et al., 2019; Mulder et
162 al., 2019; Thomson et al., 2013), but the lack of a precisely known source location for these samples renders

163 their use to characterize inland basins highly uncertain. Plainly, for a more representative sampling of the
164 Antarctic bedrock, drilling is necessary. As with offshore drilling, onshore sub-ice drilling techniques are
165 developing (Gong et al., 2019; J. W. Goodge et al., 2021; Hodgson et al., 2016; Kuhl et al., 2021; Talalay et al.,
166 2021) and have seen operation in several locations (Fig 1), with an intent to expand towards more
167 systematic coverage in the future. Notably, the alignment of these records with major ice-coring initiatives
168 has strong potential to inform glacial evolution on multiple timescales.

169 2.2.2 Indirect characterization

170 Despite the benefits of direct characterization, a systematic coverage of Antarctica requires indirect
171 characterization from geophysical data to survey the regions where no direct information exists. The major
172 techniques include ground and/or ship-based techniques including active and passive seismic methods and
173 magnetotellurics, as well as airborne techniques including radio-echo sounding (RES), gravity and magnetic
174 methods.

175 2.2.2.1 Radio-echo sounding

176 RES is an efficient geophysical method to characterize the morphology and nature of the ice-sheet bed. In
177 the context of basin studies, RES data can define both the large-scale morphology of topographic
178 depressions, but also the detailed character of the bed, as defined by along-track roughness measures.
179 While radar data can give a robust characterization of the bed at fine resolutions, hundreds of meters or
180 less, the technique cannot directly indicate a sedimentary origin, nor is it able to define the thickness or
181 properties of the sedimentary cover.

182 RES systems have been used for more than five decades to determine the thickness of ice sheets in an
183 effective way (Dustin M. Schroeder et al., 2020). Over that period, more than 1.5 million line-kilometers of
184 RES data have been collected in Antarctica, with airborne surveys predominating in recent times (Frémand,
185 Fretwell, et al., 2022; Mathieu Morlighem et al., 2020). By subtracting the radar-defined ice thickness from
186 surface-elevation data, bed topography can be determined. Surface elevation may be obtained from the RES
187 data, from other sensors (e.g. LIDAR) on the same platform, or from remote-sensing products (e.g. DEMs
188 from satellite studies). The final product is bed-elevation profiles of the ice-bed interface that are
189 interpolated to produce gridded bed-topography products. Interpolation may be done in numerous ways,
190 including direct spline-based interpolation (Fretwell et al., 2013) or geostatistical interpolation (Emma J.
191 MacKie et al., 2021); with the inclusion of ice-sheet flow data, mass-conservation approaches may be used
192 also (Mathieu Morlighem et al., 2020).

193 For the nadir-facing acquisition geometry of RES, specular and quasi-specular returns from the surface and
194 bed are typically the most prominent features in a radar trace (Haynes et al., 2018), which allows for
195 straightforward interpretation of along-profile ice thickness and bed topography. Although the earliest

196 systems were incoherent (Dustin M. Schroeder et al., 2019) the development of coherent systems (Gogineni
197 et al., 1998) and synthetic-aperture radar processing with range migration (Heliere et al., 2007; M. E. Peters
198 et al., 2007) improved the azimuth resolution of radargrams and the resulting extracted thickness profiles as
199 well as improving clutter mitigation in regions of high topographic relief and layover. More recently, swath
200 (Holschuh et al., 2020), tomographic (Paden et al., 2010), and array-based (T. J. Young et al., 2018) systems
201 as well as the availability of ultra-wideband systems (Arnold et al., 2020; Hale et al., 2016) have further
202 improved the geometric resolution of RES observations, with range resolution in the tens of centimeters and
203 along-track resolution in the tens of meters (Kjær et al., 2018).

204 The roughness of the bed encodes information on the morphologic and geologic character of the subglacial
205 interface (Jordan, Ferraccioli, Corr, et al., 2010; Rippin et al., 2014; Martin J. Siegert et al., 2005). This
206 roughness can be estimated directly from thickness profiles (Robert G. Bingham & Martin J. Siegert, 2007)
207 and – with assumptions on the fractal character of the bed – extrapolated to finer scales (T. M. Jordan et al.,
208 2017). Where perpendicular crossovers are available, the anisotropy of the bed roughness can also be
209 estimated (Cooper et al., 2019; Eisen et al., 2020). In addition to its resolvable along-profile signature, finer-
210 scale (i.e. wavelength-scale) roughness is also encoded in the bed-echo character including its abruptness (T.
211 M. Jordan et al., 2017), specularity (D. M. Schroeder et al., 2015; D. A. Young et al., 2016), and amplitude
212 distribution (Grima et al., 2019). Notably, these fine-scale relative metrics are insensitive to (even large)
213 absolute errors in ice thickness (e.g. from firm correction or surface registration). Finally, the radiometric
214 signature of bed echoes can also encode information on bed materials (Christianson et al., 2016; Tulaczyk &
215 Foley, 2020) and thermal state (Chu et al., 2018). These signatures are often difficult to interpret
216 unambiguously at the glacier to ice-sheet scale (Matsuoka, 2011), without multi-frequency (Broome &
217 Schroeder, 2022) or multi-static observations (Bienert et al., 2022) or polarimetric (Corr et al., 2007; Dall et
218 al., 2010; Frémand, Bodart, et al., 2022; Scanlan et al., 2022) observations. These approaches can
219 characterize and constrain the wavelength-scale roughness (tens of centimeters or smaller) and sub-Fresnel-
220 zone geometry (Haynes et al., 2018; T. M. Jordan et al., 2017) (meters to tens of meters) of the bed,
221 providing orders of magnitude finer-scale constraints than along-profile approaches (Bingham & Siegert,
222 2009).

223 *2.2.2.2 Gravity and magnetic data*

224 These passive techniques measure the intensity and, in some cases, the direction of the Earth's naturally
225 occurring gravity and magnetic fields. Magnetic and gravity data do not require large power sources, nor a
226 coupling to the Earth's surface, and airborne surveys have been widely deployed across Antarctica, most
227 commonly in combination with RES surveys from the same platform (Fig 1).

228 Gravity data are sensitive to the summed effects of mantle and crustal masses, including sedimentary rocks.
229 Due to their porosity, sedimentary rocks typically have lower density than the crystalline basement, causing

230 relative gravity lows over sedimentary basins (A. R. A. Aitken et al., 2016; Bell et al., 1998; Frederick et al.,
231 2016). Airborne gravity systems include several major types of gravity meter, with the conventional
232 stabilized-platform air-sea gravimeter (R. E. Bell et al., 1999) and derivations of this technology (M. Studinger
233 et al., 2008) providing the majority of data. More recently, so-called “strapdown” systems have been used,
234 which are based on inertial navigation sensors including triads of high-specification accelerometers and
235 gyroscopes rigidly attached to the aircraft (Jordan & Becker, 2018). In either approach the observed
236 accelerations are dominated by aircraft accelerations, and a well-constrained gravity solution is dependent
237 on an accurate recording of the aircraft location and elevation, and careful removal from the recorded signal
238 of aircraft accelerations and motion as well as temporal gravity variations such as tides. Accurate
239 navigational systems such as differential GNSS are therefore essential to achieve the best quality data.

240 Older spring-based meters were restricted to straight and level flights, constraining operational logistics, and
241 limiting the ability to collect other data types at the same time. This sensitivity to aircraft dynamics meant
242 accuracies of 3-5 mGal were typical (Jordan, Ferraccioli, Vaughan, et al., 2010). In recent times advances in
243 sensor technology and processing methods have allowed collection of gravity data during more dynamic
244 draped flights and an overall improvement in data quality, with accuracies of 1-2 mGal now typical (Jordan &
245 Becker, 2018; M. Studinger et al., 2008). Despite these improvements, gravity-data processing imposes a
246 low-pass filter on the data, typically 70 seconds or more, that leads to spatial resolution of 5-10 km,
247 depending on aircraft velocity. This velocity may be between 60 and 140 m/s for the fixed-wing platforms
248 used in Antarctica. A recent innovation is the adoption of helicopter-borne operations, which promises
249 further improvement in spatial resolution (Jensen & Forsberg, 2018; Wei et al., 2020). Future application of
250 strapdown gravity on slower-flying Unmanned Aerial Vehicle (UAV) platforms also holds the promise of
251 higher resolution and potentially lower-cost gravity surveys. An additional limit on the wavelengths resolved
252 by gravity surveys is the ice thickness, which means observations are often made several kilometers from the
253 bed interface, limiting the minimum resolvable wavelength. These factors limit the capacity for detection of
254 abrupt spatial changes in gravity, such as may be associated with glacial landforms and fault-bounded
255 sedimentary basins. Despite these residual limitations, the improved accuracy of gravity-sensor technology
256 allows modern airborne-gravity data to be applied with confidence at length scales > 5 kilometers.

257 The observed gravity field is a summation of source components including topography and crustal thickness,
258 as well as sedimentary-mass deficits, and to understand sedimentary basins the other factors must be
259 accounted for. Ice, subglacial lake and ocean thicknesses and bed topography, where known, are corrected
260 for using the Bouguer correction or an equivalent, which models the effect of topography and bathymetry,
261 typically assuming reference densities for rock, ice and water (Hirt et al., 2016; Scheinert et al., 2016). In
262 Antarctica, the thick ice-sheet load in the continental interior generates a Moho down-warp causing distinct
263 negative Bouguer anomalies that do not reflect crustal geology, and it is desirable to correct for this.

264 Because topographic loads may be balanced by the Moho or other masses in the deep crust or uppermost
265 mantle, for the isostatic residual anomaly, the condition is imposed that surface loads are balanced by
266 variable crustal thickness, either locally in the Airy case, or via regional flexure using elastic or visco-elastic
267 rheology (G. J. G. Paxman et al., 2017). Airy isostasy models are easy to apply and provide a consistent
268 convention for interpretation, but are prone to overcorrection, whereas flexural models may provide
269 superior removal of isostatic effects where the flexural rigidity is able to be constrained (Jordan, Ferraccioli,
270 Armadillo, et al., 2013; G. J. G. Paxman et al., 2017). Negative isostatic-residual gravity anomalies often
271 indicate sedimentary basins, although low-density basement rocks, such as granitic intrusions, can also give
272 rise to negative anomalies, requiring differentiation with other data (Jordan, Ferraccioli, Vaughan, et al.,
273 2010).

274 Despite the intricacies of processing and interpretation, sedimentary basin structure can potentially be
275 defined from gravity data for wavelengths >10 km, and for sedimentary rock thicknesses greater than ca.
276 500 m, although larger and thicker basins are resolved with more confidence. Gravity-derived thicknesses
277 are ambiguous, varying linearly with density contrast, and an inability to separate the basin source from
278 other possible sources is a limiting factor to be overcome during interpretation.

279 For magnetic data, oxidation of magnetite to hematite during weathering means that sedimentary rocks, in
280 general, have low magnetization relative to crystalline basement (Enkin et al., 2020). While low-
281 magnetization rocks do not generate a magnetic anomaly, their presence increases the distance between a
282 basement source and the aircraft sensor — this distance also includes the thickness of water and ice and the
283 height of the aircraft above the surface. Increased source-sensor separation causes anomalies to have
284 reduced amplitude and increased wavelength and sedimentary basins are characterized by reduced
285 magnetic anomaly gradients (Reid, 1980; Reid et al., 1990). Analysis of the anomaly gradients using depth-to-
286 magnetic-source estimation techniques is often applied to define the thickness and distribution of
287 sedimentary rocks (A. R. A. Aitken et al., 2014; Fausto Ferraccioli et al., 2009; Tankersley et al., 2022).

288 Airborne magnetic data are collected from magnetometers that, most commonly, are attached to aircraft by
289 a tail-boom, at wingtips, or in some cases towed. Fixed-wing surveys dominate modern data collection (A. R.
290 A. Aitken et al., 2020; Jordan & Becker, 2018; Tinto et al., 2019) but helicopter surveys are also used in
291 specific settings (Damaske et al., 2003; F. Ferraccioli et al., 2009; Fausto Ferraccioli & Bozzo, 2003; K. Gohl,
292 Denk, et al., 2013; G. Wilson et al., 2007). In contrast to gravity surveys, instrument precision is not a major
293 source of error, and improvements in practice have focused on managing the magnetic environment of
294 Antarctica, being close to the magnetic pole, and so especially vulnerable to space weather and intense
295 diurnal variations. In addition, the need for longer-range surveys and multi-year campaigns demands
296 additional care in data processing. The most recent approaches consider more fully the complexities of the
297 four-dimensional magnetic field yet (e.g. A. R. A. Aitken et al., 2020), yet the Antarctic geomagnetic

298 environment and logistical constraints remain substantial limitations on dataset accuracy relative to
299 aeromagnetic data on other continents.

300 A limitation of both gravity and magnetic approaches is the inability for airborne surveys to recover field
301 components at wavelengths longer than the scale of the survey (Scheinert et al., 2016). For this, the
302 expansion of satellite-based gravity, gravity gradiometry and magnetic data, including the GRACE, GOCE and
303 SWARM missions, has provided a crucial new understanding of the long-wavelength structure of the
304 continent (Ebbing et al., 2021; Ebbing et al., 2018; Pappa, Ebbing, & Ferraccioli, 2019; Pappa, Ebbing,
305 Ferraccioli, et al., 2019), these also underpinning more accurate compilations (Ebbing et al., 2021; A. V.
306 Golynsky et al., 2018; Hirt et al., 2016). The GOCE mission in particular has allowed new understandings of
307 crustal structure, including definition of sedimentary basins (Capponi et al., 2022; Haeger & Kaban, 2019).

308 Overall, the ability to define sedimentary basins through gravity and magnetic approaches has improved
309 substantially in recent years, with particularly more accurate gravity recovery at shorter wavelengths, and
310 the incorporation of satellite magnetic and gravity data at longer wavelengths. These improvements mean
311 that, where airborne data exist, the identification of subglacial sedimentary basins is possible for basins with
312 thicknesses greater than ca. 500m and with spatial resolutions of 10 kilometers or possibly less. These data
313 are associated with physical non-uniqueness and, given other unknowns, they do not unambiguously define
314 the geometry or physical properties of the basin fill. Unless these are otherwise constrained, these
315 uncertainties limit their use for a quantitative 3D understanding of basin morphology.

316 *2.2.2.3 Active and Passive Seismic*

317 Seismic techniques record the propagation of elastic waves in the ground, with the two main types of survey
318 being passive-seismic and active-seismic. Passive-seismic typically involves continuous observations from
319 three-component seismometer arrays with sources that may be natural or non-specific anthropogenic
320 origins (e.g. earthquakes, ambient noise). Active-seismic typically uses shorter-term, triggered observations
321 with (usually single-component) geophones and artificial sources of a controlled and survey specific nature
322 (e.g. explosives, airguns, vibrators), although hybrid approaches are also used. Seismometers or geophones
323 must be deployed in or on the ground for on-ice surveys, or in the water for marine surveys. Of these
324 methods active-seismic reflection approaches provide the more comprehensive image of basin architecture,
325 although significant ambiguities remain, including uncertainties in constraining seismic velocities and
326 geometrical biases stemming from the survey geometry.

327 Despite this, the application of active seismic techniques in Antarctica has several drawbacks. Active source
328 marine surveys can cover hundreds of kilometers per day in open water, although around Antarctica, the
329 presence of icebergs may disrupt surveying. By contrast, on-ice surveys that use explosive sources and
330 individual geophones as receivers can cover only a few km per day in Antarctic conditions (Anandakrishnan

331 et al., 1998; Brisbourne et al., 2017; Johnston et al., 2008; L. E. Peters et al., 2006; A. M. Smith, 1997; David
332 G. Vaughan et al., 2003). The use of the vibroseis method over snow with a towed streamer allows the
333 collection of tens of kilometers per day, and by this approach it has become possible to obtain larger-scale
334 surveys with several hundred kilometers per field season (Eisen et al., 2015; E. C. Smith et al., 2020).
335 Nevertheless, on-ice active seismic data are currently very limited in spatial extent (Fig 1).

336 Unlike radio waves used in RES, seismic waves can penetrate subglacial environments such as water,
337 sedimentary strata, and the basement beneath, providing crucial information necessary to understand
338 glacial dynamics. In addition, due to the simpler timing requirements (relative to RES) sources and receivers
339 can be separated, allowing for bi-static or multi-static configurations that can exploit angle-dependent
340 information from reflections. Several seismic approaches have been employed to detect and define
341 sedimentary basins in Antarctica. The tomographic approach determines the bulk velocity and thickness of a
342 geologic unit underneath the ice. Because the seismic wave speed in sedimentary basins is significantly
343 lower than in crystalline basement, the thickness and properties of such a unit can be estimated, especially
344 with long-baseline (wide-angle) reflection and refracted-wave seismic surveys (Blankenship et al., 1986;
345 Leitchenkov et al., 2016; Trey et al., 1999).

346 Seismic waves will reflect and refract at unit horizons where the acoustic impedance (defined as the product
347 of seismic velocity and density) changes. The seismic wave speed and density of sedimentary basin fill is
348 usually lower than that of crystalline basement, resulting in a generally lower acoustic impedance for
349 sedimentary basins. Furthermore, as the acoustic impedance of ice is well known, the reflection from the
350 subglacial interface can be used to determine the properties of that layer. Acoustic-impedance
351 measurements along profiles can be used to discriminate between regions of hard bedrock from sediments
352 or water at the bed. Of particular significance is the ability to discriminate different structures associated
353 with tills and tillites that have a direct link to subglacial processes at the bed (Anandakrishnan et al., 1998; H.
354 J. Horgan et al., 2021; A. Muto, Anandakrishnan, et al., 2019; Atsuhiko Muto et al., 2016; L. E. Peters et al.,
355 2006; A. M. Smith et al., 2013).

356 Seismic reflection methods can be used to map the stratigraphy of the geological units underlying the ice
357 sheet and ice shelves. The active seismic technique is especially important for resolving sub-ice-shelf
358 bathymetry and basins (Rosier et al., 2018; E. C. Smith et al., 2020). These data can be used to constrain
359 gravity-based approaches (Eisermann et al., 2020; Atsuhiko Muto et al., 2016). The identification of a
360 geologic stratigraphy indicates that a subglacial unit is of probable sedimentary origin, and the details of its
361 structure can be interpreted to understand the depositional environment, and age relationships with faults
362 and volcanic edifices (e.g. H. Horgan et al., 2005; Johnston et al., 2008; Kristoffersen et al., 2014).

363 As seismic reflection surveys have high spatial resolution, they provide a very good estimate of the ice
364 thickness and thus bed topography. In comparison to RES methods, ice-internal structure is not well
365 resolved, but seismic techniques are better able to characterize subglacial properties. Seismic profiles can be
366 analyzed in the same way as RES profiles for bed roughness, but because they very often record over a larger
367 offset (source-to-receiver distance) spread than RES methods, they are less prone to the influence of side
368 reflections and smoothing given that adequate processing is applied in the form of migration.

369 Our ability to detect and discriminate subglacial sedimentary basins in seismic reflection data is improving.
370 Because seismic-reflection-data quality increases with the square root of the number of observations, more
371 efficient data acquisition is key to improving resolution within logistical constraints. Over the last decade,
372 progress in borehole-drilling techniques (e.g. the rapid-air-movement drill system (Gibson et al., 2020)),
373 geophone design and deployment (e.g. Georods (Voigt et al., 2013)), and a combination of highly efficient
374 source-receiver systems (e.g. vibroseis-snowstream combination (Eisen et al., 2015)) have all contributed to
375 increasing the seismic data coverage and thus our ability to detect sub-ice properties (A. Muto, Alley, et al.,
376 2019; A. M. Smith et al., 2013). Nevertheless, as active seismic surveys are logistically demanding, studies
377 have been either only locally constrained or require considerable resources to cover regional distances.

378 Passive-seismic methods for detecting and studying sedimentary basins can estimate the seismic velocity
379 structure of the upper few kilometers of the crust using seismograph arrays deployed for periods of time
380 ranging from months to years. These techniques use naturally occurring seismicity within the ice sheet or
381 from earthquakes around the world, as well as seismic 'noise' from ambient sources. These surveys are
382 relatively simpler to deploy than active-source surveys as they do not require the source technology (drills
383 and explosives or a vibroseis system). Passive seismic techniques can map the thickness of sedimentary rocks
384 on a regional scale with a few seismic stations. Thus, passive techniques offer coverage of remote parts of
385 Antarctica, but at lower resolution than is possible for active seismic methods. One common method to
386 estimate the thickness of sedimentary basins is the so-called receiver function method that can be used to
387 estimate basin properties with high sensitivity to acoustic impedance contrasts at structural interfaces
388 located beneath the recording station (Ammon, 1991). Another method is to use the background signal, so-
389 called ambient noise, that can resolve broader lateral changes in seismic velocity structure (Shapiro et al.,
390 2005). Joint application of these (and other) methods has become common, providing the ability to resolve
391 sedimentary basins (Lin et al., 2012).

392 Receiver-function analysis provides images of structural interfaces below a seismic station using processing
393 that enhances seismic waves converted from S to P or P to S at structural interfaces (Ammon, 1991). The
394 depth to the sediment-bedrock interface and thus the sediment thickness is determined from the time delay
395 of the converted phase, after adjusting for ice thickness (Anandakrishnan & Winberry, 2004; Chaput et al.,
396 2014). The use of higher frequencies compared to typical receiver-function analysis (4 Hz vs < 1 Hz) allows

397 detection of sediment thicknesses of a few hundred meters and can provide some approximate constraints
398 on the velocity of the sediment layer (Dunham et al., 2020). While low-velocity relative to igneous or
399 metamorphic basement, consolidated sedimentary rocks may not provide sufficient density and velocity
400 contrast to be discernible in receiver functions.

401 Ambient-noise analysis uses short-period seismic surface waves obtained from the ambient-noise field
402 derived from non-specific sources, in particular ocean waves. By correlating records from two seismic
403 stations, the shallow structure beneath the ice sheet along the interstation path can be constrained (Pyle et
404 al., 2010; W. Shen et al., 2018). The correlation yields the Green's Function for wave propagation between
405 the stations, from which the phase and group velocity and ultimately the shear-wave velocity structure is
406 obtained. If the distribution of seismic stations is dense enough, the phase and group velocity tomography
407 maps can be used to map thicknesses of sediment and sedimentary rocks throughout the region and so
408 results are not restricted to the locations of seismographs. The use of both Rayleigh and Love waves
409 provides better results, since Love waves have superior resolution at shallow depths (Zhou et al., 2022).
410 Constraints on shallow structure from ambient-noise Rayleigh waves can be improved by also measuring the
411 ratio of horizontal to vertical displacement (Lin et al., 2012; Pourpoint et al., 2019). Joint inversion of several
412 of these datasets using a Bayesian formalism, including receiver functions, surface-wave group and phase
413 velocities, and horizontal to vertical ratios, can improve resolution of sedimentary material beneath the ice
414 sheet (Dunham et al., 2020; Pourpoint et al., 2019).

415 Sedimentary basin thicknesses have been estimated using passive seismic techniques throughout West and
416 Central Antarctica. Pourpoint et al. (2019) found thicknesses ranging from 0.1 to 1.5 km beneath seismic
417 stations near the Thwaites Glacier drainage area, with the thickest sediment in the deep topography of the
418 Byrd Basin and Thwaites Glacier bed. Dunham et al. (2020) found sediment thicknesses ranging from 0.1 to
419 0.9 km beneath seismographs in the West Antarctic Rift System (WARS) and Ellsworth Mountains region.
420 Zhou et al. (2022) mapped sedimentary basin thicknesses throughout West and Central Antarctica with
421 ambient-noise surface-wave methods. They found 4-5 km-thick basins beneath the Ross Ice Shelf but in
422 other regions of the study area maximum thicknesses were at most about 1.5 km, except in small regions
423 where spatial resolution is lacking. They interpreted the lack of thick sedimentary basins, dissimilar to
424 intracratonic basins in other continents, as indicating that basins in this region of Antarctica may have been
425 sediment starved throughout most of their post-Gondwana geological history, although erosion may also
426 have been significant.

427 *2.2.2.4 Electromagnetic and magnetotelluric*

428 Electromagnetic techniques also include active and passive techniques. Due to their limited depth
429 penetration, airborne approaches are not widely applicable to subglacial geology, although can be applied in
430 ice-free regions (Foley et al., 2015). Ground-based electric and electromagnetic techniques have seen limited

431 use in Antarctica with the most broadly applied approach in recent times being passive magnetotellurics
432 (Hill, 2020), although geomagnetic depth sounding has also been applied (Armadillo et al., 2004). The
433 magnetotelluric technique provides the capacity to image deep within the Earth and is generally applicable
434 to detect and image sedimentary basins through their electrical properties, which are commonly related to
435 water content, salinity and temperature (Gustafson et al., 2022; P. E. Wannamaker et al., 2004). Assuming
436 that subglacial sediments and sedimentary rocks are water-saturated, the key expected controls on bulk
437 resistivity values are the connected porosity of the pore space and the salinity of the waters within them,
438 defined empirically (see Glover, 2016).

439 Although a relatively old technique, the magnetotelluric method has been increasingly applied, due in large
440 part to improved ability to generate robust model solutions with high-performance computing and improved
441 sensor technologies. Magnetotelluric applications to crustal and upper-the-mantle imaging in the polar
442 regions are reviewed in Hill (2020). Building on the most recent relevant work (Gustafson et al., 2022; Key &
443 Siegfried, 2017; Kulesa et al., 2019; M. J. Siegert et al., 2018) we focus here on examining the potential
444 scope and limitations of magnetotelluric imaging of the hydrogeological and thermal properties of subglacial
445 sedimentary basins.

446 The source fields of the magnetotelluric technique are inherently wideband, ranging from ca. 10^{-5} Hz to 10^4
447 Hz, generated when electrical storms and interactions between the solar wind and the ionosphere produce
448 fluctuations in Earth's magnetic field. These fluctuations then induce correspondingly wideband telluric
449 currents in ice sheets and the underlying crust and mantle. Signal period is a proxy for depth, with longer-
450 period signals representing structure deeper in the Earth. Under favorable circumstances, and depending on
451 the bandwidth and collection procedure of the survey, temporally coincident measurements of magnetic
452 and electric potential fields allow the bulk electrical-resistivity distributions to be estimated at depths from
453 the near surface, resolved at the highest frequencies, to ca. 400 km at the lowest frequencies. Data
454 collection is typically focused in the high frequencies for near-surface studies (audio-frequency MT 10^0 Hz to
455 10^4 Hz), across a central broad band (BBMT 10^{-3} Hz to 10^2 Hz) for general crust and mantle studies, and long-
456 period MT (LPMT 10^{-1} Hz to 10^{-4} Hz) for mantle-focused studies. For the investigation of subglacial
457 sedimentary basins beneath the Antarctic Ice Sheet the higher-frequency band of the magnetotelluric
458 spectrum is of most interest. This is attractive in that high-quality magnetotelluric data can be acquired with
459 day-long station occupations if wind speeds are low ($\ll 10 \text{ m s}^{-1}$), as compared with station occupations of a
460 week or more required for upper-mantle studies.

461 Many challenges arise in ice-sheet settings related to potential violations of fundamental source-field
462 assumptions owing to the proximity to the geomagnetic south pole, high contact resistances of electrodes
463 buried in firn, and spindrift of charged snow particles generating strong broadband electrical noise (see Hill,
464 2020). The last is a particular challenge in the imaging of subglacial sediment basins because the broadband

465 frequencies exploited in doing so are particularly susceptible to noise contamination by drifting snow. A
466 second specific challenge arises when firn is absent and ice is exposed at the surface instead, forming a
467 major barrier to the deployment of electrodes and magnetometers and associated wiring. This is a problem
468 especially in coastal regions where seasonal melting and refreezing are widespread.

469 Notwithstanding these challenges, a growing number of Antarctic campaigns have demonstrated that high-
470 quality magnetotelluric data can be acquired with careful survey planning and using bespoke electrode pre-
471 amplifiers (Hill, 2020). Subglacial sedimentary basins are particularly well suited for magnetotelluric
472 exploration because they are expected to be several orders of magnitude less resistive (order of $10^{-1} - 10^1$
473 Ωm) than both the underlying crystalline crust (typically $> 10^2 \Omega\text{m}$) and the overlying ice. Cold Antarctic ice
474 has typical bulk resistivities of ca. $10^4 - 10^6 \Omega\text{m}$ but these can exceed $10^8 \Omega\text{m}$ for temperate clean-ice glaciers
475 (Kulesa, 2007).

476 Magnetotelluric studies of subglacial sedimentary basins remain limited, with only a few studies in
477 Antarctica. Although not yet widely applied, magnetotelluric surveying can reveal high-quality images of
478 subglacial sediment basins and has unique potential for detecting and defining liquid groundwater within
479 them (Gustafson et al., 2022). The use of seismic data to constrain magnetotelluric inversions with cutting-
480 edge joint inversion schemes has not yet been attempted in Antarctica but will very likely result in improved
481 resolution in the future (Key & Siegfried, 2017; Kulesa et al., 2019; M. J. Siegert et al., 2018).

482 There are two major complications for interpretation, however, in that Archie's law contains a cementation
483 exponent that has never been calibrated for subglacial sediments; and even more significantly, Archie's law
484 is not applicable where sediments have noticeable clay mineral contents requiring a significantly adapted
485 formulation (Kulesa et al., 2006). This is likely a particular problem for coastal subglacial sedimentary basins
486 where contents of marine clays are not normally negligible.

487 Finally, it is expected that a significant geothermal gradient will exist between the base and top of subglacial
488 sedimentary basins, especially where they have a vertical extent of several kilometers and are buried
489 beneath several kilometers of cold ice. Kulesa et al. (2019) demonstrated with a conceptual model that such
490 temperature gradients will likely result in a multi-fold increase in bulk resistivity between the base and top of
491 subglacial sediment basins, largely due to a temperature-controlled decrease in ionic mobility in sediment
492 pore-waters. This inference suggests that bulk resistivity models can be used to infer temperature changes in
493 subglacial sedimentary basins and implied geothermal heat flux into the ice-sheet base, a key unknown in ice
494 sheet modelling, especially in high-heat flux settings.

495 Overall, magnetotelluric measurements are powerful tools to explore subglacial sedimentary basins, the
496 associated groundwater and geothermal heat fluxes, and their interactions with the ice-sheet base. In most
497 Antarctic situations, porosity, pore-fluid salinity, clay mineral contents and temperature changes will

498 combine to control bulk resistivity magnitudes, a complication that may be further compounded for coastal
499 sediment basins. These ambiguities require external constraint to develop a quantitative interpretation of
500 sedimentary properties from bulk resistivities.

501 2.2.3 Integrated Studies

502 As we have seen above, each of the listed methods has the capacity to define the existence of sedimentary
503 basins beneath ice and, in many cases, also particular characteristics such as thickness, internal geometry,
504 seismic velocity, density, and electrical conductivity. These characteristics each may resolve different aspects
505 of the basin and, furthermore, each technique has different uncertainties and so the methods are
506 complementary. In particular, the inherent ambiguities in most available data can lead to major errors when
507 any single technique is used. For example, outcrops may be selected for erosion resistance through
508 landscape-forming processes while low-roughness topography may be caused by glacial erosion (Stewart S.
509 R. Jamieson et al., 2014) and low gravity anomalies and/or smooth magnetic gradients may be caused by
510 low-density or non-magnetic basement rocks.

511 Integrated studies that use multiple datasets are necessary to resolve these ambiguities (Grikurov et al.,
512 2003). For airborne geophysical surveys, the combination of RES, gravity and magnetic data has proved
513 powerful, and this is especially enhanced where suitable ground observations are also collected. Major
514 recent, ongoing, and upcoming data collection programs have sought to synergize multidisciplinary data
515 collection and modelling (MacGregor et al., 2021; Scambos et al., 2017). The co-interpretation of multiple
516 complex and sparse geoscience datasets has a high task-complexity, that may lead to difficulty making
517 reliable judgements (Swink & Speier, 1999). As a human-led process which relies on interpreter skill, the
518 background, knowledge and biases of the investigator can have substantial impacts on results (C. G. Wilson
519 et al., 2019). Although clearly not without uncertainty, multi-data analyses provide the potential to manage
520 subjectivity in interpretation and support the ability to make sound judgements (Alan R. A. Aitken et al.,
521 2018).

522 A consistent data-based mapping at continental scale is challenged by highly variable data quality, resolution
523 and availability, as well as the challenge of combining multiple datasets into a consistent map that accounts
524 for all data. To define basal boundary conditions, we may seek initially to define the presence or absence of
525 sedimentary basins, which is a prerequisite to understanding their thickness, age, and other properties.
526 Geostatistical and machine-learning techniques provide relatively unbiased and data-based approaches to
527 understanding this in a probabilistic sense. Li et al. (2022) applied the random forest approach with multiple
528 data types to map for all Antarctica the likelihood of sedimentary basins at the bed. Emma J. MacKie et al.
529 (2021) applied a trained logistic regression model to simulated topographic-roughness models to infer
530 geological bed type associated with the presence of sediments. Such techniques are highly valuable with
531 respect to their consistent response to data, provided those data are not too variable in their properties

532 (resolution, accuracy etc.), but they are not able always to accommodate irregularly sampled or sparse data,
533 while non-numerical data such as lithological descriptions can be problematic to include. In this work we use
534 the results of such techniques with a wide range of prior findings and datasets (Fig. 2) to develop a new
535 understanding of sedimentary basins beneath the Antarctic Ice Sheet.

536 3 Antarctica's Sedimentary Basins

537 3.1 Methods & Validation

538 We have mapped the sedimentary basin distribution continent-wide using a flexible basin-classification
539 approach applied in a GIS. The map presented here (Fig 3) is manually classified based on a wide range of
540 continent-scale datasets and derivative products. To develop the map, an initial classification into basins and
541 non-basins was automatically generated from the machine-learning-derived likelihood map (Fig 2a) of Li et
542 al. (2022), using a threshold of 0.5. From this initial point, the polygons for individual basin regions were
543 scrutinized and edited considering additional data including outcrop geology (Cox et al., 2023), along-track
544 roughness (Fig 2b), bed elevation (Fig 2c) and its spatial variability (Fig 2d), gravity magnitudes (Fig 2e) and
545 their spatial variability (Fig 2f), aeromagnetic intensities (Fig 2g) and their spatial variability (Fig 2h), and
546 estimates of sedimentary basin thickness from passive and active seismic datasets. Data visualizations, maps
547 and interpretations from many published studies were accommodated in the mapping process.

548 3.1.1 Geology classification

549 As discussed above, the principal distinction we wish to make here is between crystalline-basement-
550 dominated regions and sedimentary basins. However, a binary classification is inadequate to cover the range
551 of circumstances that the geology presents. Retaining simplicity, we classify the bed type into four main
552 classes: crystalline basement, intra-basin volcanic, and Type 1 and Type 2 sedimentary basins (Fig 3). Often,
553 the data contain characteristics of more than one of these types, due either to variable bed types present in
554 small areas, or due to transitional conditions from one type to another, and so we also have three mixed-
555 type classes, although their distribution is limited compared to the major types (Fig 3).

556 The crystalline-basement class indicates where the bed is interpreted to consist of igneous or metamorphic
557 rocks (including high-grade metasedimentary rocks), with either no sedimentary cover, or a thin veneer that
558 is below the detection thresholds of the datasets used. Typically, these regions possess the characteristics of
559 high elevation and high gravity with high spatial variability in topography, gravity, and magnetic data. Along-
560 track roughness tends to be high for this class. Type cases for this class include regions in the Transantarctic
561 Mountains, Dronning Maud Land, Marie Byrd Land and the Gamburtsev Subglacial Mountains.

562 The Type 1 basin class represents regions where sedimentary basins are preserved in relatively unmodified
563 basins, with typical characteristics of low elevation and low gravity, and low spatial variability in gravity and

564 magnetic data. Along-track roughness tends to be low. Type cases for this class include the Ross and Weddell
565 embayments, and the Wilkes, Aurora and Pensacola-Pole subglacial basins.

566 The intra-basin volcanics class includes areas where volcanic rocks are interpreted to be emplaced within a
567 Type 1 basin sequence; that is they are younger than the base of the basin and may interfinger with or
568 overlie sedimentary rocks. Typically, this class relies on outcrop data and aeromagnetic data to define the
569 extents of volcanic complexes where they are dominant. It is noted that basins may contain volcanic rocks
570 without them being evident in geophysical data and the extent of volcanic rocks is likely underestimated
571 (van Wyk de Vries et al., 2018). The type case for this class is the McMurdo Volcanic Complex in the Ross
572 Sea.

573 We define the Type 2 basin class where sedimentary rocks are known or inferred but the original
574 depositional basin is not preserved. These rocks tend to predate the formation of the present landscape, are
575 often uplifted to high elevations, may be intruded by younger igneous rocks, may be heavily eroded and may
576 have geophysical characteristics more similar to crystalline basement than Type 1 basins. The type case for
577 this class is the Beacon Supergroup, with its characteristic high elevation exposures and mesa-like
578 topography as a consequence of widespread Jurassic dolerite intrusions. Type 2 basins are prominent in the
579 Transantarctic Mountains and in the Ellsworth-Whitmore Mountains, with subglacial examples inferred in
580 Dronning Maud Land, and subglacial highlands in the Vostok and Aurora regions (Fig 3).

581 *3.1.1.1 Class Validation*

582 For validation, we may review this geological bed-type classification against the major numerical datasets
583 available to the interpretation. Summary statistics for each input dataset were calculated for each class using
584 a Zonal Statistics GIS tool. These statistics allow the distinctiveness of the class-level populations to be
585 defined in terms of differences of means, factoring in standard deviation, and so illuminate the data that
586 most strongly differentiate between classes. Figure 4 shows the extent to which the zonal mean for each
587 class differs from the mean for the entire continent. Where these differ substantially, especially in sign, that
588 dataset is a potential discriminant of the selected classes. Furthermore, we may directly compare the
589 population-level distinctiveness between classes, for which we derive Cohen's effect size (Fig 4). Values
590 above 0.8 may be considered a large effect, indicating a strong discriminant, while values below 0.5 may be
591 considered a small effect, indicating a weak discriminant.

592 The primary classification we seek is the distinction between Type 1 basins and crystalline basement. For
593 these two classes, large effect sizes are seen for topography elevation datasets, while medium effect sizes
594 are seen for free air and Bouguer gravity, topography and gravity variation and satellite gravity-gradient
595 components (Fig 4a). The ability to discriminate between crystalline basement and Type 2 basins is weaker,
596 with medium effect sizes seen for Airy Isostatic Residual Anomaly (IRA) and satellite-gravity-gradiometry

597 components (Fig 4b). The distinction between Type 1 and Type 2 basins is strong, with large effect sizes for
598 subglacial topography elevation datasets, Bouguer gravity datasets and variability measures for these, and
599 medium effect sizes for Airy IRA and high-pass-filtered Bouguer gravity (Fig 4c). Finally, the in-basin volcanics
600 class is sharply defined relative to all other classes, these being most clearly differentiated with large or
601 medium effect sizes for magnetic data-products as well as high variability in topography and gravity data.

602 The relationships highlighted above support the following as key criteria for classifying subglacial geology:
603 Type 1 basins are defined most by their low topography at large scales, accompanied by relatively high
604 Bouguer gravity, perhaps counter to expectations (note the opposite sign to topography in Fig 4a, 4c). With
605 respect to their differentiation from Type 1 basins, Type 2 basins show similar characteristics to crystalline-
606 basement, but with a stronger effect-size from gravity data, reflecting their characteristic gravity lows. Type
607 2 basins can be separated from crystalline basement by their low response in Bouguer and Airy IRA gravity
608 anomalies and satellite-gravity-gradiometry components. The magnetic dataset does not discriminate
609 strongly between these three classes but is strongly linked to the in-basin volcanics class, which is also
610 identified by high spatial variability in all datasets.

611 3.1.2 Age Classification

612 In addition to geological bed-type classification we seek to define the age of the basins which, besides their
613 importance for tectonic understanding, may reveal changing conditions for the ice sheet formation and
614 evolution through the Cenozoic, as well as differences in basal conditions associated with the age of the
615 sedimentary rocks at the surface. The interpreted age distribution indicates the evolving tectonic conditions
616 of Antarctica and its landscape, although due to the general paucity of robust age-dating outside of
617 outcropping regions, and very limited capacity for stratigraphic correlation beneath the ice, these
618 interpretations are on necessarily broad timescales.

619 For each basin, we define an interpreted age for the base and the top of the basin sequence (Fig. 5). The
620 base-of-basin age (Fig. 5a) represents a maximum bound on basin age, either from a known maximum age
621 (e.g. from a maximum deposition age), or from the interpreted age of the underlying crust. The top-of-basin
622 age (Fig. 5b) represents a minimum bound on basin age, either from a known minimum age (e.g. cooling
623 age), from a capping or intruding igneous unit or from geomorphological criteria including interpreted
624 regions of glacial erosion and deposition.

625 3.1.3 Basin Thickness

626 Except for RES data, the data types in Section 2.2 can all be used to generate models of the thickness of
627 sedimentary cover. It is possible to interpolate sedimentary thickness between existing data points, giving an
628 estimate of the thickness of sedimentary cover across the continent (Baranov et al., 2021). However, the

629 fundamental differences between basin-sensing techniques, their differing resolution and accuracy, and
630 specific features of individual surveys and models all lead to major uncertainty in defining basin thickness.

631 Figure 6 shows several models of sedimentary basin thickness, including models derived from gravity
632 (Haeger & Kaban, 2019), interpolation of seismic data (Baranov et al., 2021), passive seismic models (Zhou et
633 al., 2022), magnetic depth to basement tied to seismic-reflection data (Tankersley et al., 2022) and marine
634 seismic-reflection data (K. Hochmuth et al., 2020; Lindeque, Gohl, Wobbe, et al., 2016; Straume et al., 2019).
635 While there is some commonality between these models, there are also many differences and only the
636 seismic-reflection models show strong consistency with each other.

637 Three major factors contribute to this discrepancy. First, the resolution of techniques differs and so distinctly
638 separate features in one technique are likely to be merged in another. Consequently, thickness models will
639 differ greatly in the presence of complexity (e.g. Ross Island in Fig. 6c). Second, the physical properties
640 detected with each technique differ and, furthermore, not all techniques have agreed criteria for the
641 definition of the basin-basement interface. Finally, the different techniques have different capacity to
642 resolve deep basins, and to accurately define the base of basins accurately is challenging. For example,
643 depth to magnetic basement commonly defines sills or volcanic horizons within the basin sequence, and
644 there is often no solution possible for the basement beneath. Ultimately, while a general agreement can be
645 reached on the extent of sedimentary basins, for now, their thicknesses remain poorly constrained in
646 Antarctica, except where seismic-reflection data have been collected and analyzed alongside other
647 techniques.

648 3.2 West Antarctic Basins

649 West Antarctica, in a geomorphological division, includes the continental regions on the Pacific-facing side of
650 the chain of mountains extending from Northern Victoria Land through the Transantarctic and Pensacola
651 Mountains to Coats Land (Fig 3). This region possesses several major basin-dominated regions, in particular
652 the Ross, Amundsen and Weddell regions, and is characterized by the low-elevation topography associated
653 with these. West Antarctica's crust has a varied history, but the majority has formed since the Cambrian as a
654 result of accretionary tectonics at Gondwana's paleo-Pacific margin (Jordan et al., 2020). Older crust with an
655 affinity to cratonic regions of East Antarctica or Southern Africa may extend beneath parts of West
656 Antarctica. Precambrian basement is known to outcrop at Haag Nunataks (Riley et al., 2020) and is suggested
657 to underlie part of the Ross Embayment (Tinto et al., 2019). This basement hosts a series of basins of diverse
658 origin extending in age from the Cambrian to the Quaternary.

659 3.2.1 The Ross Embayment and Siple Coast

660 This sector of West Antarctica is bounded by the Transantarctic Mountains to the west and the West
661 Antarctic Ice Sheet (WAIS) divide to the south with the basement-dominated Marie Byrd Land to the east. In

662 Marie Byrd Land, small Type 1 basins are interpreted in glacial troughs (Fig. 7) but the major known basin
663 (Type 2) is defined by the variably metamorphosed <520 Ma to >440 Ma Swanson Formation, dominated by
664 turbidites and flysch. These rocks represent a middle-Cambrian to Ordovician basin, with sediments derived
665 from the Ross Orogen and a variety of Proterozoic sources (Yakymchuk et al., 2015). These sediments were
666 deposited along the Gondwana margin, initially on the continental slope and rise in the Cambrian – lower
667 Ordovician but possibly later in a fore-arc to accretionary-prism as a convergent-margin setting developed
668 (Jordan et al., 2020).

669 The Ross Sea is one of the most well-studied regions in Antarctica and the existence of major sedimentary
670 basins is well established, with their stratigraphy revealed in multi-channel seismic data as well as numerous
671 drill cores (Fig 1, Fig S1). These studies define a thick sequence of late Cretaceous to Quaternary sedimentary
672 rocks separated into several packages by regional unconformities (F. J. Davey & Brancolini, 1995; Lindeque,
673 Gohl, Henrys, et al., 2016; Pérez et al., 2021).

674 The Ross Sea basin has four major depocenters (Fig 7), the Victoria Land Basin, the Central Trough, the
675 Eastern Basin and the Northern Basin (F. J. Davey & Brancolini, 1995) separated by basement highs with
676 thinner sedimentary cover, the Coulman High and Central High; only Roosevelt Island appears sediment-free
677 (D. S. Wilson & Luyendyk, 2006). The West Antarctic Rift System (WARS) initiated in the late Cretaceous, but
678 with relatively little basin-fill deposited (C.S. Siddoway, 2008; Christine Smith Siddoway et al., 2004). The first
679 major sedimentary sequence (RSS-1) is discontinuous and is observed in isolated grabens in the eastern to
680 central Ross Sea, and may represent this rifting event, with thermal subsidence perhaps extending into the
681 early Cenozoic (Luyendyk et al., 2001). A later phase of Eocene to Oligocene rifting is interpreted in the
682 Victoria Land Basin (Fielding et al., 2008). A basin-wide unconformity (RSU-6) indicates a period of erosion in
683 the Oligocene, occurring not later than 26 Ma in the Eastern Basin (Kulhanek et al., 2019), potentially
684 associated with sea-level fall associated with large-scale glaciation in Antarctica. Correlation of RSU-6 into
685 the Victoria Land Basin has been problematic (cf. F. J. Davey et al., 2000; Fielding et al., 2008), but may align
686 with a mid-Oligocene unconformity that marks the end of the early rift stage of Fielding et al. (2008).
687 Subsequent to this, basin deposition was episodic, but with relatively little extension, the glacial evolution of
688 the continent being the major driver of basin evolution in most of the Ross Sea (Anderson et al., 2019; De
689 Santis et al., 1999; Kim et al., 2018; Lindeque, Gohl, Henrys, et al., 2016; Marschalek et al., 2021; Pérez et al.,
690 2021)

691 Upper Oligocene to Lower Miocene strata (RSS-2) are preserved in the major basins of the Ross Sea, but are
692 thin to absent on the basement highs (Pérez et al., 2021). These sediments are interpreted to be deposited
693 in a glacio-marine setting associated with a fluctuating ice-sheet margin including glaciation of local
694 bathymetric highs (De Santis et al., 1999). Early to middle Miocene (18-15 Ma) sedimentary deposition (RSS-
695 3 & RSS-4) is interpreted in detail in Pérez et al. (2021). In contrast to the thick and structurally segmented

696 packages of the lower sequence, this package overall is laterally continuous across the southern Ross Sea,
697 but with complex internal structure that is representative of changeable ice-sheet dynamics, as documented
698 in several drill-core records (Levy et al., 2016; Marschalek et al., 2021; R. M. McKay et al., 2016). A major
699 mid-Miocene erosional event (RSU-4), indicating the advance of a major ice sheet over the Ross Sea is
700 interpreted associated with the Mid-Miocene Climate Transition (Philip J Bart, 2003; Pérez et al., 2021). The
701 post mid-Miocene sedimentary basin record is similarly characterized by numerous and repeated ice-sheet
702 advance and retreat cycles (Anderson et al., 2019; P. J. Bart et al., 2000; Halberstadt et al., 2018; R. McKay,
703 Naish, Carter, et al., 2012; R. McKay, Naish, Powell, et al., 2012; Naish et al., 2009). Consequently, sediment
704 thicknesses are relatively low, except in deeper water in the northeast where substantial progradation of the
705 shelf edge is seen (Katharina Hochmuth & Gohl, 2019; Pérez et al., 2021), and in the west where the Terror
706 Rift has substantially deepened the bathymetry (Sauli et al., 2021; Wenman et al., 2020).

707 The Terror Rift has generated the ca. 4 km thick rhombic Discovery Graben, extending from Cape
708 Washington to, at least, Ross Island (Sauli et al., 2021), with a seismically-defined extension into the
709 southern McMurdo Ice Shelf (Johnston et al., 2008), and possibly further south (Tankersley et al., 2022).
710 Stratigraphic considerations suggest that after Eocene- Oligocene rifting, a period of thermal subsidence
711 persisted until renewed extension from ca. 13 Ma drove the renewed tectonic development of
712 accommodation space in the Discovery Graben (Fielding et al., 2008); however a more continuous evolution
713 may be considered (Granot & Dymont, 2018; Sauli et al., 2021). Within the western Ross Sea, the McMurdo
714 Volcanic Complex represents widespread and prominent volcanism, and some of these volcanoes are
715 associated with flexural basin development (e.g. H. Horgan et al., 2005; Wenman et al., 2020) generating
716 repositories of Neogene sedimentation and glacial development (R. McKay, Naish, Carter, et al., 2012; R.
717 McKay, Naish, Powell, et al., 2012; R. M. McKay et al., 2016; Naish et al., 2009).

718 The northwestern Ross Sea has a distinct Cenozoic evolution. The Northern Basin is directly associated with
719 the adjacent Adare Basin, which formed during seafloor spreading from 43 to 26 Ma, while the oceanic crust
720 beneath the Central Basin, north of the Central Trough, may have formed from 61 to 53 Ma (Cande & Stock,
721 2004). The Northern Basin is offset from the Victoria Land Basin by the Polar 3 magnetic anomaly, inferred to
722 represent 48-34 Ma alkaline intrusive rocks emplaced into a transcurrent fault zone (F. Ferraccioli et al.,
723 2009). With the implication that this fault zone extends further offshore to the Iselin Bank, Fred J. Davey et
724 al. (2021) presented a three-stage reconstruction of the northern Ross Sea involving: 10 to 26 Ma – Terror
725 Rift opening and minor extension of WARS (Granot & Dymont, 2018), 26 to 43 Ma – Opening of the Adare
726 Basin and Northern Basin; 53 to 61 Ma – Opening of the Central Basin and northern Central Trough,
727 accommodated by the Polar-3 transfer and its extension to the Iselin Rift (Fred J. Davey et al., 2021).

728 The extension of the basin-forming events known from the southern Ross Sea beneath the Ross Ice Shelf is
729 highly likely, although the structure of these basins has not been fully demonstrated, due to the lack of

730 extensive seismic data and ambiguous gravity signals (Karner et al., 2005). Recent geophysical data have
731 begun to reveal the structure of this basin: airborne geophysical surveys across the Ross Ice Shelf have
732 allowed the identification of several depocenters from depth to magnetic basement calibrated against
733 seismic-reflection data in the southern Ross Sea (Tankersley et al., 2022). These show continuation of the
734 Ross Sea systems into Eastern and Western depocenters separated by a mid-shelf high connecting with the
735 Central High. The Eastern depocenter narrows inland to a distinct trough beneath Siple Dome. A smaller
736 depocenter is located to the east of Roosevelt Island. The western depocenter beneath the Ross Ice Shelf is
737 broad with a weakly defined ridge separating two sub-basins. In addition, recent passive-seismic models
738 have mapped sedimentary thickness in the region using ambient-noise tomography, also revealing thick
739 sedimentary basins beneath the Ross Ice shelf and southern Ross Sea (Zhou et al., 2022). The structure of
740 these is different to the magnetic studies, likely reflecting the different spatial sensitivities of these
741 techniques. Similarly, the mapping of Li et al. (2022) indicates a high likelihood of major basins beneath the
742 Ross Ice Shelf (Fig 2a). Despite these first considerations being addressed, the absence of seismic-reflection
743 constraints on basin geometry and stratigraphy limits the understanding of Cenozoic deposition and erosion
744 patterns beneath the Ross Ice Shelf.

745 A further extension of the WARS into the Siple Coast region suggests a likely continuation of the basin-
746 forming processes; however, the Siple Coast has distinctly different characteristics to the Ross Embayment.
747 Although sedimentary cover is widely recognized in many geophysical surveys, sedimentary deposits are
748 apparently thinner (in general < 1 km) and not ubiquitous. Ambient-noise tomography resolves a broad basin
749 region extending ca. 400 km inland from the coast (Zhou et al., 2022). Aeromagnetic data at the coast
750 suggest several ca. 75 km wide depocenters beneath Siple Dome aligned with the previously identified Trunk
751 D Basin (Bell et al., 1998), the Crary Trough, and on the Amundsen Coast, respectively north and south of the
752 Crary Ice Rise (Tankersley et al., 2022). The southernmost of these has recently been defined in detail using
753 magnetotelluric and passive-seismic data (Gustafson et al., 2022). In the mapping of Li et al. (2022) the Siple
754 Coast region returns sedimentary-bed likelihoods dominantly between 0.25 and 0.75, indicating the
755 ambiguous nature of this region at large scales. High sedimentary-bed likelihood regions are identified for
756 the MacAyeal Ice Stream, for the Siple Dome/Trunk D Basin, the Crary Trough and the Amundsen Coast.
757 Inland, beyond the limit of the broad basin-dominated region (Zhou et al., 2022), a basement-dominated
758 pattern is seen; however, four smaller basins are identified associated with the uppermost MacAyeal Ice
759 Stream, Trunk D Basin (L. E. Peters et al., 2006), the Onset Basin linking to the Crary Trough (Bell et al., 1998;
760 L. E. Peters et al., 2006) and a southern basin linking to the Amundsen Coast (M. Studinger et al., 2001). The
761 rest of the region is here classified as mixed Type 1 basin/crystalline basement for which the exact
762 configuration of sedimentary cover in this region is not well resolved. Nonetheless there is likely to be
763 sufficient sedimentary cover for basin-influenced processes to occur widely.

764 The transition from the Ross Sea to the Siple Coast involves, in the west, several transitions in basin
765 architecture (Fig 7) – one located from the Polar-3 anomaly to Iselin Bank, which separates the Northern
766 Basin from the Victoria Land Basin and the Central Basin from the Central Trough (Fred J. Davey et al., 2021);
767 another located at the Discovery Accommodation Zone, separating the Victoria Land Basin and Central
768 Trough from the Western Ross Basin (T. J. Wilson, 1999), and a third located outboard of Shackleton Glacier
769 separating this broad basin from the narrower basins of the Amundsen Coast and Crary Trough (Tankersley
770 et al., 2022). The situation in the east is simpler, with the Eastern Basin separating at Roosevelt Island into
771 two narrower depocenters – one extending to Siple Dome, the other to MacAyeal Ice Stream (Tankersley et
772 al., 2022; Zhou et al., 2022). In general, the tendency is for narrower and more defined depocenters
773 developing inland, likely indicating a deeper exposure level inland due to repeated glaciation events
774 combined with reduced Cenozoic subsidence and sediment loading inland (Guy J. G. Paxman et al., 2019; D.
775 S. Wilson et al., 2012), and potentially stronger lithosphere under the WAIS divide.

776 3.2.2 Interior West Antarctica

777 Interior West Antarctica (Fig 8) includes a prominent low-lying region east of the WAIS divide, the central
778 West Antarctica region, including the Byrd Subglacial Basin and the Bentley Subglacial Trough (each
779 extending > 2 km below sea level.) This region is bounded to three sides by high-standing regions, the
780 Ellsworth-Whitmore and Haag regions to the west, the Thurston Island region to the north and Marie Byrd
781 Land to the northeast. To the southwest, an indistinct transition leads to the Siple Coast.

782 The Ellsworth-Whitmore Mountains preserve the oldest known sedimentary rocks in West Antarctica, with a
783 ca. 13 km-thick sequence of Cambrian to Permian sedimentary rocks (Paula Castillo et al., 2017; Craddock et
784 al., 2017). The lowermost unit, the Heritage Group, comprises lower- to middle-Cambrian sedimentary rocks
785 including a lower sequence of terrestrial volcanoclastic, shallow-marine clastic sediments and limestones, an
786 overlying sequence of transitional terrestrial to marine sedimentary rocks and, overlying these, Late-Middle
787 to Late Cambrian carbonate-dominated rocks (Curtis & Lomas, 1999). Thin transitional beds divide the
788 Heritage Group from the Upper Cambrian to Devonian Crashsite Group, deposited in a fluvial to shallow-
789 marine environment (Curtis & Lomas, 1999). The glacial-derived Whiteout Conglomerate is interpreted to
790 represent the early Permian Gondwanide glaciation at ca. 300 Ma (Isbell et al., 2008) and is overlain by the
791 Polarstar Formation including argillite, sandstone and coal measures, interpreted to represent post-glacial
792 deposition in the Gondwana Basin (Elliot et al., 2017). Overall, this basin has been interpreted to represent a
793 transition from a rift setting in the early Cambrian to a passive-margin setting extending into the Permian
794 (Paula Castillo et al., 2017; Craddock et al., 2017). Isolated exposures elsewhere in the Ellsworth-Whitmore
795 Block (Cox et al., 2023) also possess sedimentary rocks and we infer the unexposed region to be of mixed
796 class, preserving the Paleozoic basin intruded by younger granite suites.

797 Seismic observations suggest that the central West Antarctica region is not occupied by a thick, broad low-
798 velocity sedimentary basin (Zhou et al., 2022), but sedimentary rocks are likely to exist in low-lying regions
799 (Li et al., 2022). The low-elevation areas possess markedly smooth beds, and in many cases low isostatic-
800 residual gravity anomalies indicating relatively young sedimentary rocks are present (Jordan, Ferraccioli,
801 Vaughan, et al., 2010). Three basins are interpreted in this region, each with different glacial catchments: the
802 Pine Island Rift Basin underlies the upper Pine Island Glacier catchment (Jordan, Ferraccioli, Vaughan, et al.,
803 2010); the Byrd Subglacial Basin underlies the upper portion of the Thwaites Glacier catchment (M.
804 Studinger et al., 2001); and the Bentley Subglacial Trough flanks the Ellsworth-Whitmore block, connecting
805 to the Ferrigno Rift Basin (Bingham et al., 2012). The thickness of sedimentary rocks in these is variable but
806 locally may be up to 2 km thick. The geometry of these basins indicates several phases of extension, with ca.
807 E-W oriented basins overprinted by later extension generating ca. NE-SW aligned basins (Fig 8). The former
808 set may relate to structures in the southern Weddell Sea while the latter are aligned with WARS rift axis and
809 the Siple Coast basins.

810 The nature of the bed in the glacial troughs connecting these inland basins to the coast is not clearly defined.
811 Evidence from seismic and RES data suggests in each case a complex bed evolving with, in places, thick and
812 partially lithified sedimentary deposits, and in other places basement rocks or volcanoes (Alley et al., 2021;
813 Bingham et al., 2012; Brisbourne et al., 2017; A. Muto, Alley, et al., 2019; A. Muto, Anandakrishnan, et al.,
814 2019; Atsuhiko Muto et al., 2016; A. M. Smith et al., 2013). These are classed as mixed-crust, similar to the
815 Siple Coast region, implying a bed condition that is not well resolved within the trough, but likely contains
816 enough sedimentary material to support enhanced till production and hydrogeology (Alley et al., 2021).

817 3.2.3 Pacific Margin

818 The Pacific margin of West Antarctica includes the basin regions of the Amundsen and Bellingshausen Seas,
819 and the extension of this margin along the western Antarctic Peninsula (Fig 8). Each of these is characterized
820 by a thick sequence of sedimentary rocks on the continental shelf, with up to 7 km in the Amundsen Sea and
821 5 km in the Bellingshausen Sea (K. Hochmuth et al., 2020; Lindeque, Gohl, Wobbe, et al., 2016). Based on a
822 partial continuity of Cenozoic seismic stratigraphy extending from the eastern Ross Sea, the Pacific margin
823 preserves, from west to east, a progressively younger base-of-basin, from 80-67 Ma in the Ross Sea to 36 Ma
824 on the Antarctic Peninsula margin, and correspondingly a younger onset of transitional glacial conditions,
825 from 34-30 Ma in the Ross Sea to 21 Ma in the eastern Amundsen Sea, and 25 Ma on the Antarctic Peninsula
826 margin, (Lindeque, Gohl, Wobbe, et al., 2016). In the transition to glacial Antarctica, and in subsequent
827 glacial conditions, these basins record selective deposition focused especially in the Amundsen Sea
828 Embayment and the eastern Bellingshausen Sea (K. Hochmuth et al., 2020; Lindeque, Gohl, Wobbe, et al.,
829 2016). This margin has substantial shelf-edge progradation, since the middle to late Miocene in the

830 Amundsen Sea and since the late Miocene/early Pliocene for the Bellingshausen Sea, and the early Pliocene
831 for the Antarctic Peninsula margin (K. Hochmuth et al., 2020).

832 The Amundsen Sea Embayment receives sediments from the Pine Island and Thwaites Glaciers and
833 possesses the thickest accumulation of sedimentary rocks on the Pacific margin. The inner shelf, however, is
834 dominated by exposed basement, extending 200 to 250 km from the coast (K. Gohl, Denk, et al., 2013).
835 Within this region some minor basin regions are interpreted where both the bed and the magnetic data are
836 relatively smooth. The middle and outer shelf are thickly sedimented, comprising basal strata from early
837 Cretaceous rifting, a thick passive-margin sequence of Late Cretaceous to Oligocene sediments, and
838 Early/Middle Miocene to Pleistocene characterized by episodic glacial advances and progradation of the
839 shelf edge, especially during the Pliocene (K. Gohl, Denk, et al., 2013; Karsten Gohl et al., 2021; K. Gohl,
840 Uenzelmann-Neben, et al., 2013).

841 3.2.4 South Shetland and South Orkney Shelf

842 At the northern Antarctic Peninsula, the Pacific margin of Antarctica changes from a passive margin to a
843 convergent margin with the former Phoenix Plate (Antarctic Plate) descending under the South Shetland
844 Islands. The main features of this margin are the South Shetland Trench and the active spreading center in
845 Bransfield Strait behind, both associated with ongoing basin-forming processes. At the South Shetland
846 Trench, the margin preserves a thick accretionary complex and fore-arc system imposed on the older
847 continental shelf (Maldonado et al., 1994). These sediments were predominantly accumulated during
848 subduction of the former Phoenix Plate, which ceased between 3.6-2.6 Ma, but also preserve evidence of
849 younger deformation suggesting ongoing thrust faulting (Maldonado et al., 1994). Since ca. 4 Ma, the
850 Bransfield Basin is actively subsiding through rifting with segmented depocenters up to 2 km thick, and with
851 active volcanism and seismicity (Almendros et al., 2020).

852 On the opposite side of the Antarctic Peninsula shelf, the Powell Basin records rifting of the South Orkney
853 microcontinent from the Antarctic Peninsula, with rifting commencing in the late Eocene or early Oligocene,
854 progressing to seafloor spreading from ca. 30 to ca. 20 Ma (Eagles & Livermore, 2002). The adjacent Jane
855 Basin opened in a back-arc setting from ca. 18 to ca. 14 Ma (Bohoyo et al., 2002). Across these basins,
856 sediments are deposited in several sequences including syn- to post-rift packages initially in individual
857 depocenters, transitioning to a broader shared sequence since the mid-Miocene (Lindeque et al., 2013;
858 Maldonado et al., 2006).

859 3.2.5 Antarctic Peninsula and Weddell Sea

860 The Antarctic Peninsula and the Weddell Sea record the evolution of the Weddell Sea Rift with a partly
861 shared basin evolution in the Mesozoic to Cenozoic. The oldest sedimentary rocks on the Antarctic Peninsula
862 are preserved in the Trinity Peninsula Group, outcropping on the northern Antarctic Peninsula. These rocks

863 comprise an upper Carboniferous to Triassic sequence that formed on the margin of Gondwana in
864 association with erosion of continental magmatic-arc material (P. Castillo et al., 2015). The Triassic LeMay
865 Group outcropping on Alexander Island was deposited in a fore-arc accretionary complex coincident with
866 ongoing Triassic arc-magmatism in the southern Antarctic Peninsula (Willan, 2003). The Late Jurassic to Early
867 Cretaceous Fossil Bluff Group represents a thick sequence of fore-arc deposits derived from adjacent
868 magmatic arcs (Riley et al., 2012). Considering their current setting, all these basins are classed as Type 2
869 basins.

870 The Jurassic-Cretaceous Latady Group outcrops on the southeastern Antarctic Peninsula, representing the
871 formation of a progressively deepening basin from 185 to 140 Ma, with several kilometers of sediment
872 deposited (M. A. Hunter & Cantrill, 2006). Early Jurassic to early-Middle Jurassic terrestrial to shallow-marine
873 formations occupy smaller depocenters in grabens or half-grabens, with a transition to a deep-marine
874 environment from the late-Middle Jurassic onwards associated with Weddell Sea rifting (M. A. Hunter &
875 Cantrill, 2006). More sparse outcrops of similarly-aged rocks are found to the north in the Larsen Basin.
876 Although a distinct depocenter, the Larsen Basin preserves a similar evolution from a terrestrial to shallow-
877 marine syn-rift setting in the Early to Middle Jurassic, transitioning to a deep-marine setting from the Late
878 Jurassic (Hathway, 2000). The northern Antarctic Peninsula preserves key upper Mesozoic to lower Cenozoic
879 sequences exposed in the James Ross Basin. These sequences preserve a critical record of the high-latitude
880 paleoenvironment at the Cretaceous-Tertiary boundary and also support a better knowledge of
881 paleogeography of Antarctica (Bowman et al., 2016; Francis et al., 2006).

882 The formation of the Weddell Sea Rift System is interpreted to commence in line with the above transition
883 from a magmatic-arc setting to back-arc extension at 180-177 Ma (Riley et al., 2020), with the onset of
884 seafloor spreading by 147 Ma (König & Jokat, 2006). The Weddell Sea contains the thickest known
885 sedimentary basin in Antarctica (Fig 6), with up to 15 km of sedimentary rocks (Leitchenkov & Kudryavtzev,
886 1997; Straume et al., 2019). T. A. Jordan et al. (2017) defined distinct northern and southern provinces from
887 magnetic fabrics, indicating two distinct phases of rifting: in the south, east-west extension is interpreted
888 due to the motion, and possibly rotation, of the Ellsworth-Whitmore and Haag blocks from a position
889 adjacent to the East Antarctic margin, north of the Pensacola Mountains. Movement of the Haag/Ellsworth-
890 Whitmore microcontinent likely ceased by ca. 175 Ma, based on the ages of granites emplaced along the
891 marginal Pagano Shear Zone (Jordan, Ferraccioli, Ross, et al., 2013). Modelling of Bouguer gravity anomalies
892 has resolved highly-thinned continental crust with a bowl-shaped basin geometry beneath the Ronne-
893 Filchner Ice Shelf (T. A. Jordan et al., 2017; Leitchenkov & Kudryavtzev, 1997). Distinct positive Bouguer
894 gravity anomalies occur around the margins of the Ronne-Filchner Ice Shelf (Fig 2e), including the Weddell
895 Rift Anomaly, Filchner Rift and Evans-Rutford Rift Basin. The tectonic significance of these anomalies is not
896 clear and they may represent crustal thinning, but with less thick sedimentary fill than is seen in the central

897 basin, or they may reflect regional isostatic compensation of sedimentary loads deposited after rifting when
898 the crust had regained its strength, as suggested in the Ross Sea (Karner et al., 2005).

899 After development of the Southern Weddell Sea Rift System, continental rifting between Southern Africa
900 and Antarctica became the dominant tectonic process (König & Jokat, 2006) forming the Northern Weddell
901 Sea Rift System. The northern province possesses a NE-SW magnetic fabric, and potentially oceanic to
902 transitional crust (Jordan et al., 2020). This phase of extension appears to crosscut the older back-arc system
903 (T. A. Jordan et al., 2017) and is associated with magmatism giving rise to the Orion and Explora magnetic
904 anomalies (Fig. 9). These magnetic anomalies approximately coincide with the continent-ocean transition,
905 and they may reflect seaward-dipping reflector sequences (Kristoffersen et al., 2014), potentially emplaced
906 ca. 150-138 Ma (König & Jokat, 2006). The onset-age of northern Weddell Sea rifting is not uniquely defined:
907 in one model, onset of extension is suggested by 167 Ma with ocean-crust forming by 147 Ma (König &
908 Jokat, 2006), but an alternative model suggests the Northern Weddell Sea Rift reflects separation of a single
909 Skytrain Plate from Southern Africa and the Falkland Plateau between 180 and 156 Ma, followed by 90
910 degree rotation of the entire Skytrain Plate into its current position by ca. 126 Ma (Eagles & Eisermann,
911 2020).

912 Regardless of the tectonic model, interpreted sedimentary-rock thicknesses and gravity anomalies are
913 continuous throughout the central part of the Weddell Embayment. This suggests that most of the
914 sedimentary fill was deposited after tectonic motions ceased, likely due to thermal subsidence associated
915 with ongoing slow spreading at the margin. The oldest sedimentary horizons were deposited over the
916 seaward-dipping reflectors and the oceanic crust from ca. 160 to 145 Ma, with ongoing deposition
917 continuing until at least ca. 114 Ma in the southeastern Weddell Sea (Rogenhagen et al., 2004). Progressively
918 younger deposition proceeded toward the northwest, in line with the generation of oceanic crust and its
919 subsidence (Lindeque et al., 2013). The youngest sediments of the pre-glacial regime may be as young as
920 mid-Miocene, with deposition controlled by the proto-Weddell gyre (Lindeque et al., 2013).

921 Glacial influences on the northern Weddell Sea are substantial, with major sedimentary packages deposited
922 associated with the transition to glacial conditions, in the Oligocene (in the southeast) to early Miocene (in
923 the northwest), and to full glacial conditions in the mid-Miocene (Lindeque et al., 2013). Substantial shelf
924 progradation has occurred since the late Miocene (Katharina Hochmuth & Gohl, 2019). The youngest cover
925 relates to Quaternary sediments recovered in marine sediment cores which preserve normally consolidated,
926 over-compacted sediments and glacial till (Hillenbrand et al., 2014) as well as glacio-marine landforms in
927 seabed topography (Arndt et al., 2017). The distribution of these young units is not comprehensively
928 mapped, and their thickness and age are likely to be highly variable. Nevertheless, we infer that the Weddell
929 Sea has received sediment continuously since the Early Jurassic. To the south of the Ronne-Filchner Ice Shelf,
930 accumulations of water-saturated sediments are identified beneath the Bungenstock Ice Rise and extending

931 into the Institute Ice Stream (M. J. Siegert et al., 2016). These sedimentary deposits overlie a relatively
932 shallow basement but are associated with elevated ice velocity suggesting their potential to control ice-
933 sheet dynamics (M. J. Siegert et al., 2016).

934 3.3 East Antarctic Basins

935 3.3.1 Weddell Coast

936 The continental shelf in the eastern Weddell Sea preserves a sedimentary basin extending along the shelf
937 from the Filchner Rift to the Fimbul Ice Shelf. The basin is associated with a volcanic rifted margin that
938 initiated in the Jurassic (Jokat & Herter, 2016; Kristoffersen et al., 2014), but also has upper Cenozoic to
939 Quaternary sediment deposition recording repeated glacial advances (Hillenbrand et al., 2014; Huang &
940 Jokat, 2016; Kristoffersen et al., 2014). Magnetic data indicate the geology of the underlying basement with
941 high frequency content indicating relatively thin basin cover throughout this basin. Magnetic data also image
942 the Explora anomaly (Fig 9), associated with Jurassic magmatism (R. J. Hunter et al., 1996) and a seaward-
943 dipping reflector sequence, the Explora Wedge (Kristoffersen et al., 2014). Seismic exploration on the
944 Ekström Ice Shelf has demonstrated the Explora Wedge to extend beneath the ice shelf, with overlying
945 sedimentary rocks of up to 1 km thickness (Kristoffersen et al., 2014). The boundary is marked by a
946 prominent magnetic gradient that extends along the entire basin, which we infer to delineate the extent of
947 the seaward-dipping reflector sequence. Landward from this magnetic boundary, the basin is characterized
948 by smooth topography with several ice rises interpreted as representing grounded ice on remnants of shelf
949 sediments while adjacent troughs were eroded (Kristoffersen et al., 2014).

950 Inland, as well as extensive crystalline bed, several phases of basin formation are recorded. The oldest phase
951 is preserved in outcrops in the Pensacola Mountains (Fig 9). The early Cambrian Hannah Ridge Formation
952 was deposited after 563 Ma and prior to granite intrusion dated at 505 Ma (Curtis et al., 2004). The Hannah
953 Ridge Formation is overlain by the Nelson Limestone and the Gambacorta Formation volcanics, dated at 501
954 Ma. Overlying these, the Late Cambrian Wiens Formation and Late Cambrian to Ordovician Neptune Group
955 were deposited during and after the Ross Orogeny (Curtis et al., 2004). Similar rocks may also be preserved
956 in the Argentina and Shackleton Ranges (K. R. Evans et al., 2018). The second major phase comprises the
957 Devonian to Permian Beacon Supergroup, including the Upper Devonian Dover Sandstone, the
958 Carboniferous-Permian Gale Mudstone and the Permian Pecora Formation (Curtis, 2002). As elsewhere, the
959 Beacon Supergroup is preserved with characteristic mesa-like landforms in the Polar Gap Subglacial
960 Highlands (G. J. G. Paxman et al., 2019) between Support Force and Recovery glaciers (Fig 9). Outliers of the
961 Beacon Supergroup also occur on the Theron Mountains north of Slessor Glacier (Cox et al., 2023). There is
962 no evidence for Beacon Supergroup to the north of the Theron Mountains, although the Paleozoic rocks of
963 the Urfjell Group and Amelang Formation outcrop in western Dronning Maud Land (Cox et al., 2023).

964 Several Type 1 basins are inferred, with a dominant westerly trend, and characterized by low topography,
965 negative isostatic residual gravity anomalies and smooth beds. Major basins exist to the northeast and to the
966 south of the Polar Gap Subglacial Highlands extending to the Recovery Subglacial Highlands (Fig 9). The
967 southern basin, the Pensacola-Pole Basin, occupies an elongate trough 150-200 km wide. Sedimentary rocks
968 in this basin thicken inland reaching a thickness of 3.6 ± 1.1 km (G. J. G. Paxman et al., 2019). The basin fill is
969 interpreted to be dominated by the Beacon Supergroup, indicated by the presence of magnetic features
970 interpreted to represent Jurassic dolerites, but also there is interpreted younger cover of up to 1 km
971 thickness (G. J. G. Paxman et al., 2019). We define the Foundation Basin as a smaller aligned depocenter with
972 similar characteristics. The northern Recovery Basin occurs inland from Recovery Glacier. No thickness for
973 this basin is defined, but its geophysical character is similar to the Pensacola-Pole basin. We suggest that the
974 topography and morphology of the Foundation, Pensacola-Pole and Recovery subglacial sedimentary basins
975 formed during Jurassic-Cretaceous rifting. The topographic basins were later incised by glaciers, removing
976 several kilometers of sediments from glacier troughs (G. J. G. Paxman et al., 2017). These troughs do not
977 host major basin fill today. To the north, another major basin is interpreted associated with the Slessor
978 Glacier (Shepherd et al., 2006). This basin (Fig 9) has a particularly smooth bed throughout (Bamber et al.,
979 2006; Eisen et al., 2020) and models of magnetic data suggest 3 km of post-Jurassic fill (Bamber et al., 2006).

980 3.3.2 Dronning Maud Land and Enderby Land

981 Dronning Maud Land preserves evidence for a series of basin-forming events. The most prominent is the
982 Jurassic rifting associated with the Jutul-Penck Graben system, associated with localized crustal thinning
983 associated with the Jutulstraumen and Pencksokket troughs, with high isostatic residual gravity, and smooth
984 magnetic-field patterns (F. Ferraccioli, Jones, Curtis, & Leat, 2005; F. Ferraccioli, Jones, Curtis, Leat, et al.,
985 2005; Riedel et al., 2013). Interpreted Type 1 basins in the interior Dronning Maud Land region (Fig 9) are
986 parallel and may also represent this event.

987 Sedimentary rocks of the ca. 1.1 Ga Ritscherflya Supergroup are exposed adjacent to Jutulstraumen,
988 representing a ca. 2 km thick basin forming on the eastern edge of the Grunehogna Craton, in an interpreted
989 arc-proximal setting (Marschall et al., 2013). A series of north-south oriented Type 2 basins is interpreted in
990 interior Dronning Maud Land based on negative isostatic residual gravity and reduced subglacial roughness
991 relative to their surroundings (Fig 3). One of these was modelled in the work of Eagles et al. (2018) who
992 identified a sedimentary bed incised by a preserved fluvial landscape. The age of these basins is highly
993 uncertain, although they overlie magnetic trends of the Tonian Ocean Arc Super Terrane (Ruppel et al.,
994 2018), and are aligned with interpreted late Pan-African structures in the Sør Rondane region (Mieth &
995 Jokat, 2014).

996 The Dronning Maud Land Escarpment (Eagles et al., 2018) separates the basins of the interior from
997 interpreted Type 1 basins along the coastal plain and continental shelf (Fig 9). The coastal escarpment basin

998 is characterized by low, flat and smooth bed topography, sloping gently southward overall (Eisen et al., 2020)
999 and, onshore, negative isostatic residual gravity. Numerous ice rises are present associated with sedimentary
1000 banks, interpreted as remnant shelf sediments following erosion of the adjacent troughs. These basins are
1001 interpreted to reflect depocenters formed initially during the late Jurassic to Cretaceous denudation of the
1002 escarpment, and received sediment as part of the sedimentary pathway to the major depocenters of the
1003 Riiser-Larsen Sea (Eagles et al., 2018). Further regions along the front of the escarpment, and in localized
1004 topographic lows, also have relatively high basin likelihood (Li et al., 2022), and may represent piedmont
1005 deposits.

1006 The Ragnhild Trough (Fig 10) is a major topographic feature cutting through the Dronning Maud Land
1007 Escarpment. Its coastal portion is interpreted to possess a fill of low-density sedimentary material (Eagles et
1008 al., 2018), and is topographically smooth (Eisen et al., 2020) and is included here in the escarpment basin.
1009 Inland, the trough forms two ca. 100 km wide sub-troughs either side of Belgica Highlands (Belgicafjella),
1010 respectively called West and Central Ragnhild Troughs, with low gravity, low to moderate topographic
1011 roughness and low magnetic roughness. To the east is the crystalline bed of the Queen Fabiola Mountains
1012 block. These linear troughs are interpreted as rifts forming during Paleozoic to Mesozoic rifting. Similar
1013 troughs are interpreted in Enderby Land, connecting to the west branch of the Lambert Rift System (Fig 10).

1014 The continental shelf fringing the Cosmonauts Sea is narrow, at ca. 70 km width (Davis et al., 2018). Two
1015 separate depocenters are defined with the western depocenter having less rugged topography and lower
1016 sediment volume relative to the eastern depocenter (Davis et al., 2018). Seismic data over the shelf edge
1017 image a relatively thin package (0.5 to 2 km) of pre- to syn-rift sediments, with a more voluminous post-rift
1018 sequence (Stagg et al., 2004). While sedimentation on the shelf may be relatively limited, a substantial
1019 sediment volume was transported to the continental rise since the late Miocene (K. Hochmuth et al., 2020).

1020 3.3.3 Lambert Graben and Prydz Bay

1021 Mac. Robertson Land is dominated by crystalline basement, with basins associated with the Lambert Rift
1022 System. The Lambert Rift System has a cruciform geometry, with the north-south-aligned main branch
1023 extending inland for over 1500 km, complemented by eastern and western branches (Fig 10). Subsidence is
1024 greatest in the northern portion of the main branch, with more limited subsidence to the south, suggesting
1025 that the eastern and western branches may have accommodated differential strain. Smaller aligned basins
1026 are found in Mac. Robertson Land, including the exposed Beaver Lake Basin. The Beaver Lake Basin
1027 preserves the mid-Permian to upper-Triassic Amery Group, comprising clastic sedimentary rocks, with coals
1028 in the lower sequence (McLoughlin & Drinnan, 1997). These rocks represent a terrestrial depositional setting
1029 with overall north-directed sediment transport. Seismic studies on the Amery Ice Shelf resolve multiple
1030 layers of sedimentary rocks, with a thin layer of young sediments overlying an older package of interpreted
1031 glaciomarine origin (McMahon & Lackie, 2006). In turn this overlies a > 5 km-thick sequence of rift-related

1032 sedimentary rocks (Mishra et al., 1999). Cenozoic glaciomarine fjordal sedimentary rocks are mapped from
1033 within the Lambert Graben, indicating a series of glacial-retreat events since the Oligocene or younger, and
1034 also significant Cenozoic uplift, with exposures preserved at up to 1500 m elevation (Hambrey & McKelvey,
1035 2000).

1036 Inland, the southern branch of the Lambert Rift System occupies the trough to the Mellor Glacier, while the
1037 eastern branch occupies the trough to the Lambert Glacier, and the western branch occupies the catchment
1038 of the Fisher Glacier (F. Ferraccioli et al., 2011). Each has characteristics of low isostatic residual gravity
1039 anomalies and smooth topography. The southern branch has several further depocenters indicated
1040 upstream (Fig 10).

1041 Offshore, the Prydz Bay Basin is well-surveyed with relatively dense seismic coverage and multiple drill cores
1042 (Fig 1). The inner shelf is dominated by thick accumulations of Permian to Early Cretaceous sediments, with a
1043 thin veneer of Cenozoic cover (Stagg et al., 2004). On the outer shelf a sequence is recorded prograding
1044 toward the northeast through the Cenozoic, marked by several erosion surfaces and marine deposition
1045 events (Whitehead et al., 2006). Quaternary deposition is inferred to be present throughout the region
1046 (Whitehead et al., 2006). The Mac. Robertson Shelf preserves a relatively thin cover of syn- to post-rift
1047 sedimentary rocks (Stagg et al., 2004), with a comparable Cenozoic sequence to the Prydz Bay Basin
1048 (Whitehead et al., 2006).

1049 3.3.4 Princess Elizabeth Land and Queen Mary Land

1050 The continental shelf offshore from Princess Elizabeth Land preserves a thin cover of upper Paleozoic to
1051 Cenozoic sedimentary rocks (Davis et al., 2018), with interpreted Precambrian basement at Drygalski Island
1052 (Fig 11), and, at Gaussberg, a volcano dated at 56 ± 5 ka (Smellie & Collerson, 2021). Inland, the Princess
1053 Elizabeth Land region is dominated by crystalline basement, but several regions are identified with subdued
1054 magnetic responses and relatively smooth topography that may represent remnant sedimentary basins.
1055 These are arrayed along the tectonic structure of the Gaussberg Rift, which may share an evolution with the
1056 Lambert Rift system (D. A. Golynsky & Golynsky, 2007). A large basin (the Wilhelm II Basin) is identified with
1057 similar characteristics to the better-known Knox Basin further east (Fig 11). The interior of Princess Elizabeth
1058 Land, until recently, had one of the largest data gaps in Antarctica (Cui et al., 2020). Early work identified a
1059 significant lake (Lake Snow Eagle) and associated canyon system (Stewart S.R. Jamieson et al., 2016) likely
1060 aligned with tectonic structures (Fig 10). More recent subglacial topography (Cui et al., 2020) identified a
1061 topographic depression that is aligned en-echelon with the Wilhelm II Basin and Lake Snow Eagle (Fig 10).
1062 We infer a sedimentary basin in this depression although other geophysical results are not yet available for
1063 corroboration.

1064 Queen Mary Land has the well-resolved and substantial Knox Rift system including several sedimentary
1065 depocenters aligned perpendicular to the coast sedimentary (Maritati et al., 2016). The basin system may
1066 extend over 1000 km inland (Fig 11). This basin possesses up to 3 km of sedimentary-rock fill that is
1067 interpreted to date primarily to the Permian-Triassic (Maritati et al., 2016; Maritati et al., 2020). The region
1068 also preserves the Neoproterozoic to Ediacaran Sandow Group, exposed at the fringes of the Knox Basin
1069 (Mikhalsky et al., 2020). The coastal region is dominated by Precambrian crystalline basement, including
1070 beneath the Shackleton Ice Shelf, with moderate to thin sedimentary cover interpreted for the Bruce Rise
1071 and the Knox Coast shelf. The Knox coastal plain preserves a low-relief surface (Eisen et al., 2020) potentially
1072 indicative of a thin and relatively young sedimentary cover.

1073 3.3.5 Vostok and Gamburtsev Highlands

1074 The East Antarctic interior is defined by the subglacial highlands of the Vostok and Gamburtsev regions (Fig
1075 11). Subglacial Lake Vostok has been investigated with seismic techniques that return equivocal results (M.
1076 Siegert et al., 2011). Receiver-function studies recorded a low-velocity zone beneath the lake bed,
1077 interpreted to represent a 4-5 km thickness of sedimentary rocks above a crystalline bed (Isanina et al.,
1078 2009). However, later seismic-refraction experiments suggested that the lake bed is instead characterized by
1079 a relatively thin cover of sediments over an acoustically-fast basement, likely to be crystalline basement
1080 (Leitchenkov et al., 2016). The latter study resolved a lower-velocity bedrock for the highlands to the west of
1081 Lake Vostok. Lake Vostok and its western shore possesses predicted moderate to high sedimentary basin
1082 likelihood (Li et al., 2022), indicated by low isostatic residual gravity anomalies and smooth magnetic-field
1083 anomalies (Michael Studinger et al., 2003). These characteristics notably do not extend to the eastern shore.
1084 While a thick Type 1 sedimentary basin in Lake Vostok may not be supported, a Type 2 basin is interpreted
1085 extending along the Vostok Subglacial Highland to the west of and beneath Lake Vostok (Fig 11). This may
1086 represent a flexural basin formed in response to collisional processes in the Neoproterozoic (Michael
1087 Studinger et al., 2003).

1088 The Vostok Highlands are separated from the Gamburtsev Subglacial Mountains (GSM) by a prominent low-
1089 lying region with a relatively smooth bed, also including Lake Sovetskaya and Lake 90°E (Fig 11), forming the
1090 eastern branch of the East Antarctic Rift System (EARS) (F. Ferraccioli et al., 2011). This region is interpreted
1091 as a Type 1 sedimentary basin, although it is not associated with a gravity low, suggesting sedimentary fill is
1092 limited in thickness. The main range of the GSM is dominated by high-elevation topography, high along-track
1093 roughness, and high spatial variability in elevation and magnetic data (Fig 2), all indicative of crystalline
1094 basement. To the west, a broad area with low and smooth topography and low gravity separates the GSM
1095 from the Recovery Subglacial Highlands, suggesting a basin with substantial sedimentary fill, forming the
1096 western branch of the EARS (F. Ferraccioli et al., 2011). The southern flank of the GSM is also marked by a
1097 substantial gravity low, and relatively low roughness, indicating a possible sedimentary basin (Fig 3). The

1098 origin of this basin is not known, but it is aligned parallel to the South Pole Basin, and it may be an uplifted
1099 remnant of that basin or part of an older basin system (cf McLean et al., 2008).

1100 3.3.6 Wilkes Land and Terre Adelie

1101 Wilkes Land preserves an extensive sedimentary basin system including several major depocenters including
1102 the Aurora, Vincennes and Sabrina basins (A. R. A. Aitken et al., 2014). These basins are characterized by
1103 thick accumulations of sedimentary rocks, with as much as 10 km of fill possible in the Aurora Basin, but
1104 more typically ca. 5 km in Aurora, ca. 4 km in Vincennes and ca. 2 km in Sabrina Basin (A.R.A. Aitken et al.,
1105 2016; A. R. A. Aitken et al., 2014). The Aurora and Vincennes basins are characterized most fundamentally by
1106 low gravity, a very smooth surface, and subdued magnetic signals- this same characteristic defining the
1107 southward extension of the Aurora Basin (Fig 11). The Sabrina Basin has less smooth topography and more
1108 variable magnetic data, nevertheless, geophysical models suggest a preserved sedimentary basin of up to 3
1109 km thickness that has been variably eroded by ice-ice-sheet activity, exposing basement in places (A.R.A.
1110 Aitken et al., 2016). These inland basins are separated from the Sabrina Coast by a basement ridge, likely
1111 also a feature of glacial erosion.

1112 Tonian to Ediacaran sedimentary rocks have been found in glacial erratics from the Windmill Islands,
1113 indicating an early basin forming phase in this region with potential links to the Centralian Superbasin of
1114 Australia (Maritati et al., 2019). The region preserves several subglacial highlands that are interpreted in
1115 gravity models to be sedimentary in nature, including Highlands A, B and C, the region north of the Aurora
1116 Basin, and the Belgica Subglacial Highlands (A.R.A. Aitken et al., 2016). Thermochronology suggests that the
1117 highlands were uplifted and peneplained in the Permian-Triassic (Maritati et al., 2020), with the main phase
1118 of rifting at this time. Although the region was potentially reactivated during Jurassic-Cretaceous rifting
1119 events, to date, no evidence of this exists locally.

1120 Offshore, sedimentary sequences along the Australian-Antarctic margin define four major sequences
1121 separated by unconformities of age 95-80 Ma, 65-58 Ma, 50-45 Ma and 34 Ma (Sauermilch et al., 2019). The
1122 first sequence represents the rift-derived basin; the sequence is characterized by deltaic sediment
1123 deposition derived from continental river systems, while the third may derive from clockwise-circulating
1124 bottom currents developing in the Paleocene – Eocene with a decrease in sediment input (Sauermilch et al.,
1125 2019). The Sabrina Shelf sedimentary basin may have begun forming at this time, with a distinctive
1126 terrestrial palynoflora interpreted to date to the latest Paleocene to earliest Eocene (C. Smith et al., 2019).
1127 The Sabrina Shelf is covered by post-Cretaceous sedimentary cover with variable thickness up to 1.3 km
1128 seismically imaged (Gulick et al., 2017; Montelli et al., 2019). Paleocene to late-Miocene strata record a
1129 history of Cenozoic ice-sheet evolution including the identification of marine-terminating glaciers in the early
1130 to middle Eocene, a series of retreat and advance events in the Oligocene and Miocene, and an expanded
1131 East Antarctic Ice Sheet since the late Miocene (Gulick et al., 2017). The fourth offshore sequence represents

1132 the glacial development of the margin with, in particular, the deposition of a high volume of sediments since
1133 the Oligocene, including apparently variable supply from glacial outlets through time (K. Hochmuth et al.,
1134 2020; Katharina Hochmuth et al., 2022).

1135 The Terre Adelie Craton provides the eastern boundary to this basin region, with a basement-dominated
1136 ridge extending 1800 km inland from Porpoise Bay. Several smaller basins are identified within this ridge
1137 including the Frost, Astrolabe and Adventure subglacial troughs. Smooth beds (Eisen et al., 2020) and low
1138 gravity suggest these depressions host sedimentary basins, although their age is not known (A. R. A. Aitken
1139 et al., 2014; Frederick et al., 2016). Offshore Terre Adelie, seismic data record the transition from a
1140 deformed Cretaceous rift on the innermost shelf, through a Paleocene to Eocene transpressional phase,
1141 younging to Plio-Pleistocene strata at the shelf edge (De Santis et al., 2003), representing progradation of
1142 the shelf since the Eocene (Katharina Hochmuth & Gohl, 2019). Maximum observed sedimentary thickness is
1143 1.6 km (De Santis et al., 2003). The Mertz and Adelie banks are prominent bathymetric features representing
1144 remnant shelf-sediments, with adjacent basins incised by past glacial action (Beaman et al., 2011).

1145 3.3.7 Wilkes Subglacial Basin, South Pole Basin and Transantarctic Mountains

1146 The Beacon Supergroup is prominent along the Transantarctic Mountains (Fig 12) extending from northern
1147 Victoria Land, where outcrops are relatively sparse, to prominent and near-continuous exposures extending
1148 from David Glacier to the Ohio Range (Elliot et al., 2017). The Beacon Supergroup comprises the basal Taylor
1149 Group and the overlying Victoria Group. The Taylor Group consists of Devonian clastic sedimentary rocks,
1150 predominated by shallow-marine sediments grading to fluvial sediments (Bradshaw, 2013). The
1151 unconformably overlying Victoria Group and regional equivalents consist of Permian-Triassic siliciclastic and
1152 volcaniclastic rocks also including glacial deposits and coal beds (Elliot et al., 2017). Ongoing sedimentation
1153 into the Jurassic is identified from younger rocks exposed along the Transantarctic Mountains including the
1154 Section Peak Formation of northern Victoria land, the Mawson Formation of southern Victoria Land and the
1155 Hanson Formation in the central Transantarctic Mountains (Elliot et al., 2017). The sequence is overlain and
1156 intruded by mafic magmatic rocks of the Ferrar Group, often forming the caps to mesa-like exposures. In the
1157 context of their exposed extent the Beacon Supergroup are classed as Type 2 basins.

1158 Likely Beacon Supergroup correlatives are exposed at Horn Bluff, on the Wilkes Land coast, and magnetic-
1159 field anomalies consistent with Ferrar Group dolerite intrusions are found throughout the northern Wilkes
1160 Subglacial Basin (Fausto Ferraccioli et al., 2009). From these observations we may infer the Beacon
1161 Supergroup as the dominant sedimentary fill in the Wilkes Subglacial Basin. The Wilkes Subglacial Basin
1162 extends for 1600 km along the edge of the Terre Adelie Craton. The basin may be divided into a southern
1163 sub-basin, which consists of a single broad depocenter, with a substantial thickness of sedimentary rocks (ca.
1164 5 km) extending to 81°S, in line with Byrd Glacier (Frederick et al., 2016). Thinner cover extends southwards
1165 to roughly 84°S, in line with the southern end of the Miller Range. The northern sub-basin consists of three

1166 smaller depocenters and more variable sedimentary cover (Frederick et al., 2016). Magnetic analysis
1167 suggests possible rifting post-dating the intrusion of the Ferrar Group, and interpreted to be Cretaceous in
1168 age, possibly with Cenozoic reactivation (Fausto Ferraccioli et al., 2009; Jordan, Ferraccioli, Armadillo, et al.,
1169 2013). The discontinuity between these basin regimes (Fig 12) connects to David Glacier and is aligned with
1170 several right-lateral transcurrent faults in northern Victoria Land (Fausto Ferraccioli et al., 2009), that also
1171 influenced the Cenozoic evolution of the Ross Sea (Salvini et al., 1997). The Wilkes Subglacial Basin is
1172 continuous with a further subglacial sedimentary basin located near the South Pole (P. E. Wannamaker et al.,
1173 2004). The furthest extent of the South Pole Basin is aligned with a structural lineament extending from the
1174 South Pole through the Transantarctic Mountains near the Reedy Glacier (Fig 12).

1175 Several Neoproterozoic to early Paleozoic sedimentary packages occur along the Transantarctic Mountains.
1176 Ediacaran sedimentary rocks are preserved including the Berg Group (northern Victoria Land) and the
1177 Beardmore Group (central and southern Transantarctic Mountains). Metasedimentary units along the
1178 Transantarctic Mountains include the Rennick Schist and Priestley Formation (northern Victoria Land) and
1179 Skelton Group (southern Victoria Land) (John W. Goodge, 2020). Detrital zircon populations indicate these
1180 units were deposited after ca 1000 Ma, while Ross Orogeny metamorphism and granite intrusions provide a
1181 lower bound of 600 – 550 Ma; volcanic horizons in the Skelton Glacier area and Beardmore Group return
1182 compatible ages of 670-650 Ma Transantarctic Mountains (John W. Goodge, 2020). The Transantarctic
1183 Mountains also preserve extensive lower Paleozoic successions. These include in northern Victoria Land the
1184 Bowers Supergroup, comprising the Sledgers, Mariners and Leap Year Groups, exposed in the Bowers
1185 Terrane and the Robertson Bay Group exposed in the Robertson Bay Terrane. The Bowers Supergroup was
1186 deposited in a marine to terrestrial setting in the Cambrian, deposition beginning prior to 520 Ma and
1187 ceasing after 480 Ma (John W. Goodge, 2020). The Robertson Bay Group was deposited in a deep marine
1188 setting in the early Ordovician, after 490-465 Ma.

1189 The Transantarctic Mountains between David Glacier and Byrd Glacier does not preserve a comparable
1190 lower Paleozoic sequence, but south of Byrd Glacier the Cambrian-Ordovician Byrd Group is interpreted to
1191 extend to the Shackleton Glacier (John W. Goodge, 2020). The Byrd Group contains a lower sequence of
1192 carbonate rocks (Shackleton Limestone, 525-515 Ma) transitioning upwards to carbonate-clastics (Holyoake
1193 Formation) and then siliciclastic sedimentary rocks (Starshot Formation and Douglas Conglomerate, 515 –
1194 480 Ma). These are interpreted to represent the transition from a pre-Ross Orogeny carbonate platform to
1195 syn-orogenic molasse deposit Transantarctic Mountains (John W. Goodge, 2020). The southern
1196 Transantarctic Mountains, extending from the Queen Maud Range to the Wisconsin Range, preserve the
1197 lower Paleozoic siliciclastic LaGorce Formation and Duncan Formation. These formations contain detrital
1198 zircons dated at ca. 560-550 Ma, suggesting they were deposited in the early Cambrian and are intruded by

1199 hypabyssal volcanic rocks of the Liv Group dated at 526 Ma. The Liv Group preserves an early Cambrian
1200 lower sequence of silicic volcanics and a middle to late Cambrian upper sequence of bimodal volcanics.

1201 4 Tectonic architecture, basin formation and the paleolandscape of 1202 Antarctica

1203 Antarctica's sedimentary basins have developed in several key phases in accordance with the evolving plate-
1204 tectonic system. Early phases associated with Pre-Ediacaran tectonic events are well defined at the regional
1205 scale; however, their plate-tectonic setting remains in many cases cryptic with respect to the global plate
1206 system. The Type 1 basins recognized in this study have predominantly developed since the Ediacaran and
1207 we focus on these.

1208 4.1 Tectonic structure of Antarctica's lithosphere

1209 The development of sedimentary basins occurs in parallel with the development of the crust and the
1210 lithospheric mantle beneath. The structure of the crust and mantle have been investigated in a number of
1211 recent studies that reveal key features of relevance to understanding the basin distribution (An et al., 2015;
1212 Chaput et al., 2014; Hazzard et al., 2023; Lloyd et al., 2015; Lloyd et al., 2020; Pappa, Ebbing, & Ferraccioli,
1213 2019; Weisen Shen et al., 2017; W. Shen et al., 2018). Most critical to basin forming is the development of
1214 accommodation space due to tectonic subsidence. Most commonly, the thinning of the lithosphere under
1215 extension is the main driver of tectonic subsidence.

1216 Antarctica's crustal thickness (Fig 13a) reflects, to a large degree, the history of extension events that have
1217 occurred since Pangea times, and thinner crust is highly correlated with the presence of major basins,
1218 whereas basement-dominated regions tend to have substantially thicker crust. This is most notable in the
1219 Ross and Weddell regions where very thin crust (thickness < 15 km) is linked to the major basin systems in
1220 these regions. This relationship is not universal, with the southern Wilkes Basin and the Aurora Basin being
1221 underlain by thicker crust (thickness > 30 km), suggesting that subsidence for these basins potentially was
1222 not linked to intense crustal thinning. Type 2 basins often overlie thick crust including those in the Vostok
1223 Highlands, Transantarctic Mountains and Dronning Maud Land regions.

1224 In addition to effects on crustal thickness, lithospheric thinning may lead to the upwelling of asthenospheric
1225 mantle. Initially, a surface uplift is typical due to mantle heating, and then a prolonged post-rift thermal
1226 subsidence phase as the mantle cools over hundreds of millions of years. Lithospheric thickness (Fig 13b) is
1227 closely associated with the thermal state of the mantle, and areas of thin lithosphere are associated with
1228 recent to ongoing tectonic events. Thin lithosphere in West Antarctica is associated with the WARS, and
1229 recent higher-resolution models (Hazzard et al., 2023) suggest it may be less than 30 km thick in regions with
1230 recent volcanism including the Terror Rift, Marie Byrd Land, the Siple Coast and the Antarctic Peninsula.

1231 Thicker lithosphere is found through the Eastern Basin of the Ross Sea, central West Antarctica and
1232 Ellsworth-Whitmore and Haag regions. The Jurassic Weddell Sea Rift System has a lithosphere thickness of
1233 ca. 100 km.

1234 In central East Antarctica the thickest lithosphere, exceeding 200 km thickness, is centered on the Recovery
1235 Subglacial Highlands, the Gamburtsev Subglacial Mountains and the Vostok Highlands (Fig 13b). The effect of
1236 the East Antarctic Rift System on the lithosphere is not clearly delineated, although narrow rifts of ca. 100
1237 km width may be below the resolution of the seismic models for East Antarctica. The major basins of East
1238 Antarctica are not all clearly associated with thinned lithosphere and notably Aurora, Vincennes, South Pole
1239 and Southern Wilkes basins all overlie lithosphere exceeding 150 km thickness. The lack of basin-aligned
1240 thermal anomalies suggests that these basins are probably associated with rifting occurring prior to the
1241 Jurassic. The Lambert, Slessor Glacier and northern Wilkes basins are associated with thinner lithosphere,
1242 supporting a more recent (post-Triassic) rifting and thermal reactivation in those basins. Thinned lithosphere
1243 is observed around the East Antarctic margin including lithospheric embayments beneath northern Victoria
1244 Land, the southern Transantarctic Mountains, Dronning Maud Land, Enderby Land, the Sabrina Coast and
1245 Terre Adelie (Fig 13b).

1246 In rifting, crustal- and lithospheric-scale structures control the locus of deformation, and strongly influence
1247 the shape and internal structure of basins. Integrated lithospheric-scale structures were investigated by Stål
1248 et al. (2019), who analyzed bed topography, gravity, and seismic tomography models to delineate the major
1249 boundaries of the lithosphere (Fig 13c). We apply a multiscale edge-detection approach to the Bouguer
1250 gravity anomaly (Fig 13d). Phase-congruent multiscale edges (Kovesi, 1999) were delineated for 6 scales with
1251 upward-continued datasets at 20, 30, 40, 50, 60 and 80 km height. At each height, three sub-scales were
1252 analyzed for phase congruency using windows of 3, 6 and 12 times the height. Ultimately, the analysis
1253 resolves phase-congruent structures between 60 km and 960 km width, including finer-scaled structures
1254 than the integrated lithospheric analysis.

1255 Both analyses indicate major basin-bounding structures of the lithosphere including the WARS-bounding
1256 structures of the Transantarctic Mountains front and Bentley Subglacial Trough but also several more subtle
1257 basin-aligned features including in the Ross Sea, and along the Siple Coast, the Pine Island Rift and the Byrd
1258 Subglacial Basin (Fig 13c). The boundaries of the Weddell Sea Rift system are clearly defined including the
1259 boundary with Palmer Land (the Palmer Land Lineament) and the Filchner Trough (the Filchner Trough
1260 Lineament), again with several smaller structures associated with the internal structure of the basin. The
1261 gravity analysis defines additional lineaments associated with the Orion and Explora magnetic anomalies (Fig
1262 13d)

1263 In East Antarctica, the analyses delineate major basin-bounding structures including both the eastern and
1264 western edges of the northern Wilkes Subglacial Basin. The western boundary (the Wilkes Adelie Lineament)
1265 extends inland for at least 1200 km, while the eastern boundary (the Matusевич Glacier Lineament) is
1266 truncated against the Transantarctic Mountains front near David Glacier. Numerous cross-basin structures
1267 are seen including the division of northern and southern Wilkes Subglacial Basin, near David Glacier, the
1268 boundary with the South Pole Basin near Nimrod Glacier, and the truncation of the South Pole Basin near
1269 Reedy Glacier (Fig 13). Beyond, the Polar Gap Subglacial Highlands are bounded by lineaments associated
1270 with Support Force and Recovery Glaciers, and the final boundary of the Beacon Supergroup basin is seen
1271 aligned with Bailey Glacier. Beyond Bailey Glacier the north-south-oriented Coats Land lineament relates to
1272 basement structures, likely of Precambrian age, with a minor basin formed to its west.

1273 The Adventure Subglacial Trench is bounded to the west by a prominent north-south oriented lineament
1274 (the Adventure Trough Lineament) while a parallel structure to the west bounds the Belgica Subglacial
1275 Highlands from the Aurora Subglacial Basin (the Concordia Lineament). The southern boundary of the Aurora
1276 Subglacial Basin possesses a substantial gravity boundary, linked to a topographic boundary and truncation
1277 of magnetic trends (A. R. A. Aitken et al., 2014). This boundary is not associated with a lineament in either
1278 analysis (Fig 13) indicating a diffuse gradient that is not phase-congruent and may indicate a shallow-dipping
1279 structure. The northern edge of the Aurora Subglacial Basin is associated with a lineament (the Aurora
1280 Lineament) trending northwest-southeast towards the Knox Coast. The northwest-southeast lineament is
1281 disrupted by the north-south-trending Highland B Lineament and a similar structure to the west defines the
1282 eastern boundary of the Knox Subglacial Basin (the Knox Basin Lineament). The Lambert region has a
1283 complex structure including, in the analysis of Stål et al. (2019) the main north-south graben, although this is
1284 less obvious in the gravity analysis, and secondary east-west to northwest-southeast boundaries aligned with
1285 basins (Fig 13c). In the gravity-data analysis, additional northeast-southwest lineaments are identified
1286 aligned with the Ruker magnetic anomaly (the Ruker Lineament) and the Gamburtsev Suture representing
1287 structures in the Precambrian basement (F. Ferraccioli et al., 2011; McLean et al., 2009).

1288 At the largest scale, we can see in these analyses and models the division of East Antarctica into several
1289 major domains by prominent sets of lineaments along structural culminations, marked by dashed lines in
1290 Figure 13. The first lineament set is observed extending along the Terre Adelie Highlands, bounding the
1291 Wilkes Subglacial Basin from the Aurora Subglacial Basin region. This trend reflects fundamental boundaries
1292 in the geometry of the Mawson continent and its Neoproterozoic margin (A. R. A. Aitken et al., 2016; M.
1293 Studinger et al., 2004). The second lineament set extends from near Nimrod Glacier, along the Vostok
1294 Subglacial Highlands, where lineaments bound the Vostok Highlands Basin and Lake Vostok Basin, to the
1295 coast near the West Ice Shelf. A potential sub-set to the west extends along a similar trend transecting the
1296 Gamburtsev Subglacial Mountains, Princess Elizabeth Land and emerging into Prydz Bay. In part this trend

1297 may represent the East Antarctic Rift System (F. Ferraccioli et al., 2011) but also is aligned with a proposed
1298 fundamental lithospheric boundary associated with Neoproterozoic collision (Mulder et al., 2019; Michael
1299 Studinger et al., 2003). The third set of lineaments extends from Reedy Glacier, through South Pole,
1300 extending along the Recovery Subglacial Highlands, and then either side of the Fuji Subglacial Highlands, with
1301 branches emerging into Lutzow-Holm bay, the West Ragnhild Trough and possibly also Borchgrevinkisen. In
1302 its southern portion, this structure separates the South Pole Basin from the Pensacola-Pole Basin and is
1303 linked to the formation of the Pensacola Embayment, interpreted in the late Neoproterozoic (Jordan et al.,
1304 2022). To the north, the Fuji Subglacial Highlands culmination separates the basin-dominated regions to the
1305 west (Recovery, Slessor and interior Dronning Maud Land), and east (Lambert).

1306 These lineament sets represent fundamental structures of the Antarctic lithosphere dating to at least the
1307 Neoproterozoic, but their impact on later tectonics and basins is profound. In a Gondwana reconstruction,
1308 the Fuji Subglacial Highlands lineament trend is aligned with the eventual Africa-Madagascar-Sri Lanka triple
1309 junction, the Vostok Highlands lineament trend is aligned with the Kerguelen Plateau, and the Terre Adelle
1310 Highlands trend is linked to the George V fracture zone of Australian-Antarctic basin (Fig 14). The four
1311 domains of East Antarctica have clearly different basin systems with distinct geometries and structural
1312 trends, with broadly, the Pensacola-Recovery-Slessor rift system (G. J. G. Paxman et al., 2017; G. J. G.
1313 Paxman et al., 2019), the EARS (F. Ferraccioli et al., 2011), the Aurora-Vincennes-Sabrina system (A. R. A.
1314 Aitken et al., 2014), and the Wilkes Subglacial Basin system (Fausto Ferraccioli et al., 2009; Jordan,
1315 Ferraccioli, Armadillo, et al., 2013; Jordan et al., 2022).

1316 4.2 Basin forming phase 1- Ediacaran to Carboniferous

1317 During the Ediacaran to early Cambrian, a continuous East Antarctica was formed as part of Gondwana,
1318 assembled through the East-African (ca. 650 to ca. 550 Ma) and Kuunga (ca. 550 to ca. 490 Ma) orogens. The
1319 exact locations of the associated lithospheric boundaries beneath the ice sheet are not known well. Type 2
1320 basins in the continental interior potentially formed during these events, including in Dronning Maud Land,
1321 the Vostok Highlands, the Aurora/Sabrina region and the Knox region. In the same timeframe, the edge of
1322 East Antarctica was evolving as a passive margin (Jordan et al., 2022) with associated basin forming events
1323 (John W. Goodge, 2020). Ediacaran subduction was initiated along the paleo-Pacific margin of Gondwana.
1324 The onset of the Ross Orogeny, marked by metamorphism from 615 Ma and magmatism from 590- 565 Ma
1325 (John W. Goodge, 2020) and associated deformation events, saw a change in the locus and nature of basin
1326 formation towards the edge of the craton, with the orogeny ending ca. 470 Ma when the margin retreated
1327 (John W. Goodge, 2020).

1328 Cambrian to Ordovician sedimentary basins deposited along this margin are interpreted to have formed in
1329 association with arc-related magmatism of the Ross Orogeny, continuing into the post-tectonic phase. Basins

1330 typically include an Early to Middle Cambrian sequence of pre- to syn-orogenic units (e.g. Bowers
1331 Supergroup, Byrd Group, Hannah Ridge Formation, Heritage Group) and a Late Cambrian to Ordovician syn-
1332 to post-orogenic sequence (e.g. the Robertson Bay Group, the Swanson Formation, Neptune Group,
1333 Crashsite Group). Both the Ellsworth-Whitmore and western Marie Byrd Land blocks were probably adjacent
1334 to East Antarctica at this time (Jordan et al., 2020). Global tectonic reconstructions of this time period lack
1335 detail relative to those from the Devonian onwards, and for regional tectonic reconstructions of this time
1336 period the reader is referred to regional syntheses (e.g. Boger, 2011; John W. Goodge, 2020). Cambro-
1337 Ordovician basement exhumation occurred inland from the central Transantarctic Mountains region as
1338 recorded in low-temperature thermochronology data (Fitzgerald & Goodge, 2022).

1339 The Devonian is marked by the deposition of the lower Beacon Supergroup in an interpreted continental
1340 retro-arc setting within Gondwana (Bradshaw, 2013). This basin is exposed as Type 2 in the mountains from
1341 Northern Victoria Land to the Theron Mountains and is preserved as Type 1 in the subglacial hinterland. The
1342 distinction of Type 1 and Type 2 in this case is primarily a consequence of later uplift of the Transantarctic
1343 Mountains and potentially also downfaulting of the hinterland (Fausto Ferraccioli et al., 2009). We infer for
1344 the Devonian a single sedimentary basin system (the Beacon Basin) with low elevation throughout. The
1345 system was divided along-strike into distinct depocenters with up to nine major divisions along its length (Fig
1346 13). The internal divisions are marked by changing thickness and morphology of the Type 1 basins, while for
1347 Type 2 basins in the Transantarctic Mountains the variable extent of Beacon Supergroup exposures along-
1348 strike may represent initial thickness variations coupled with differential uplift in later events (Brenn et al.,
1349 2017; Weisen Shen et al., 2017; P. Wannamaker et al., 2017). Offsets to the basin margins and the uplifted
1350 parts are also seen (Fig 12). The end of this subsidence episode is not well constrained but must predate
1351 lower-Permian glaciogenic deposits that mark the onset of the second phase (Elliot et al., 2017).

1352 4.3 Basin forming phase 2- Permian to Triassic

1353 Following the amalgamation of Pangea at ca. 320 Ma, the Permian marked a distinct change in the tectonic
1354 setting of Antarctica. Permian-Triassic Antarctica saw ongoing subduction at the West Antarctic-
1355 Panthalassan margin, while the Tethyan margin was subjected to rifting from ca. 300 Ma to ca. 200 Ma
1356 (Müller et al., 2019; A. Young et al., 2019). During this period several microcontinents rifted at different
1357 times, but the main Cimmerian terranes separated from Pangea from 280 to 270 Ma (Fig 14a). The Antarctic
1358 Peninsula preserves arc-proximal sedimentary rocks from this period (P. Castillo et al., 2015), but the most
1359 extensive known sedimentary deposits are found along the Transantarctic Mountains, including exposures
1360 from Northern Victoria Land to the Shackleton Range (Elliot et al., 2017) which are all considered equivalents
1361 of the Victoria Group of the Beacon Supergroup. Similar rocks in the Ellsworth Mountains may also be
1362 stratigraphic correlatives, since relocated due to motion of the Ellsworth-Whitmore Block (T. A. Jordan et al.,
1363 2017) (Fig 14a). A continuation of Victoria Group equivalent sequences into the Wilkes Subglacial basin,

1364 South Pole Basin and Pensacola-Pole Basin is likely (Fausto Ferraccioli et al., 2009; G. J. G. Paxman et al.,
1365 2019; P. E. Wannamaker et al., 2004).

1366 Exhumation of the East Antarctic coast at least from Prydz Bay to George IV Land occurred between ca. 350
1367 and ca. 200 Ma, likely in response to Tethyan rifting (Lisker et al., 2007; Maritati et al., 2020; Tochilin et al.,
1368 2012) although influenced by glacial erosion (Rolland et al., 2019). This was accompanied by formation of
1369 several major basins including Lambert, Knox and Aurora basins (Maritati et al., 2020) and likely an extensive
1370 network of smaller basins within East Antarctica (Fig 14a). The Pangean landscape and basins persisted until
1371 the Early Jurassic Karoo-Ferrar LIP (183 Ma) when Gondwana breakup commenced.

1372 4.4 Basin forming phase 3 - Jurassic to Eocene

1373 The Jurassic to Eocene tectonic setting of Antarctica was dominated by the protracted and progressive
1374 fragmentation of Gondwana (Fig 14), which led to the formation of marginal basins and ultimately led to an
1375 isolated Antarctic continent. Rifting progressed in a 'clockwise' direction with first South America and Africa
1376 (from 177 Ma), India, Sri Lanka and Madagascar (from 135 Ma), Australia (from 100 Ma), and Zealandia
1377 (from 82 Ma). This process is relatively well recorded in the sedimentary basins of the Antarctic margin.

1378 Subsidence linked to Gondwana dispersal began in the Weddell Sea region ca. 180-177 Ma (Riley et al.,
1379 2020). The pre-cursor to continental breakup is thought to have been extensive magmatism and
1380 emplacement of the Karoo-Ferrar Large Igneous Province at ca. 183 Ma (Burgess et al., 2015). For the main
1381 Weddell Sea basins, one suite of models suggests a two-stage development with Early Jurassic motion of the
1382 Haag-Ellsworth-Whitmore microcontinent that led to the development of the Southern Weddell Sea Rift
1383 System (T. A. Jordan et al., 2017), including rifting at the margins of the Weddell Sea (Evans-Rutford Basin
1384 and Filchner Trough). Subsequently, rifting occurred in the Northern Weddell Sea Rift Basin and the Riiser-
1385 Larsen Sea, beginning associated with breakup between Southern Africa and Antarctica before ca. 167 Ma
1386 (König & Jokat, 2006). The Weddell and Riiser-Larsen seas continued to open together, with associated basin
1387 formation offshore, until 126 Ma after which time Atlantic Ocean (Fig 14b) opening led to separate
1388 kinematics for these regions (König & Jokat, 2006). In East Antarctica, the Jutul-Penck Graben system (F.
1389 Ferraccioli, Jones, Curtis, Leat, et al., 2005; Riedel et al., 2012) and the Slessor Glacier Basin experienced
1390 Jurassic to early Cretaceous extension in line with the departure of Africa and South America (Fig 14b). The
1391 thermal history of the Shackleton Range suggests a heating episode between 180 – 135 Ma indicating
1392 possible sedimentary burial during this time, before rapid cooling at ca 130 Ma (Krohne et al., 2016).

1393 An alternative tectonic model for the Weddell Sea region suggests that the entire Weddell Sea Rift System is
1394 part of a single larger Skytrain tectonic plate, including much of the central and southern Antarctic Peninsula
1395 Plate (Eagles & Eisermann, 2020). In this model the Northern Weddell Sea Rift reflects separation of the
1396 Skytrain Plate from Southern Africa and the Falkland Plateau between 180 and 156 Ma, followed by 90°

1397 counterclockwise rotation of the entire Skytrain Plate into its current position by ca. 126 Ma (Eagles &
1398 Eisermann, 2020). In contrast with the previous model this model does not include Jurassic opening of the
1399 southern Weddell Sea, and the plate motion implies 200-400 km of shortening between the Skytrain Plate
1400 and East Antarctica during the Cretaceous.

1401 Rifting of Madagascar and greater India from Antarctica had commenced by the early Cretaceous with
1402 oceanic crust forming in the Enderby Basin from 133 Ma (Jokat et al., 2021). This process may have involved
1403 an initial separation between East Antarctica and the Elan Bank and Southern Kerguelen Plateau, with by ca.
1404 115 Ma a ridge-jump to north of the Elan Bank associated with the Kerguelen Plume (Gaina et al., 2007;
1405 Gibbons et al., 2013), although an entirely pre-Kerguelen evolution is possible (Jokat et al., 2021). From 120
1406 Ma, igneous rocks from the Kerguelen Plume formed much of the Southern Kerguelen Plateau and also are
1407 prominent in the basins of Enderby and Davis Seas (Davis et al., 2018). The potential effects of the rifting of
1408 greater India on East Antarctica's landscape and onshore basins remains ill-defined. Limited
1409 thermochronology detects early Cretaceous cooling in the Lambert region (Lisker et al., 2007), linked to
1410 brittle deformation structures (Phillips & Läufer, 2009), although later studies propose an igneous origin for
1411 thermal resetting (Tochilin et al., 2012), while the Shackleton range experienced rapid cooling at ca 130 Ma
1412 (Krohne et al., 2016).

1413 The geometry of the Lambert Rift is characteristic of two distinct structural orientations that dominate this
1414 sector of East Antarctica: one is aligned parallel to the early-spreading isochrons in the Cosmonauts Sea
1415 margin, and the other is aligned to the early-spreading isochrons of the Enderby Basin (Fig 14b). These
1416 structural orientations may be associated with much older events, and reactivation may have occurred in
1417 response to events associated with the opening of the Enderby Basin (130 – 115 Ma (Gibbons et al., 2013))
1418 and the Cosmonauts Sea (<120 Ma (Jokat et al., 2010)), either separately, or due to strain-partitioning
1419 associated with contemporaneous rifting.

1420 The impact of greater India rifting on the margin of Western Australia, at the time contiguous with East
1421 Antarctica, is more well defined, and may form a key template to understand East Antarctica. After the end
1422 of Permian-Triassic rifting, renewed subsidence of the Perth and Mentelle basins occurred from the mid-
1423 Jurassic to early Cretaceous, with the breakup phase associated with oblique northwest-southeast extension
1424 aligned with spreading in the Perth Abyssal Plain (Williams et al., 2013). Onshore structures for this period
1425 include dextral strike-slip on north-south oriented structures, en-echelon folding and sinistral motion on
1426 northwest-southeast transfer faults (Song & Cawood, 2000). The late Jurassic sedimentary fill of the
1427 Mentelle Basin suggests dominant detrital sources located in East Antarctica during this time, indicating
1428 active erosion of inland regions (Maritati et al., 2021). Following these a widespread Valanginian
1429 unconformity and eruption of the Bunbury Basalt at 137- 130 Ma (Olierook et al., 2016) mark breakup and

1430 widespread uplift. The Perth Basin is continuous with the Knox and Aurora subglacial basins, which are
1431 structurally similar (Fig 14b).

1432 In the mid-Cretaceous the oblique motion of Australia from Antarctica (Fig 14c) commenced at ca. 100 Ma,
1433 but this did not proceed to separation until 83 Ma (Williams et al., 2019). In contrast to Africa and India,
1434 Australia did not move away rapidly, with slow spreading persisting until ca. 45 Ma (Williams et al., 2019),
1435 and the Tasman Gateway was not opened until 33 Ma (Howie D. Scher et al., 2015). Spreading on this margin
1436 west of the George V fracture zone between 57-50 Ma may have been accommodated by sinistral
1437 transtension in East Antarctica and tectonic deepening of the Adventure and Astrolabe subglacial troughs
1438 (Eagles, 2019). The adjacent margins preserve the evolution of this post-rift system including, since the early
1439 Paleogene, a major influence from evolving glacial and oceanographic systems (De Santis et al., 2003; Escutia
1440 et al., 2005; K. Hochmuth et al., 2020; Sauermilch et al., 2019).

1441 Initial east-west extension in the Ross Sea is interpreted with a broad basin developing between 105 and 83
1442 Ma (Jordan et al., 2020). This phase of rifting in the Ross Sea is characterized by lower-crustal exhumation
1443 along low-angle detachment faults (Christine Smith Siddoway et al., 2004). Up to 100 km of diffuse extension
1444 may be accommodated on these shear zones (C.S. Siddoway, 2008), and this phase of extension is associated
1445 with crustal thinning and magmatism but not the development of major accommodation space (Lindeque,
1446 Gohl, Henrys, et al., 2016). The predominance of crustal thinning over basin development may have been a
1447 consequence of weak lower crust (Karner et al., 2005). This wide rift event has also been associated with a
1448 potential plateau collapse (Bialas et al., 2007). With separation of Zealandia at 83 Ma the translation of
1449 Marie Byrd Land trends towards the northwest and the rift system is interpreted to extend southward into
1450 the Siple Coast and Amundsen regions (Jordan et al., 2020), also evolving from a more diffuse wide-rift to a
1451 more focused narrow-rift mode, likely due to increasing rheological strength (Harry et al., 2018; Huerta &
1452 Harry, 2007). The opening of the Tasman Sea and Pacific-Antarctic Ridge from 83 Ma to 52 Ma
1453 accommodated the majority of the relative motion of Zealandia and the Pacific Plate relative to Antarctica
1454 (Gibbons et al., 2013). In the northern Ross Sea, opening of the Central Basin is interpreted between 61- 53
1455 Ma (Fred J. Davey et al., 2021). From 52 Ma, the opening of the Macquarie Ridge and Adare Basin is
1456 associated with translation and rotation of Marie Byrd Land and the Eastern Basin, initially to the northeast,
1457 and then to the east (Fig 14).

1458 4.5 Basin forming phase 4 – Eocene to Present

1459 Post mid-Eocene, plate-tectonic motions in Antarctica were restricted to a few key areas. The western Ross
1460 Sea was in extension with corresponding seafloor spreading in the Adare Basin from 43 to 26 Ma, and also
1461 extension in the Terror Rift (F. J. Davey et al., 2016; Granot & Dymant, 2018). Although the amount of
1462 extension was limited, the effects on the bathymetry of the continental shelf, and the association with

1463 volcanism, were important local drivers of basin evolution. Neogene rifting is interpreted to extend into the
1464 interior West Antarctica including the Bentley Subglacial Trough (Lloyd et al., 2015), Pine Island Rift (Jordan,
1465 Ferraccioli, Vaughan, et al., 2010), Byrd Subglacial Basin (W. Shen et al., 2018) and the Ferrigno Rift (Bingham
1466 et al., 2012). Tectonic subsidence through this period has occurred in the Ross, Siple Coast and Central West
1467 Antarctica regions (Fig 15) (Guy J. G. Paxman et al., 2019).

1468 Subduction of the Aluk Plate (part of the Phoenix Plate) progressively ceased from south to north over time,
1469 as the West Antarctic-Aluk Ridge moved north and ultimately ceased subduction in the Neogene (Burton-
1470 Johnson & Riley, 2015). The evolution of a more complex margin to the north occurred in line with complex
1471 tectonics of the Scotia Sea (van de Lagemaat et al., 2021). This included the opening of the Powell (30-20
1472 Ma) and Jane (18-14 Ma) basins in a back-arc setting, and the convergent South Shetland margin, comprising
1473 a fore-arc basin and accretionary prism (Maldonado et al., 1994), and since 4 Ma, rifting in the Bransfield
1474 Basin (Almendros et al., 2020). In the Eocene, tectonic processes occurring to the north of Antarctica
1475 remained important as the Drake Passage allowed throughflow by 42 Ma (H. D. Scher & Martin, 2006) and
1476 the Tasman Gateway by 33 Ma (Howie D. Scher et al., 2015). Through the Oligocene these gateways
1477 developed more fully (van de Lagemaat et al., 2021), allowing by the Miocene a fully-developed Antarctic
1478 Circumpolar Current.

1479 Despite these regional tectonic events, by far the major influence on Antarctica's basin-forming processes in
1480 this period was the glacial influence as the ice sheet developed, with many cycles of advance and retreat
1481 causing major unconformities, substantial onshore erosion (Guy J. G. Paxman et al., 2019) and fluctuating
1482 sediment volumes deposited around the margins (Katharina Hochmuth & Gohl, 2019; Pérez et al., 2021).
1483 Understanding the resulting landscape of eroded basement regions, post-glacial sedimentary basins and the
1484 geomorphological features from both tectonic and glacial processes is essential to constrain the past,
1485 present and future behavior of the Antarctic Ice Sheet.

1486 5 Implications for Antarctic Ice Sheet dynamics

1487 5.1 Basin-associated processes and their potential impact on the cryosphere

1488 Ice sheets and glaciers flow by three main mechanisms: internal ice deformation, basal sliding and
1489 deformation of basal material. The first of these is ubiquitous among ice masses, but the second and third
1490 are conditional on the presence of basal water. Furthermore, the third is dependent on the availability of
1491 deformable sediments at the bed. For water to exist beneath an ice sheet basal heat is needed: this can
1492 come from geothermal sources and, especially if ice flow is rapid, from basal motion and internal ice
1493 deformation. Thus, the dynamics of fast-flowing ice are dominated by basal-flow processes that allow speeds
1494 more than 50 m yr^{-1} , and often several 100 m yr^{-1} .

1495 The availability of subglacial water is essential to both basal sliding and sediment deformation. In addition to
1496 ice-sheet melting, for a permeable bed we must consider the potential for water to be exchanged between
1497 the ice-sheet/bed interface, any actively deforming till layer, and the strata beneath which may tap deep
1498 groundwater reserves (Gustafson et al., 2022). The role of groundwater in subglacial hydrological systems is
1499 important to ice flow for two main reasons. The first reason is that groundwater comprises a source of water
1500 in addition to that melted from ice. For example, Christoffersen et al. (2014) suggest groundwater may
1501 contribute up to half of the water available beneath ice streams in the Siple Coast. The second reason is that
1502 groundwater flow allows heat to be transported vertically and laterally through the subglacial system (Gooch
1503 et al., 2016; Kulesa et al., 2019) thus representing a governing mechanism of advective heat transport to
1504 the ice-sheet base.

1505 Hydraulic gradients in subglacial sedimentary basins vary over glacial cycles during the growth and decay of
1506 the ice sheet. This process has a positive feedback with ice sheet retreat and advance: as retreating ice
1507 sheets thin, unloading of the basin causes groundwater to be discharged into the subglacial system (Gooch
1508 et al., 2016; Li et al., 2022; Person et al., 2012). The opposite may occur when the ice sheet thickens,
1509 directing water away from the ice-sheet base and storing it in subglacial sedimentary basins (Gooch et al.,
1510 2016). In this manner, the groundwater system modulates interactions between basal water systems and
1511 the underlying sedimentary basins to exert control on the lubrication of the ice-sheet base and thus impact
1512 ice flow. Numerical modelling indicates that, even in situations of fast retreat, the rate of groundwater
1513 discharge can be of comparable magnitude to the expected basal-melt rate, and this feedback is likely to
1514 contribute substantially to ice-sheet dynamics (Li et al., 2022). Furthermore, past retreat and advance events
1515 can store 'fossil' hydraulic head in aquifers for later release (Gooch et al., 2016; Person et al., 2012).

1516 From what we understand from formerly-glaciated regions (D. J. A. Evans et al., 2006) and from geophysical
1517 observations of subglacial Antarctica (Alley et al., 2021; Anandakrishnan et al., 1998; Christianson et al.,
1518 2016; A. Muto, Alley, et al., 2019; M. J. Siegert et al., 2016; A. M. Smith, 1997; A. M. Smith et al., 2013), the
1519 deformation of basal material is a dominant process within major ice streams and, consequently, exerts
1520 control on ice-sheet flow. InSAR depiction of surface-ice-flow velocities (Mouginot et al., 2019) and
1521 geophysical measurements of the subglacial system (Anandakrishnan et al., 1998; Brisbourne et al., 2017;
1522 Christianson et al., 2016; A. Muto, Alley, et al., 2019; Atsuhiko Muto et al., 2016; L. E. Peters et al., 2006; A.
1523 M. Smith et al., 2013; David G. Vaughan et al., 2003) allow us to pinpoint the onset of enhanced ice flow and
1524 the basal boundary conditions that permit it: for example, the onset of Whillans Ice Stream coincides with
1525 the availability of sedimentary material identified through aerogeophysical (Bell et al., 1998) and seismic
1526 (Anandakrishnan et al., 1998) data. The mechanics of subglacial sediment are complex and time variable,
1527 with hydration and fluid overpressure in general leading to weaker rheology while compaction and de-
1528 watering lead to stiffer rheology. This sensitivity to water supply can lead to relatively abrupt changes in flow

1529 (Catania et al., 2012; Christoffersen et al., 2014; A. M. Smith et al., 2013). Meanwhile, sediment deposition in
1530 a grounding zone wedge and subsequent compaction associated with tidal loading may stabilize the
1531 grounding zone (Christianson et al., 2016). The deformation of the sediment commonly involves two layers:
1532 a relatively thin upper active zone, at most a few meters thick dilated by high-pressure water within pores
1533 that acts to reduce its material strength; and a thicker over-compacted basal unit that is stiffer and
1534 contributes little to flow (D. J. A. Evans et al., 2006).

1535 Basal sediments originate from two main sources: accumulations of marine sediments deposited during
1536 previous times of deglaciation, and from the erosion of bedrock either locally or upstream. Recent marine
1537 deposits are likely to be present at lower elevations and will often be widespread, prompting zones of more
1538 continuous bed deformation (D. J. A. Evans et al., 2006). Without recent marine sediments, sediment supply
1539 must be sustained through glacial erosion, and this may be a limiting factor on till continuity. Glacial erosion
1540 is accomplished through a variety of processes, and these are fundamentally reliant on heterogeneities in
1541 the bedrock, including joints, especially their spacing and orientation (Hooyer et al., 2012), and lithological
1542 variations including competency contrasts, layer thicknesses, and structural orientation relative to flow
1543 (Krabbendam & Glasser, 2011; Lane et al., 2015). In comparison to the competent and massive structure
1544 more typical of igneous and metamorphic basement, sedimentary rocks provide more opportunities for
1545 quarrying to occur, and a higher likelihood of abrasion where the rocks are less competent (Krabbendam &
1546 Glasser, 2011). Finally, to sustain a continuous till layer, sediments eroded upstream must be transported,
1547 which is predominantly achieved via the subglacial-hydrology system, which, depending on erosion rate and
1548 water flux, may be supply-limited or transport-capacity limited (Delaney et al., 2019).

1549 Both subglacial water and thin horizons of weak basal sediments may be present in areas of crystalline
1550 basement as well as in sedimentary-basin regions. Before considering basin settings, it is instructive to
1551 consider an ice-stream catchment with a structurally massive and impermeable bed throughout, such as a
1552 granite or gneiss bedrock. For such a bed we may consider as a priority the supply of basal water, which
1553 must be derived from basal melting and/or surface melting transported to the bed via fractures and moulins-
1554 (Schoof, 2010). The latter, while certainly important, depends on surface-melting conditions that, for now,
1555 are limited to certain coastal regions of Antarctica, although they may be more widespread in the future
1556 (Tuckett et al., 2019). For the former, a sustained high flow-speed and/or geothermal heat flux is needed.
1557 With an impermeable bed, geothermal heat flux for a given location will be near constant, and so temporal
1558 variations in basal-melt rate will depend solely on ice-stream flow processes. In addition to water, sediment
1559 must be supplied through erosion of the crystalline basement, which is likely to be highly resistant to erosion
1560 (Krabbendam & Glasser, 2011) potentially restricting supply. We may now consider how the presence of a
1561 sedimentary bed influences ice-sheet dynamics.

1562 Several factors associated with sedimentary-basin formation increase the likelihood that regions containing
1563 sedimentary basins will possess enhanced ice flow. These are: 1) a favorable source for sustained supply of
1564 sediment from more erodible bedrock and/or recent marine sediments (Bell et al., 1998); 2) the supply of
1565 subglacial water through groundwater discharge, tied to glacial unloading (Christoffersen et al., 2014; M. J.
1566 Siegert et al., 2018); 3) different organization of subglacial water systems including transitions between
1567 distributed and channelized flow, and flow routing between catchments (Christoffersen et al., 2014; Dustin
1568 M Schroeder et al., 2013); 4) the opportunity through groundwater circulation to advect heat from depth to
1569 the ice-sheet bed (Gooch et al., 2016). In addition, the tendency for basin-dominated regions to possess
1570 relatively smooth topography at all scales promotes ice-stream boundaries defined by ice-sheet dynamics,
1571 including basal processes (Catania et al., 2012). Finally, we may consider the effects of ongoing basin-
1572 forming processes on the morphology of ice-shelf cavities that are critical for ice-sheet stability (J. A. Smith
1573 et al., 2019).

1574 5.2 Antarctic sedimentary basins and ice sheet dynamics

1575 Although the specifics of when, where and how sedimentary basins have influenced ice-sheet dynamics in
1576 Antarctica remain to be defined, the mechanisms listed above are enhanced in catchments containing
1577 sedimentary basins. Consequently, we may consider if the presence of subglacial sedimentary basins within
1578 a glacial catchment is associated with more dynamic behaviour, and if this impact on ice-sheet dynamics may
1579 be expressed for the modern-day ice sheet.

1580 Sedimentary basins are an important modulating influence on geothermal heat flux (GHF) and can act either
1581 to inhibit or enhance surface GHF. In Antarctica, the overall statistical relationship with heat flux from deep-
1582 seated sources (Lösing & Ebbing, 2021) is almost null for Type 1 basins relative to crystalline basement,
1583 although Type 2 basins are systematically associated with lower GHF (small effect size). In West Antarctica,
1584 where heat flux is generally high, higher heat flux is found within basin regions (Fig 16a). These regions
1585 include the Siple Coast with highest high heat flux in the south, but less to the north. Extending from the
1586 Byrd Subglacial Basin to the Ferrigno Rift is an elevated high heat flux region, with concentrations beneath
1587 basins including the Byrd Subglacial Basin and the Pine Island Rift Basin. Tectonically-active regions including
1588 the Terror Rift and the Bransfield Strait region have high heat flux relative to tectonically older regions such
1589 as the Weddell Sea that have more moderate heat flux (Fig 16a). Variations in heat flux in East Antarctica are
1590 not clearly associated with basins except for the tendency for very low GHF to occur only in areas without
1591 Type 1 basins. Selected basins, including the Foundation Basin, South Pole Basin, the Northern Wilkes Basin,
1592 and the Prydz Bay Basin show elevated heat flux relative to their surrounding areas. In contrast the Aurora-
1593 Vincennes and southern Wilkes subglacial basins show reduced heat flux relative to their surrounding areas.
1594 The large-scale heat flux shown here represents the crustal and lithospheric structure beneath the basin
1595 and, excepting volcanism, is a stable boundary condition for ice-sheet dynamics. The time-variable influence

1596 of basins on heat flux at the bed is likely to be substantial where fluid circulation is coupled with a high
1597 thermal gradient, and fluid conduits such as deformation zones are also important (Tankersley et al., 2022).

1598 Fast flowing ice, as defined by surface-ice velocity (Mouginot et al., 2019) has overall only a weak spatial
1599 association with the presence of basins (Fig 16b). Type 1 basins have a higher average velocity (24 m yr^{-1})
1600 than either crystalline bed (19 m yr^{-1}) or Type 2 basins (11 m yr^{-1}), but with very small effect size given the
1601 large spatial variability in velocity ($\sigma \approx 70 \text{ m yr}^{-1}$). However, although many of Antarctica's fastest-flowing
1602 glaciers flow over crystalline bedrock or a mixed bed, many of these possess sedimentary basins preserved in
1603 the upper catchment (Fig 16b).

1604 The slipperiness at the ice-bed interface is expressed by the basal-friction coefficient, which relates basal
1605 sliding velocity to basal shear stress. It is a direct measure of the subglacial environment and encapsulates
1606 the effect of both subglacial water and deformable sediment. The model-inferred basal-friction coefficient is
1607 generally lower where there is fast-flowing ice and higher near topographic divides, but also may associate
1608 with the presence of basins (Fig 16c). The model-inferred basal-friction coefficient is closely correlated with
1609 the basin distribution, with a mean for Type 1 basins of $93 (\text{Pa yr/m})^{1/2}$ contrasting with a mean of 127 and
1610 $134 (\text{Pa yr/m})^{1/2}$ in crystalline basement and Type 2 basins respectively. Overall, this relationship has a
1611 medium effect size given regional variability ($\sigma \approx 70 (\text{Pa yr/m})^{1/2}$).

1612 Basal-friction coefficient is related to basin coverage in several ways. In several ice-stream systems,
1613 sedimentary basins occur in the fast-flowing lower catchment and low basal-friction coefficient is seen.
1614 Examples include Mercer and Whillans; MacAyeal and Bindschadler; and Institute ice streams draining the
1615 West Antarctic Ice Sheet and Academy and Support Force; Jutulstraumen; West and Central Ragnhild; and
1616 Cook ice streams draining the East Antarctic Ice Sheet. Often however for major catchments ice in the fast-
1617 flowing lower catchment flows over a crystalline or mixed bed, with the basin confined to the upper
1618 catchment, the downstream part having been eroded (A.R.A. Aitken et al., 2016; G. J. G. Paxman et al.,
1619 2017). Examples include Thwaites and Pine Island; Recovery and Slessor; Lambert, Mellor and Fisher;
1620 Denman and Scott; Totten and the ice streams draining from the southern Wilkes Subglacial Basin through
1621 the Transantarctic Mountains including Byrd, Skelton and David glaciers. For these ice streams, low basal-
1622 friction coefficient extends far into the sedimentary-basin region despite the surface velocity being relatively
1623 slow, suggesting that basal sliding can propagate into the upstream basin. A final relationship is that for
1624 slow-moving ice such as at Kamb Ice Stream, and at drainage divides (e.g. for South Pole), we see basin
1625 regions associated with moderate to high basal-friction coefficient, indicating that basal sliding is limited.

1626 We may also review the association of basins with the subglacial-hydrology system (Fig 16d). Subglacial lakes
1627 are found throughout Antarctica (Livingstone et al., 2022) and occur across all bed classes. Of 675 lakes, 260
1628 (39%) occur over crystalline bedrock, while 239 (35%) occur over Type 1 basins, and 114 (17%) over Type 2

1629 basins. For comparison, the area taken up by these bed classes is 40%, 47% and 8% respectively.
1630 Furthermore, of 140 hydraulically-active lakes we find 96 (69%) occur over Type 1 basins, while of 502 stable
1631 lakes only 137 occur over this class (27%). This represents a tendency for stable lakes to occur close to ice
1632 divides, while active lakes occur more frequently towards the ice-sheet margins (Livingstone et al., 2022).
1633 Besides subglacial lakes, basal-fluid flux is driven by hydraulic-potential gradients from the high-potential
1634 divides towards the ice sheet margins. These networks do not necessarily follow the same flow-routing as
1635 the ice and can cross boundaries to ice flow (Fig 16d). Unless the ice-sheet-surface slope is steep and
1636 oriented transverse to the bed slope, the subglacial water flux will be preferentially concentrated into
1637 topographic basins and form highly dynamic flow networks (Dow et al., 2022; Le Brocq et al., 2013), and so
1638 there is a natural association of high-volume subglacial water flux and sedimentary basins (Fig 16d). Several
1639 notable examples include the Recovery Lakes that overlie the Recovery Basin with flow directed towards
1640 Recovery Glacier; the Pensacola-Pole Basin with flow directed to Academy and Support Force glaciers; and
1641 the Byrd Subglacial Basin with flow directed towards Thwaites Glacier. Lake Vostok drains into the Wilkes
1642 Subglacial Basin, and from there flow is directed towards Cook Glacier, and also through the Transantarctic
1643 Mountains. Finally, Dome C has flow directed into the Aurora Subglacial Basin and from there towards
1644 Vanderford Glacier.

1645 At Thwaites Glacier, the transition from distributed to channelized flow may be correlated to the change
1646 from sedimentary basin to crystalline bed (Dustin M Schroeder et al., 2013) and bed-type transitions in other
1647 catchments (Fig 16d) may also be critical thresholds for the hydrology system. The interaction of high-flux
1648 hydrology networks, including active lakes, with higher-permeability sedimentary beds is fundamental to the
1649 subglacial hydrology of Antarctica and may exert a critical influence on ice-sheet dynamics. An important
1650 consideration is where subglacial hydrology follows different routing to the ice flow: ice retreat and
1651 unloading in one catchment, along with increased basal melting, may enhance water flux that is potentially
1652 routed into another catchment, and so may help propagate dynamic behavior from one catchment to
1653 another (Wright et al., 2008). In some regions, high sensitivity to variable subglacial-hydrology network
1654 structure may lead to cross-catchment vulnerabilities and the propagation of dynamic behavior between ice
1655 streams (Alley et al., 1994; D. G. Vaughan et al., 2008; Wright et al., 2008).

1656 The preceding discussion indicates associations between the presence of sedimentary basins and enhanced
1657 ice-sheet flow. In a sedimentary-basin setting, this sliding may occur in deformable till layers facilitated by
1658 more extensive basal till and from hydrogeological processes that may provide substantial amounts of
1659 subglacial water. Enhanced groundwater discharge to the bed is associated with additional feedbacks,
1660 including heat advection within the basin and temporally-variable water discharge and recharge coupled
1661 with ice unloading and loading histories. The expected groundwater response includes an ongoing long-term
1662 response from deep aquifers activated by unloading since Last Glacial Maximum, and shorter-term

1663 responses from shallower aquifers activated by more recent mass loss (Christoffersen et al., 2014; Gustafson
1664 et al., 2022; Li et al., 2022).

1665 A substantial role for subglacial sedimentary basins in governing the basal conditions of the ice sheet is well
1666 supported by both models and data, but a well-defined relationship between subglacial sedimentary basins
1667 and ice-sheet flow remains elusive, with many cross-associations with other boundary conditions and
1668 complex time- and space-variable interactions. In particular, the potential effects of these basin-facilitated
1669 processes on large scale glacial flow are yet to be systematically assessed.

1670 6 Future directions in Antarctic Subglacial Sedimentary Basins research

1671 Knowledge of sedimentary basins beneath the Antarctic Ice Sheet has expanded greatly in recent decades,
1672 and key concepts relating to their influence on ice-sheet dynamics have been identified. Despite this, for a
1673 full realization of their value for understanding global tectonics, paleolandscape evolution and the dynamic
1674 behavior of ice sheets with changing climate, there is a pressing need to continue to progress several key
1675 themes.

1676 6.1 Sedimentary basin definition and characterization

1677 Despite substantial recent advances, mapping the presence of sedimentary rocks beneath thick ice remains a
1678 significant challenge. The more widely available datasets from airborne geophysics can provide a strong
1679 indication of the presence of a sedimentary basin, subject to certain ambiguities.

1680 Small-scale variations in the solid earth, for example geothermal heat flux (McCormack et al., 2022) and
1681 topography (E. J. MacKie et al., 2020) may have large impacts on ice-sheet dynamics. For consistent mapping
1682 at a continent scale, improved coverage is needed to fill remaining data gaps, and to improve data quality in
1683 areas with, low resolution, less accurate or poorly geolocated data. The newest topographic compilation,
1684 Bedmap3 ,(Frémand, Fretwell, et al., 2022) is based on a 500m along-line resolution. Taking this as a
1685 benchmark, we consider the requirements for airborne data to resolve subglacial geology at this resolution.
1686 To maximize non-aliased signal, magnetic intensity data should be collected with a line-separation
1687 comparable to the source-sensor separation (Reid, 1980). Gravity data may be more widely separated
1688 without loss of non-aliased signal. In much of Antarctica, due to thick ice, the source-sensor separation is
1689 several kilometers, and so there is little gain from closely-spaced magnetic and gravity surveys. Regions with
1690 thinner ice may benefit in principle but are limited by several additional factors, in particular airborne
1691 gravity systems require along-line data filtering that, for most fixed-wing platforms, limit along-line
1692 resolutions to 5-10 kilometers wavelength.

1693 RES has no similar physical limitation on resolution and the bed can be sampled at fine scales along lines.
1694 Fine-scale along-line sampling allows for sub-survey resolution data products to be generated in 2D using

1695 physical and/or statistical techniques (Frémand, Fretwell, et al., 2022; E. J. MacKie et al., 2020; Mathieu
1696 Morlighem et al., 2020). The need for closely-spaced RES data depends on the characteristics of the ice-
1697 sheet bed and the ice-sheet flow, and a variable radar line-spacing of 500 to 2.5 km across the continent is
1698 likely to improve the fidelity of bed-topography data products across all scales. Across all airborne data
1699 types, finer resolution demands a reduced aircraft velocity, for which helicopter surveys are one solution
1700 (Wei et al., 2020), or alternatively, slow-flying UAVs are an emerging technology for practical deployment in
1701 the future (Teisberg et al., 2022). Ship-based airborne operations may also allow surveys to reach coastal
1702 data gaps where onshore infrastructure is not available.

1703 Ground-based geophysical-data collection, including active- and passive-seismic and magnetotelluric
1704 methods, remains limited in Antarctica and it is a significant challenge to achieve a systematic continent-
1705 wide coverage. Large-scale passive-seismic deployments, with stations spaced tens of kilometers apart or
1706 more, have been used with success to image the nature of the crust and the mantle including basins (W.
1707 Shen et al., 2018; Zhou et al., 2022). The current network of passive-seismic stations, mostly in West
1708 Antarctica (Fig 1), could feasibly be expanded to a continent-scale network with accompanying
1709 magnetotelluric data within a manageable logistical footprint. Smaller-scale deployments with station
1710 spacings of kilometers are capable of imaging the ice bed geology conditions for individual ice streams and are
1711 fundamental to understanding the impact of sedimentary basins on ice sheet dynamics Active-
1712 (Anandakrishnan & Winberry, 2004; Gustafson et al., 2022; L. E. Peters et al., 2006). Active seismic
1713 experiments remain resource-intensive and logistically challenging although the implementation of vibrator
1714 sources and snow-streamer technologies is a substantial step forward to increase the efficiency, resolution
1715 and accuracy of data collection but an(Eisen et al., 2015). These more intensive approaches initially may be
1716 targeted towards key catchments, however expanded deployment of these technologies would be of
1717 immense benefit to understanding geologic bed conditions for ice dynamics.

1718 Finally, it is necessary to enhance capability for field verification of bed characteristics to inform and
1719 constrain geophysical observations. Several initiatives are under way to develop further drilling technologies
1720 to access the subglacial geology, including systems designed with differing logistical footprints and with
1721 different capacity to reach the bed through thick ice (Gong et al., 2019; J. W. Goodge et al., 2021; Hodgson
1722 et al., 2016; Kuhl et al., 2021; Talalay et al., 2021). Maintaining strong engagement with ice-coring and hot-
1723 water-drilling communities is desirable to synergize efforts where feasible. In the context of basins research,
1724 and the study of their interactions with glacial systems, a critical problem remains that representative
1725 samples are likely to be found under thick and especially wet-based ice, for which drilling technologies are
1726 not yet optimized. The capacity to recover long stratigraphic cores is of particular value to basins research.

1727 As well as the detection of basins, we may seek to better define the geometry of basins, including their
1728 thickness and overall morphology but also their internal structure. Defining the thickness of Antarctica's

1729 sedimentary basins is a clear next step that demands a new approach able to combine multiple diverse
1730 datasets so that all are accommodated in the problem formulation, and so the solution. Also important are
1731 faults and stratigraphy, which provide critical controls on fluid flow within the basins. Consequently, these
1732 dictate the hydrogeological response to changing glacial load and so advective heat transport to the ice-
1733 sheet bed (Tankersley et al., 2022). The sensitivity of gravity and magnetic data to internal basin structure
1734 may be limited by density and magnetization contrasts between sedimentary rocks which are relatively low
1735 in comparison to the contrast with the basement and other features such as intrusions and volcanic rocks.
1736 While passive-seismic and magnetotelluric data provide some additional constraints, active-seismic data
1737 have in other regions proved most effective for developing a good appreciation of intra-basin structure.
1738 Finally, while the physical properties of the basins, including density, seismic velocity and its anisotropy,
1739 electrical conductivity and other characteristics may be defined from geophysical data, to define their
1740 relationship with ice-sheet dynamics it is necessary to translate these into mechanical and hydrogeological
1741 properties. A particular challenge is to define topological properties defined largely by orientations and
1742 connections (e.g. permeability, stratigraphic layering and its orientation, fracture density and orientation)
1743 that have most bearing on both the hydrogeological system (Person et al., 2012) and also the erodibility of
1744 sedimentary bedrock (Krabbendam & Glasser, 2011; Lane et al., 2015).

1745 6.2 Sedimentary basins as a record of glacial change

1746 A profound quality of sedimentary basins is their capacity to record sensitively the conditions of their
1747 formation which provides knowledge of tectonic and surface processes, and past ice, ocean, and climate
1748 conditions. Sampling of sedimentary records from basins provides key benchmarks and constraints on the
1749 behavior of the ice sheet in the past, which supports an improved capacity to define ice-sheet dynamic
1750 processes in models of potential future ice-sheet change. While many studies have investigated the Antarctic
1751 margin, these studies remain limited in extent and are clustered in a few areas (Fig 1). With dynamic
1752 instabilities dominating catchment-scale ice-stream behavior, more comprehensive coverage is required to
1753 understand the dynamic response of the Antarctic Ice Sheet logistically-sheet to changing climate. Innovative
1754 approaches to marine drilling (e.g. K. Gohl et al., 2017) may allow more agile, safer and less logistically
1755 demanding investigations.

1756 In addition to obtaining records of changing conditions from drill cores, spatial patterns of erosion and
1757 sedimentation are closely linked to past glacial cycles (Anderson et al., 2019; K. Hochmuth et al., 2020; Pérez
1758 et al., 2021) and can be used to understand systematic instabilities within catchments (A.R.A. Aitken et al.,
1759 2016). The structure of sedimentary basins can be used for the reconstruction of paleo-landscapes, offshore
1760 and onshore, which is important for understanding the long-term stability of the ice-sheet structure (K.
1761 Hochmuth et al., 2020; S. S. Jamieson et al., 2010; Guy J. G. Paxman et al., 2019). Paleotopographic

1762 reconstruction is also critical in the effort to model past ice-sheet behavior with realistic topographic and
1763 basal boundary conditions, rather than relying on modern-day formulations (Katharina Hochmuth & Gohl,
1764 2019; Guy J. G. Paxman et al., 2020). An important factor here is not just the reconstruction of topographic
1765 elevation, but also the changing geology of the ice-sheet bed through time.

1766 6.3 Understanding cryosphere interactions

1767 While the fundamental principles of the interactions between sedimentary basins, sediments and water at
1768 the ice-sheet bed and ice-sheet flow have been known for some time ,(Alley et al., 1987; Bell et al., 1998;
1769 Blankenship et al., 1986; Christoffersen et al., 2014) their overall role in controlling Antarctic Ice Sheet
1770 dynamics remains ill-defined. Knowledge of these interactions in Antarctica is growing, but it is evident that
1771 much further work needs be done to provide a systematic understanding of how these complex boundary
1772 conditions interact with the ice sheet to focus, enhance, inhibit or otherwise influence glacial-change
1773 processes associated with a warming climate (Kennicutt et al., 2019).

1774 Hydrogeologic interactions of sedimentary basins with subglacial hydrology and the cryosphere are
1775 understood largely through model studies (Christoffersen et al., 2014; Gooch et al., 2016; Li et al., 2022) and
1776 through studies of the former Northern H hemisphere ice sheets (Person et al., 2007). It is not clear yet how
1777 these model concepts may translate to Antarctic conditions, and a robust and Antarctic-specific
1778 understanding of their role in the dynamics of the Antarctic Ice Sheet is a core challenge requiring both
1779 targeted model studies and expanded observations of the bed. Critical concepts to be defined further
1780 include the role of sedimentary basins for sustaining subglacial water supply, and the interactions of aquifer
1781 systems with subglacial lakes and hydrological flow organization on different timescales. Understanding how
1782 Antarctica's aquifers respond to a changing ice sheet may be an essential factor in understanding their
1783 vulnerability in retreat, as the release of water during glacial unloading, if substantial, could be a critical
1784 positive feedback promoting accelerated ice-sheet flow (Schoof, 2010) and also ice-shelf destabilization (Le
1785 Brocq et al., 2013).

1786 Sedimentary basins are an important factor in controlling geothermal heat flux, firstly through the tendency
1787 to insulate the crust beneath, leading to warmer conditions beneath and secondly, through efficiently that
1788 may further enhance melting ice-the capacity for fluid circulation within the basin to efficiently transport
1789 heat from depth to the surface, also potentially accessing saline waters (Gustafson et al., 2022). Heat
1790 advection is especially important as a positive feedback associated with ice sheet unloading (Gooch et al.,
1791 2016). Essential concepts to be defined further include mapping temperature gradients, water contents and
1792 salinity within basins, as well as the association of these with high ambient temperatures associated with
1793 rifting, magmatism, or high crustal heat production. Perhaps the most limiting factor is the identification of

1794 the internal basin structure, and so the necessary conduits for fluid circulation, their orientation and
1795 connectivity.

1796 A sustained supply of flow-capable sediment is an important factor enabling sustained fast ice-sheet flow.
1797 This requires either a base of marine sediments, deposited during a past retreat, or a reliably erodible
1798 bedrock. In the latter case, while the presence of the sedimentary bed is known to be an important
1799 condition, studies of formerly-glaciated regions show there is a high degree of sensitivity to the nature of the
1800 sedimentary rocks, including the dip and strike of the strata, bedding-layer thicknesses, the competency of
1801 the different lithologies, and the intensity and spacing of joints and other fractures (Hooyer et al., 2012;
1802 Krabbendam & Glasser, 2011; Lane et al., 2015). Characterization of these fine-scale details in a subglacial
1803 setting is problematic in the absence of high-resolution data, however, an understanding of the depositional
1804 setting, large-scale structure and broad lithology variations within basins may allow these factors to be
1805 assessed in a probabilistic sense bearing in mind analogues from formerly glaciated regions.

1806 6.4 Coupling mapping with ice-sheet models for predictive capacity

1807 A major frontier for basins research in Antarctica is the coupling of the knowledge of subglacial geology with
1808 ice-sheet models to understand the influence of bed conditions on basal processes and to enable better
1809 predictions of sea level change and other impacts on ocean and climate. The first challenge in doing so is the
1810 identification of the basin characteristics and processes that are most relevant to dynamic ice-sheet
1811 behavior: in particular we may wish to understand more precisely the influence of basin location within the
1812 catchment relative to the grounding zone, the effects of variable basin thickness, and variations at different
1813 scales of properties such as porosity, lithology, permeability, structural orientation and mechanical
1814 erodibility. Incorporating representations of these factors in ice-sheet models may be enabled in the future
1815 through inclusion of adaptive sliding laws and better coupled hydrology and hydrogeology modelling.

1816 Other challenges include the successful representation in ice-sheet models of evolving sedimentary systems
1817 under ice, including spatially-variable and anisotropic bedrock erosion, the re-distribution of subglacial
1818 sediments through subglacial sediment transport and time-variable subglacial hydrology on ice-sheet flow,
1819 water outflux and sediment deposition on ice shelves and their cavities. Many ice-sheet models are now able
1820 to accommodate at least some of these processes in parameterized forms, allowing their influence to be
1821 assessed alongside other processes (e.g. Delaney et al., 2019; Lowry et al., 2020; Pollard & DeConto, 2020).

1822 7 Conclusion

1823 The presence of sedimentary basins in Antarctica, their potential impact on ice-sheet dynamics, and their
1824 ability to record change has long been known. Except in some regions with access to outcrops and/or ship-
1825 based science, a comprehensive understanding has been lacking due to ice cover and remoteness restricting
1826 access. In recent years, the geophysical community has developed improved approaches to characterize

1827 subglacial geology, through improved equipment and data collection, and advances in data processing and
1828 analysis targeted to the unique environment of Antarctica. Large amounts of data have been collected, and
1829 crucially these are readily available to the broader community in compilations at continent-scale. Numerical
1830 data-analysis techniques including machine learning are providing advanced capability to map the
1831 distribution of sedimentary basins.

1832 Key outcomes from the growing understanding of Antarctica's sedimentary basins are the definition of
1833 feedbacks with ice-sheet processes that have the capacity to influence the future Antarctic Ice Sheet, in
1834 particular through the potential supply of increased water and heat to the ice-sheet bed as a consequence of
1835 retreat. Around the continent, a system-level understanding is emerging that connects subglacial processes
1836 at the ice-sheet bed to marine-depositional systems (K. Hochmuth et al., 2020; Guy J. G. Paxman et al., 2019;
1837 Pollard & DeConto, 2020). A persistent finding beneath the ice sheet, on the continental shelf, and beyond,
1838 is that glacial processes are the dominant factor in the development of Antarctica's sedimentary basins since
1839 at least the Eocene, signifying the dynamic nature of the Antarctic Ice Sheet (Noble et al., 2020).

1840 Despite the progress made it is notable that the records we have for Antarctica are, relative to many other
1841 parts of the world, very limited in their distribution, resolution and scope. Across all data, critical gaps
1842 remain in our coverage of Antarctica's basins, and, due to high logistical thresholds, data redundancy and
1843 repeatability are often low. There is a critical need to define in expanded form the importance of subglacial
1844 sedimentary basins for controlling dynamic ice-sheet flow, especially to characterize the feedbacks and
1845 instabilities that may dictate the response of Antarctica's ice sheet to changing climate. Finally, it is essential
1846 that these findings are incorporated in numerical ice-sheet models to underpin a better predictive capacity
1847 for future ice-sheet change.

1848 8 Acknowledgements

1849 This work rests upon an enormous body of knowledge, and we thank all who have contributed to the
1850 acquisition, processing, analysis and modelling of data and to providing a rich base of interpretations to draw
1851 on. We thank a broad range of collaborators for conversations that helped to develop the manuscript,
1852 including Pippa Whitehouse, Jamin Greenbaum and Katharina Hochmuth. We thank the Editorial Board for
1853 the invitation for this review article. Reviews from Fausto Ferraccioli and an anonymous reviewer, and
1854 editorial comments from Associate Editor Rob Bingham helped to improve the manuscript. The authors
1855 acknowledge funding support from the following bodies Australian Research Council Special Research
1856 Initiative, Australian Centre for Excellence in Antarctic Science (Project Number SR200100008). China
1857 Scholarship Council–The University of Western Australia joint Ph.D. scholarship (201806170054). Natural
1858 Environment Research Council grants NE/S006621/1, NE/R010838/1 NE/G013071/2, NE/F016646/2. British

1859 Antarctic Survey Palaeo Environments, Ice Sheets and Climate Change team. National Science Foundation
1860 Graduate Research Fellowship under Grant No. DGE-1656518.

1861 9 Open Research

1862 The map of Antarctic sedimentary basins as presented here (version 1.04) is available in GIS-ready format
1863 from the Zenodo repository [<https://doi.org/10.5281/zenodo.7984586>]. An updateable version for ongoing
1864 community development is available from GitHub [<https://github.com/LL-Geo/AntarcticBasins/tree/main>] or
1865 Zenodo [<https://doi.org/10.5281/zenodo.7955584>]. Data used in mapping are available from sources as
1866 cited in text.

1867 10 References

1868

- 1869 Aitken, A. R. A., Betts, P. G., Young, D. A., Blankenship, D. D., Roberts, J. L., & Siegert, M. J. (2016). The
1870 Australo-Antarctic Columbia to Gondwana transition. *Gondwana Research*, 29(0), 136-152.
1871 <https://doi.org/10.1016/j.gr.2014.10.019>
- 1872 Aitken, A. R. A., Occhipinti, S. A., Lindsay, M. D., & Trench, A. (2018). A role for data richness mapping in
1873 exploration decision making. *Ore Geology Reviews*, 99, 398-410.
1874 <https://doi.org/10.1016/j.oregeorev.2018.07.002>
- 1875 Aitken, A. R. A., Ramos, L. N., Roberts, J. L., Greenbaum, J. S., Jong, L. M., Young, D. A., & Blankenship, D. D.
1876 (2020). A Magnetic Data Correction Workflow for Sparse, Four-Dimensional Data. *Journal of*
1877 *Geophysical Research: Solid Earth*, 125(10). <https://doi.org/10.1029/2020jb019825>
- 1878 Aitken, A. R. A., Roberts, J. L., Van Ommen, T. D., Young, D. A., Greenbaum, J. S., Blankenship, D. D., &
1879 Siegert, M. J. (2016). Repeated large-scale retreat and advance of Totten Glacier indicated by inland
1880 bed erosion. *Nature*, 533, 385-389. <https://doi.org/10.1038/nature17447>
- 1881 Aitken, A. R. A., Young, D. A., Ferraccioli, F., Betts, P. G., Greenbaum, J. S., Richter, T. G., et al. (2014). The
1882 subglacial geology of Wilkes Land, East Antarctica. *Geophysical Research Letters*, 41(7), 2390-2400.
1883 <https://doi.org/10.1002/2014gl059405>
- 1884 Allen, P. A., Eriksson, P. G., Alkmim, F. F., Betts, P. G., Catuneanu, O., Mazumder, R., et al. (2015). Chapter 2
1885 Classification of basins, with special reference to Proterozoic examples. *Geological Society, London,*
1886 *Memoirs*, 43(1), 5-28. <https://doi.org/10.1144/m43.2>
- 1887 Alley, R. B., Anandakrishnan, S., Bentley, C. R., & Lord, N. (1994). A water-piracy hypothesis for the
1888 stagnation of Ice Stream C, Antarctica. *Annals of Glaciology*, 20, 187-194.
1889 <https://doi.org/10.3189/1994AoG20-1-187-194>
- 1890 Alley, R. B., Blankenship, D. D., Bentley, C. R., & Rooney, S. T. (1987). Till beneath ice stream B: 3. Till
1891 deformation: Evidence and implications. *Journal of Geophysical Research: Solid Earth*, 92(B9), 8921-
1892 8929. <https://doi.org/10.1029/JB092iB09p08921>
- 1893 Alley, R. B., Holschuh, N., MacAyeal, D. R., Parizek, B. R., Zoet, L., Riverman, K., et al. (2021). Bedforms of
1894 Thwaites Glacier, West Antarctica: Character and Origin. *Journal of Geophysical Research: Earth*
1895 *Surface*, 126(12). <https://doi.org/10.1029/2021jf006339>
- 1896 Almendros, J., Wilcock, W., Soule, D., Teixidó, T., Vizcaíno, L., Ardanaz, O., et al. (2020). BRAVOSEIS:
1897 Geophysical investigation of rifting and volcanism in the Bransfield Strait, Antarctica. *Journal of*
1898 *South American Earth Sciences*, 104, 102834. <https://doi.org/10.1016/j.jsames.2020.102834>
- 1899 Ammon, C. J. (1991). The isolation of receiver effects from teleseismic P waveforms. *Bulletin - Seismological*
1900 *Society of America*, 81(6), 2504-2510. <https://doi.org/10.1785/BSSA0810062504>

1901 An, M., Wiens, D. A., Zhao, Y., Feng, M., Nyblade, A. A., Kanao, M., et al. (2015). S-velocity model and
1902 inferred Moho topography beneath the Antarctic Plate from Rayleigh waves. *Journal of Geophysical*
1903 *Research: Solid Earth*, 120(1), 2014JB011332. <https://doi.org/10.1002/2014JB011332>
1904 Anandakrishnan, S., Blankenship, D. D., Alley, R. B., & Stoffa, P. L. (1998). Influence of subglacial geology on
1905 the position of a West Antarctic ice stream from seismic observations. *Nature*, 394(6688), 62-65.
1906 <https://doi.org/10.1038/27889>
1907 Anandakrishnan, S., Voigt, D. E., Burkett, P. G., Long, B., & Henry, R. (2000). Deployment of a broadband
1908 seismic network in West Antarctica. *Geophysical Research Letters*, 27(14), 2053-2056.
1909 <https://doi.org/10.1029/1999GL011189>
1910 Anandakrishnan, S., & Winberry, J. P. (2004). Antarctic subglacial sedimentary layer thickness from receiver
1911 function analysis. *Global and Planetary Change*, 42(1-4), 167-176.
1912 <https://doi.org/10.1016/j.gloplacha.2003.10.005>
1913 Anderson, J. B., Simkins, L. M., Bart, P. J., De Santis, L., Halberstadt, A. R. W., Olivo, E., & Greenwood, S. L.
1914 (2019). Seismic and geomorphic records of Antarctic Ice Sheet evolution in the Ross Sea and
1915 controlling factors in its behaviour. *Geological Society, London, Special Publications*, 475(1), 223-240.
1916 <https://doi.org/10.1144/sp475.5>
1917 Armadillo, E., Ferraccioli, F., Tabellario, G., & Bozzo, E. (2004). Electrical structure across a major ice-covered
1918 fault belt in Northern Victoria Land (East Antarctica). *Geophysical Research Letters*, 31(10).
1919 <https://doi.org/10.1029/2004GL019903>
1920 Arndt, J. E., Hillenbrand, C. D., Grobe, H., Kuhn, G., & Wacker, L. (2017). Evidence for a dynamic grounding
1921 line in outer Filchner Trough, Antarctica, until the early Holocene. *Geology*, 45(11), 1035-1038.
1922 <https://doi.org/10.1130/G39398.1>
1923 Arnold, E., Leuschen, C., Rodriguez-Morales, F., Li, J., Paden, J., Hale, R., & Keshmiri, S. (2020). CReSIS
1924 airborne radars and platforms for ice and snow sounding. *Annals of Glaciology*, 61(81), 58-67.
1925 <https://doi.org/10.1017/aog.2019.37>
1926 Bailey, J. T., Evans, S., & Robin, G. D. Q. (1964). Radio echo sounding of polar ice sheets. *Nature*, 204(4957),
1927 420-421. <https://doi.org/10.1038/204420a0>
1928 Bamber, J. L., Ferraccioli, F., Joughin, I., Shepherd, T., Rippin, D. M., Siegert, M. J., & Vaughan, D. G. (2006).
1929 East Antarctic ice stream tributary underlain by major sedimentary basin. *Geology*, 34(1), 33-36.
1930 <https://doi.org/10.1130/G22160.1>
1931 Baranov, A., Morelli, A., & Chuvaev, A. (2021). ANTASed – An Updated Sediment Model for Antarctica.
1932 *Frontiers in Earth Science*, 9. <https://doi.org/10.3389/feart.2021.722699>
1933 Bart, P. J. (2003). Were West Antarctic ice sheet grounding events in the Ross Sea a consequence of East
1934 Antarctic ice sheet expansion during the middle Miocene? *Earth and Planetary Science Letters*,
1935 216(1-2), 93-107. [https://doi.org/10.1016/S0012-821X\(03\)00509-0](https://doi.org/10.1016/S0012-821X(03)00509-0)
1936 Bart, P. J., Anderson, J. B., Trincardi, F., & Shipp, S. S. (2000). Seismic data from the Northern basin, Ross Sea,
1937 record extreme expansions of the East Antarctic Ice Sheet during the late Neogene. *Marine Geology*,
1938 166(1-4), 31-50. [https://doi.org/10.1016/S0025-3227\(00\)00006-2](https://doi.org/10.1016/S0025-3227(00)00006-2)
1939 Batchelor, C. L., Montelli, A., Ottesen, D., Evans, J., Dowdeswell, E. K., Christie, F. D. W., & Dowdeswell, J. A.
1940 (2020). New insights into the formation of submarine glacial landforms from high-resolution
1941 Autonomous Underwater Vehicle data. *Geomorphology*, 370.
1942 <https://doi.org/10.1016/j.geomorph.2020.107396>
1943 Beaman, R. J., O'Brien, P. E., Post, A. L., & De Santis, L. (2011). A new high-resolution bathymetry model for
1944 the Terre Adélie and George V continental margin, East Antarctica. *Antarctic Science*, 23(1), 95-103.
1945 <https://doi.org/10.1017/S095410201000074X>
1946 Behrendt, J. C., Meister, L., & Henderson, J. R. (1966). Airborne geophysical study in the Pensacola
1947 Mountains of Antarctica. *Science*, 153(3742), 1373-1376.
1948 <https://doi.org/10.1126/science.153.3742.1373>
1949 Bell, R., Small, C., & Arko, R. (1999). Development of a new generation gravity map of Antarctica: ADGRAV
1950 Antarctic Digital Gravity Synthesis. *Annali di Geofisica*, 42. <https://doi.org/10.4401/ag-3720>

- 1951 Bell, R. E., Blankenship, D. D., Finn, C. A., Morse, D. L., Scambos, T. A., Brozena, J. M., & Hodge, S. M. (1998).
1952 Influence of subglacial geology on the onset of a West antarctic ice stream from aerogeophysical
1953 observations. *Nature*, 394(6688), 58-62. <https://doi.org/10.1038/27883>
- 1954 Bell, R. E., Childers, V. A., Arko, R. A., Blankenship, D. D., & Brozena, J. M. (1999). Airborne gravity and precise
1955 positioning for geologic applications. *Journal of Geophysical Research: Solid Earth*, 104(B7), 15281-
1956 15292. <https://doi.org/10.1029/1999jb900122>
- 1957 Bentley, C. R., Crary, A. P., Ostenso, N. A., & Thiel, E. C. (1960). Structure of West Antarctica. *Science*,
1958 131(3394), 131-136. <https://doi.org/10.1126/science.131.3394.131>
- 1959 Bialas, R., Buck, R., Studinger, M., & Fitzgerald, P. (2007). Plateau collapse model for the Transantarctic
1960 Mountains--West Antarctic Rift System: Insights from numerical experiments. *Geology*, 35, 687-690.
1961 <https://doi.org/10.1130/G23825A.1>
- 1962 Bienert, N. L., Schroeder, D. M., Peters, S. T., MacKie, E. J., Dawson, E. J., Siegfried, M., et al. (2022). Post-
1963 Processing Synchronized Bistatic Radar for Long Offset Glacier Sounding. *IEEE Transactions on*
1964 *Geoscience and Remote Sensing*, 1-1. <https://doi.org/10.1109/tgrs.2022.3147172>
- 1965 Bingham, R. G., Ferraccioli, F., King, E. C., Larter, R. D., Pritchard, H. D., Smith, A. M., & Vaughan, D. G. (2012).
1966 Inland thinning of West Antarctic Ice Sheet steered along subglacial rifts. *Nature*, 487(7408), 468-
1967 471. <https://doi.org/10.1038/nature11292>
- 1968 Bingham, R. G., & Siegert, M. J. (2007). Radar-derived bed roughness characterization of Institute and Möller
1969 ice streams, West Antarctica, and comparison with Siple Coast ice streams. *Geophysical Research*
1970 *Letters*, 34(21). <https://doi.org/10.1029/2007GL031483>
- 1971 Bingham, R. G., & Siegert, M. J. (2007). Radio-echo sounding over polar ice masses. *Journal of Environmental*
1972 *and Engineering Geophysics*, 12(1), 47-62. <https://doi.org/10.2113/jeeeg12.1.47>
- 1973 Bingham, R. G., & Siegert, M. J. (2009). Quantifying subglacial bed roughness in Antarctica: implications for
1974 ice-sheet dynamics and history. *Quaternary Science Reviews*, 28(3), 223-236.
1975 <https://doi.org/10.1016/j.quascirev.2008.10.014>
- 1976 Blankenship, D. D., Bentley, C. R., Rooney, S., & Alley, R. B. (1986). Seismic measurements reveal a saturated
1977 porous layer beneath an active Antarctic ice stream. *Nature*, 322(6074), 54-57.
1978 <https://doi.org/10.1038/322054a0>
- 1979 Boger, S. D. (2011). Antarctica — Before and after Gondwana. *Gondwana Research*, 19(2), 335-371.
1980 <https://doi.org/10.1016/j.jgr.2010.09.003>
- 1981 Bohoyo, F., Galindo-Zaldívar, J., Maldonado, A., Schreider, A. A., & Surinach, E. (2002). Basin development
1982 subsequent to ridge-trench collision: The Jane Basin, Antarctica. *Marine Geophysical Research*, 23(5-
1983 6), 413-421. <https://doi.org/10.1023/b:mari.0000018194.18098.0d>
- 1984 Bowman, V., Ineson, J., Riding, J., Crame, J., Francis, J., Condon, D., et al. (2016). The Paleocene of Antarctica:
1985 Dinoflagellate cyst biostratigraphy, chronostratigraphy and implications for the palaeo-Pacific
1986 margin of Gondwana. *Gondwana Research*, 38, 132-148. <https://doi.org/10.1016/j.jgr.2015.10.018>
- 1987 Bradshaw, M. A. (2013). The Taylor Group (Beacon Supergroup): the Devonian sediments of Antarctica.
1988 *Geological Society, London, Special Publications*, 381(1), 67-97. <https://doi.org/10.1144/SP381.23>
- 1989 Brenn, G. R., Hansen, S. E., & Park, Y. (2017). Variable thermal loading and flexural uplift along the
1990 Transantarctic Mountains, Antarctica. *Geology*, 45(5), 463-466. <https://doi.org/10.1130/g38784.1>
- 1991 Brisbourne, A. M., Smith, A. M., Vaughan, D. G., King, E. C., Davies, D., Bingham, R. G., et al. (2017). Bed
1992 conditions of Pine Island Glacier, West Antarctica. *Journal of Geophysical Research: Earth Surface*,
1993 122(1), 419-433. <https://doi.org/10.1002/2016jf004033>
- 1994 Broome, A. L., & Schroeder, D. M. (2022). A Radiometrically Precise Multi-Frequency Ice-Penetrating Radar
1995 Architecture. *IEEE Transactions on Geoscience and Remote Sensing*, 60, 1-15.
1996 <https://doi.org/10.1109/tgrs.2021.3099801>
- 1997 Burgess, S. D., Bowring, S. A., Fleming, T. H., & Elliot, D. H. (2015). High-precision geochronology links the
1998 Ferrar large igneous province with early-Jurassic ocean anoxia and biotic crisis. *Earth and Planetary*
1999 *Science Letters*, 415, 90-99. <https://doi.org/10.1016/j.epsl.2015.01.037>

2000 Burton-Johnson, A., & Riley, T. R. (2015). Autochthonous v. accreted terrane development of continental
2001 margins: a revised in situ tectonic history of the Antarctic Peninsula. *Journal of the Geological*
2002 *Society*, 172(6), 822-835. <https://doi.org/10.1144/jgs2014-110>
2003 Cande, S. C., & Stock, J. M. (2004) Cenozoic reconstructions of the australia-new zealand-south pacific sector
2004 of antarctica. In: *Vol. 151. Geophysical Monograph Series* (pp. 5-17).
2005 Capponi, M., Sampietro, D., Ebbing, J., & Ferraccioli, F. (2022). Antarctica 3-D crustal structure investigation
2006 by means of the Bayesian gravity inversion: the Wilkes Land case study. *Geophysical Journal*
2007 *International*, 229(3), 2147-2161. <https://doi.org/10.1093/gji/ggac036>
2008 Castillo, P., Fanning, C. M., Fernandez, R., Poblete, F., & Hervé, F. (2017). Provenance and age constraints of
2009 Paleozoic siliciclastic rocks from the Ellsworth Mountains in West Antarctica, as determined by
2010 detrital zircon geochronology. *GSA Bulletin*, 129(11-12), 1568-1584.
2011 <https://doi.org/10.1130/b31686.1>
2012 Castillo, P., Lacassie, J. P., Augustsson, C., & Hervé, F. (2015). Petrography and geochemistry of the
2013 Carboniferous-Triassic Trinity Peninsula Group, West Antarctica: Implications for provenance and
2014 tectonic setting. *Geological Magazine*, 152(4), 575-588.
2015 <https://doi.org/10.1017/S0016756814000454>
2016 Catania, G., Hulbe, C., Conway, H., Scambos, T. A., & Raymond, C. F. (2012). Variability in the mass flux of the
2017 Ross ice streams, West Antarctica, over the last millennium. *Journal of Glaciology*, 58(210), 741-752.
2018 <https://doi.org/10.3189/2012JoG11J219>
2019 Chaput, J., Aster, R. C., Huerta, A., Sun, X., Lloyd, A., Wiens, D., et al. (2014). The crustal thickness of West
2020 Antarctica. *Journal of Geophysical Research: Solid Earth*, 119(1), 378-395.
2021 <https://doi.org/10.1002/2013JB010642>
2022 Christianson, K., Jacobel, R. W., Horgan, H. J., Alley, R. B., Anandakrishnan, S., Holland, D. M., & DallaSanta, K.
2023 J. (2016). Basal conditions at the grounding zone of Whillans Ice Stream, West Antarctica, from ice-
2024 penetrating radar. *Journal of Geophysical Research: Earth Surface*, 121(11), 1954-1983.
2025 <https://doi.org/10.1002/2015JF003806>
2026 Christoffersen, P., Bougamont, M., Carter, S. P., Fricker, H. A., & Tulaczyk, S. (2014). Significant groundwater
2027 contribution to Antarctic ice streams hydrologic budget. *Geophysical Research Letters*, 41(6), 2003-
2028 2010. <https://doi.org/10.1002/2014GL059250>
2029 Chu, W., Schroeder, D. M., Seroussi, H., Creyts, T. T., & Bell, R. E. (2018). Complex Basal Thermal Transition
2030 Near the Onset of Petermann Glacier, Greenland. *Journal of Geophysical Research: Earth Surface*,
2031 123(5), 985-995. <https://doi.org/10.1029/2017JF004561>
2032 Cianfarra, P., & Salvini, F. (2016). Origin of the Adventure Subglacial Trench linked to Cenozoic extension in
2033 the East Antarctic Craton. *Tectonophysics*, 670, 30-37. <https://doi.org/10.1016/j.tecto.2015.12.011>
2034 Cooper, M. A., Jordan, T. M., Schroeder, D. M., Siegert, M. J., Williams, C. N., & Bamber, J. L. (2019).
2035 Subglacial roughness of the Greenland Ice Sheet: relationship with contemporary ice velocity and
2036 geology. *The Cryosphere*, 13(11), 3093-3115. <https://doi.org/10.5194/tc-13-3093-2019>
2037 Corr, H., Ferraccioli, F., Frearson, N., Jordan, T., Robinson, C., Armadillo, E., et al. (2007). Airborne radio-echo
2038 sounding of the Wilkes Subglacial Basin, the Transantarctic Mountains, and the Dome C region. 55-
2039 63.
2040 Cox, S. C., Smith Lyttle, B., Elkind, S., Smith Siddoway, C., Morin, P., Capponi, G., et al. (2023). A continent-
2041 wide detailed geological map dataset of Antarctica. *Scientific Data*, 10(1), 250.
2042 <https://doi.org/10.1038/s41597-023-02152-9>
2043 Craddock, J. P., Fitzgerald, P., Konstantinou, A., Nereson, A., & Thomas, R. J. (2017). Detrital zircon
2044 provenance of upper Cambrian-Permian strata and tectonic evolution of the Ellsworth Mountains,
2045 West Antarctica. *Gondwana Research*, 45, 191-207. <https://doi.org/10.1016/j.gr.2016.11.011>
2046 Cui, X., Jeofry, H., Greenbaum, J. S., Guo, J., Li, L., Lindzey, L. E., et al. (2020). Bed topography of Princess
2047 Elizabeth Land in East Antarctica. *Earth Syst. Sci. Data*, 12(4), 2765-2774.
2048 <https://doi.org/10.5194/essd-12-2765-2020>

2049 Curtis, M. L. (2002). Palaeozoic to Mesozoic polyphase deformation of the Patuxent Range, Pensacola
2050 Mountains, Antarctica. *Antarctic Science*, 14(2), 175-183.
2051 <https://doi.org/10.1017/S0954102002000743>

2052 Curtis, M. L., & Lomas, S. A. (1999). Late Cambrian stratigraphy of the Heritage Range, Ellsworth Mountains:
2053 Implications for basin evolution. *Antarctic Science*, 11(1), 63-77.
2054 <https://doi.org/10.1017/s0954102099000103>

2055 Curtis, M. L., Millar, I. L., Storey, B. C., & Fanning, M. (2004). Structural and geochronological constraints of
2056 early Ross orogenic deformation in the Pensacola Mountains, Antarctica. *Bulletin of the Geological*
2057 *Society of America*, 116(5-6), 619-636. <https://doi.org/10.1130/B25170.1>

2058 Dall, J., Kristensen, S. S., Krozer, V., Hernández, C. C., Vidkjær, J., Kusk, A., et al. (2010). ESA'S
2059 POLarimetric Airborne Radar Ice Sounder (POLARIS): design and first results. *IET Radar, Sonar & Navigation*, 4(3), 488-496. <https://doi.org/10.1049/iet-rsn.2009.0035>

2060 Damaske, D., Ferraccioli, F., & Bozzo, E. (2003). Aeromagnetic anomaly investigations along the Antarctic
2061 coast between Yule Bay and Mertz Glacier. *Terra Antartica*, 10, 85-96.

2062 Davey, F. J., & Brancolini, G. (1995). The Late Mesozoic and Cenozoic structural setting of the Ross Sea
2063 region. *Geology and Seismic Stratigraphy of the Antarctic Margin*, 68, 167-182.
2064 <https://doi.org/10.1029/AR068p0167>

2065 Davey, F. J., Brancolini, G., Hamilton, R. J., Henrys, S. A., Sorlien, C. C., & Bartek, L. R. (2000). A revised
2066 correlation of the seismic stratigraphy at the Cape Roberts drill sites with the seismic stratigraphy of
2067 the Victoria Land Basin, Antarctica. *Terra Antarctica*, 7(3), 215-220.

2068 Davey, F. J., Cande, S., & Stock, J. (2021). Cenozoic continental rifting in the north-western Ross Sea. *New*
2069 *Zealand Journal of Geology and Geophysics*, 1-8. <https://doi.org/10.1080/00288306.2021.1891942>

2070 Davey, F. J., Granot, R., Cande, S. C., Stock, J. M., Selvans, M., & Ferraccioli, F. (2016). Synchronous oceanic
2071 spreading and continental rifting in West Antarctica. *Geophysical Research Letters*, 43(12), 6162-
2072 6169. <https://doi.org/10.1002/2016GL069087>

2073 Davies, D., Bingham, R. G., Graham, A. G. C., Spagnolo, M., Dutrieux, P., Vaughan, D. G., et al. (2017). High-
2074 resolution sub-ice-shelf seafloor records of twentieth century ungrounding and retreat of Pine Island
2075 Glacier, West Antarctica. *Journal of Geophysical Research: Earth Surface*, 122(9), 1698-1714.
2076 <https://doi.org/10.1002/2017jf004311>

2077 Davis, J. K., Lawver, L. A., Norton, I., Dalziel, I., & Gahagan, L. M. (2018). The crustal structure of the Enderby
2078 Basin, East Antarctica. *Marine Geophysical Research*, 40, 1-16. <https://doi.org/10.1007/s11001-018-9356-5>

2079 Dawson, E. J., Schroeder, D. M., Chu, W., Mantelli, E., & Seroussi, H. (2022). Ice mass loss sensitivity to the
2080 Antarctic ice sheet basal thermal state. *Nature Communications*, 13(1), 4957.
2081 <https://doi.org/10.1038/s41467-022-32632-2>

2082 De Santis, L., Brancolini, G., & Donda, F. (2003). Seismo-stratigraphic analysis of the Wilkes Land continental
2083 margin (East Antarctica): Influence of glacially driven processes on the Cenozoic deposition. *Deep-*
2084 *Sea Research Part II: Topical Studies in Oceanography*, 50(8-9), 1563-1594.
2085 [https://doi.org/10.1016/s0967-0645\(03\)00079-1](https://doi.org/10.1016/s0967-0645(03)00079-1)

2086 De Santis, L., Prato, S., Brancolini, G., Lovo, M., & Torelli, L. (1999). The Eastern Ross Sea continental shelf
2087 during the Cenozoic: Implications for the West Antarctic ice sheet development. *Global and*
2088 *Planetary Change*, 23(1-4), 173-196. [https://doi.org/10.1016/s0921-8181\(99\)00056-9](https://doi.org/10.1016/s0921-8181(99)00056-9)

2089 Delaney, I., Werder, M. A., & Farinotti, D. (2019). A Numerical Model for Fluvial Transport of Subglacial
2090 Sediment. *Journal of Geophysical Research: Earth Surface*, 124(8), 2197-2223.
2091 <https://doi.org/10.1029/2019JF005004>

2092 Dow, C. F., Ross, N., Jeofry, H., Siu, K., & Siegert, M. J. (2022). Antarctic basal environment shaped by high-
2093 pressure flow through a subglacial river system. *Nature Geoscience*, 15(11), 892-898.
2094 <https://doi.org/10.1038/s41561-022-01059-1>

2095
2096

2097 Dowdeswell, J. A., Evans, J., Mugford, R., Griffiths, G., McPhail, S., Millard, N., et al. (2008). Autonomous
2098 underwater vehicles (AUVs) and investigations of the ice-ocean interface in Antarctic and Arctic
2099 waters. *Journal of Glaciology*, 54(187), 661-672. <https://doi.org/10.3189/002214308786570773>
2100 Dunham, C. K., O'Donnell, J. P., Stuart, G. W., Brisbourne, A. M., Rost, S., Jordan, T. A., et al. (2020). A joint
2101 inversion of receiver function and Rayleigh wave phase velocity dispersion data to estimate crustal
2102 structure in West Antarctica. *Geophysical Journal International*, 223(3), 1644-1657.
2103 <https://doi.org/10.1093/gji/ggaa398>
2104 Eagles, G. (2019). A little spin in the Indian Ocean plate circuit. *Tectonophysics*, 754, 80-100.
2105 <https://doi.org/10.1016/j.tecto.2019.01.015>
2106 Eagles, G., & Eisermann, H. (2020). The Skytrain plate and tectonic evolution of southwest Gondwana since
2107 Jurassic times. *Scientific Reports*, 10(1), 19994. <https://doi.org/10.1038/s41598-020-77070-6>
2108 Eagles, G., Karlsson, N. B., Ruppel, A., Steinhage, D., Jokat, W., & Läufer, A. (2018). Erosion at extended
2109 continental margins: Insights from new aerogeophysical data in eastern Dronning Maud Land.
2110 *Gondwana Research*, 63, 105-116. <https://doi.org/10.1016/j.gr.2018.05.011>
2111 Eagles, G., & Livermore, R. A. (2002). Opening history of Powell Basin, Antarctic Peninsula. *Marine Geology*,
2112 185(3-4), 195-205. [https://doi.org/10.1016/s0025-3227\(02\)00191-3](https://doi.org/10.1016/s0025-3227(02)00191-3)
2113 Ebbing, J., Dilixiati, Y., Haas, P., Ferraccioli, F., & Scheiber-Enslin, S. (2021). East Antarctica magnetically
2114 linked to its ancient neighbours in Gondwana. *Scientific Reports*, 11(1).
2115 <https://doi.org/10.1038/s41598-021-84834-1>
2116 Ebbing, J., Haas, P., Ferraccioli, F., Pappa, F., Szwillus, W., & Bouman, J. (2018). Earth tectonics as seen by
2117 GOCE - Enhanced satellite gravity gradient imaging. *Scientific Reports*, 8(1).
2118 <https://doi.org/10.1038/s41598-018-34733-9>
2119 Eisen, O., Hofstede, C., Diez, A., Kristoffersen, Y., Lambrecht, A., Mayer, C., et al. (2015). On-ice vibroseis and
2120 snowstreamer systems for geoscientific research. *Polar Science*, 9(1), 51-65.
2121 <https://doi.org/10.1016/j.polar.2014.10.003>
2122 Eisen, O., Winter, A., Steinhage, D., Kleiner, T., & Humbert, A. (2020). Basal roughness of the East Antarctic
2123 Ice Sheet in relation to flow speed and basal thermal state. *Annals of Glaciology*, 61(81), 162-175.
2124 <https://doi.org/10.1017/aog.2020.47>
2125 Eisermann, H., Eagles, G., Ruppel, A., Smith, E. C., & Jokat, W. (2020). Bathymetry Beneath Ice Shelves of
2126 Western Dronning Maud Land, East Antarctica, and Implications on Ice Shelf Stability. *Geophysical*
2127 *Research Letters*, 47(12), e2019GL086724. <https://doi.org/10.1029/2019GL086724>
2128 Elliot, D. H., Fanning, C. M., Isbell, J. L., & Hulett, S. R. W. (2017). The Permo-Triassic Gondwana sequence,
2129 central Transantarctic Mountains, Antarctica: Zircon geochronology, provenance, and basin
2130 evolution. *Geosphere*, 13(1), 155-178. <https://doi.org/10.1130/ges01345.1>
2131 Enkin, R. J., Hamilton, T. S., & Morris, W. A. (2020). The Henkel Petrophysical Plot: Mineralogy and Lithology
2132 From Physical Properties. *Geochemistry, Geophysics, Geosystems*, 21(1), e2019GC008818.
2133 <https://doi.org/10.1029/2019GC008818>
2134 Escutia, C., De Santis, L., Donda, F., Dunbar, R. B., Cooper, A. K., Brancolini, G., & Eittrheim, S. L. (2005).
2135 Cenozoic ice sheet history from East Antarctic Wilkes Land continental margin sediments. *Global and*
2136 *Planetary Change*, 45(1), 51-81. <https://doi.org/10.1016/j.gloplacha.2004.09.010>
2137 Evans, D. J. A., Phillips, E. R., Hiemstra, J. F., & Auton, C. A. (2006). Subglacial till: Formation, sedimentary
2138 characteristics and classification. *Earth-Science Reviews*, 78(1), 115-176.
2139 <https://doi.org/10.1016/j.earscirev.2006.04.001>
2140 Evans, K. R., McKenna, L. W., Lieberman, B. S., Weichert, W. D., & Macleod, K. G. (2018). Geology of the
2141 Nelson Limestone, Postel Nunatak, Patuxent Range, Antarctica. *Antarctic Science*, 30(1), 29-43.
2142 <https://doi.org/10.1017/S0954102017000396>
2143 Evans, S., & Robin, G. D. Q. (1966). Glacier depth-sounding from the air. *Nature*, 210(5039), 883-885.
2144 <https://doi.org/10.1038/210883a0>
2145 Evenick, J. C. (2021). Glimpses into Earth's history using a revised global sedimentary basin map. *Earth-*
2146 *Science Reviews*, 215. <https://doi.org/10.1016/j.earscirev.2021.103564>

2147 Ferraccioli, F., Armadillo, E., Jordan, T., Bozzo, E., & Corr, H. (2009). Aeromagnetic exploration over the East
2148 Antarctic Ice Sheet: A new view of the Wilkes Subglacial Basin. *Tectonophysics*, 478(1), 62-77.
2149 <https://doi.org/10.1016/j.tecto.2009.03.013>

2150 Ferraccioli, F., Armadillo, E., Zunino, A., Bozzo, E., Rocchi, S., & Armienti, P. (2009). Magmatic and tectonic
2151 patterns over the Northern Victoria Land sector of the Transantarctic Mountains from new
2152 aeromagnetic imaging. *Tectonophysics*, 478(1-2), 43-61. <https://doi.org/10.1016/j.tecto.2008.11.028>

2153 Ferraccioli, F., & Bozzo, E. (2003). Cenozoic strike-slip faulting from the eastern margin of the Wilkes
2154 Subglacial Basin to the western margin of the Ross Sea Rift: an aeromagnetic connection. *Geological
2155 Society, London, Special Publications*, 210(1), 109-133.
2156 <https://doi.org/10.1144/GSL.SP.2003.210.01.07>

2157 Ferraccioli, F., Finn, C. A., Jordan, T. A., Bell, R. E., Anderson, L. M., & Damaske, D. (2011). East Antarctic
2158 rifting triggers uplift of the Gamburtsev Mountains. *Nature*, 479(7373), 388-392.
2159 <https://doi.org/10.1038/nature10566>

2160 Ferraccioli, F., Forsberg, R., Olesen, A., Jordan, T., Matsuoka, K., Zakrajsek, A., & Ghidella, M. (2020).
2161 *Processed line aeromagnetic data over the Recovery Lakes region and interior Dronning Maud Land,
2162 East Antarctica (2013) [Data set]. UK Polar Data Centre, Natural Environment Research Council, UK
2163 Research & Innovation.* . <https://doi.org/10.5285/849E2215-95B0-4275-88B8-50E18E3F8D56>

2164 Ferraccioli, F., Jones, P. C., Curtis, M. L., & Leat, P. T. (2005). Subglacial imprints of early Gondwana break-up
2165 as identified from high resolution aerogeophysical data over western Dronning Maud Land, East
2166 Antarctica. *Terra Nova*, 17(6), 573-579. <https://doi.org/10.1111/j.1365-3121.2005.00651.x>

2167 Ferraccioli, F., Jones, P. C., Curtis, M. L., Leat, P. T., & Riley, T. R. (2005). Tectonic and magmatic patterns in
2168 the Jutulstraumen rift (?) region, East Antarctica, as imaged by high-resolution aeromagnetic data.
2169 *Earth, Planets and Space*, 57(8), 767-780. <https://doi.org/10.1186/bf03351856>

2170 Ferrar, H. (1907). *Report on the field-geology of the region explored during the "Discovery" Antarctic
2171 Expedition, 1901-1904.* Retrieved from

2172 Fielding, C. R., Whittaker, J., Henrys, S. A., Wilson, T. J., & Naish, T. R. (2008). Seismic facies and stratigraphy
2173 of the Cenozoic succession in McMurdo Sound, Antarctica: Implications for tectonic, climatic and
2174 glacial history. *Palaeogeography, Palaeoclimatology, Palaeoecology*, 260(1-2), 8-29.
2175 <https://doi.org/10.1016/j.palaeo.2007.08.016>

2176 Fitzgerald, P. G., & Goodge, J. W. (2022). Exhumation and tectonic history of inaccessible subglacial interior
2177 East Antarctica from thermochronology on glacial erratics. *Nature Communications*, 13(1), 6217.
2178 <https://doi.org/10.1038/s41467-022-33791-y>

2179 Foley, N., Tulaczyk, S., Auken, E., Schamper, C., Dugan, H., Mikucki, J., et al. (2015). Helicopter-borne
2180 transient electromagnetics in high-latitude environments: An application in the McMurdo Dry
2181 Valleys, Antarctica. *GEOPHYSICS*, 81, WA87-WA99. <https://doi.org/10.1190/geo2015-0186.1>

2182 Forsberg, R., Olesen, A. V., Ferraccioli, F., Jordan, T. A., Matsuoka, K., Zakrajsek, A., et al. (2018). Exploring
2183 the Recovery Lakes region and interior Dronning Maud Land, East Antarctica, with airborne gravity,
2184 magnetic and radar measurements. *Geological Society, London, Special Publications*, 461(1), 23-34.
2185 <https://doi.org/10.1144/SP461.17>

2186 Francis, J. E., Pirrie, D., & Crame, J. A. (2006). *Cretaceous–Tertiary High-Latitude Palaeoenvironments: James
2187 Ross Basin, Antarctica*: Geological Society of London. <https://doi.org/10.1144/gsl.Sp.2006.258>

2188 Frederick, B. C., Young, D. A., Blankenship, D. D., Richter, T. G., Kempf, S. D., Ferraccioli, F., & Siegert, M. J.
2189 (2016). Distribution of subglacial sediments across the Wilkes Subglacial Basin, East Antarctica.
2190 *Journal of Geophysical Research F: Earth Surface*, 121(4), 790-813.
2191 <https://doi.org/10.1002/2015jf003760>

2192 Frémand, A. C., Bodart, J. A., Jordan, T. A., Ferraccioli, F., Robinson, C., Corr, H. F. J., et al. (2022). British
2193 Antarctic Survey's aerogeophysical data: releasing 25 years of airborne gravity, magnetic, and radar
2194 datasets over Antarctica. *Earth Syst. Sci. Data*, 14(7), 3379-3410. [https://doi.org/10.5194/essd-14-
2195 3379-2022](https://doi.org/10.5194/essd-14-3379-2022)

2196 Frémand, A. C., Fretwell, P., Bodart, J., Pritchard, H. D., Aitken, A., Bamber, J. L., et al. (2022). Antarctic
2197 Bedmap data: FAIR sharing of 60 years of ice bed, surface and thickness data. *Earth Syst. Sci. Data*
2198 *Discuss.*, 2022, 1-25. <https://doi.org/10.5194/essd-2022-355>
2199 Fretwell, P., Pritchard, H. D., Vaughan, D. G., Bamber, J. L., Barrand, N. E., Bell, R., et al. (2013). Bedmap2:
2200 Improved ice bed, surface and thickness datasets for Antarctica. *Cryosphere*, 7(1), 375-393.
2201 <https://doi.org/10.5194/tc-7-375-2013>
2202 Gaina, C., Müller, R. D., Brown, B., Ishihara, T., & Ivanov, S. (2007). Breakup and early seafloor spreading
2203 between India and Antarctica. *Geophysical Journal International*, 170(1), 151-169.
2204 <https://doi.org/10.1111/j.1365-246X.2007.03450.x>
2205 Gibbons, A. D., Whittaker, J. M., & Müller, R. D. (2013). The breakup of East Gondwana: Assimilating
2206 constraints from Cretaceous ocean basins around India into a best-fit tectonic model. *Journal of*
2207 *Geophysical Research: Solid Earth*, 118(3), 808-822. <https://doi.org/10.1002/jgrb.50079>
2208 Gibson, C., Boeckmann, G., Meulemans, Z., Kuhl, T., Koehler, J., Johnson, J., & Slawny, K. (2020). RAM-2 Drill
2209 system development: an upgrade of the Rapid Air Movement Drill. *Annals of Glaciology*, 62, 1-10.
2210 <https://doi.org/10.1017/aog.2020.72>
2211 Glover, P. (2016). Archie's law – a reappraisal. *Solid Earth*, 7, 1157-1169. [https://doi.org/10.5194/se-7-](https://doi.org/10.5194/se-7-1157-2016)
2212 [1157-2016](https://doi.org/10.5194/se-7-1157-2016)
2213 Gogineni, S., Chuah, T., Allen, C., Jezek, K., & Moore, R. K. (1998). An improved coherent radar depth
2214 sounder. *Journal of Glaciology*, 44(148), 659-669. <https://doi.org/10.3189/s0022143000002161>
2215 Gohl, K., Denk, A., Eagles, G., & Wobbe, F. (2013). Deciphering tectonic phases of the Amundsen Sea
2216 Embayment shelf, West Antarctica, From a magnetic anomaly grid. *Tectonophysics*, 585, 113-123.
2217 <https://doi.org/10.1016/j.tecto.2012.06.036>
2218 Gohl, K., Freudenthal, T., Hillenbrand, C. D., Klages, J., Larter, R., Bickert, T., et al. (2017). MeBo70 Seabed
2219 Drilling on a Polar Continental Shelf: Operational Report and Lessons From Drilling in the Amundsen
2220 Sea Embayment of West Antarctica. *Geochemistry, Geophysics, Geosystems*, 18(11), 4235-4250.
2221 <https://doi.org/10.1002/2017GC007081>
2222 Gohl, K., Uenzelmann-Neben, G., Gille-Petzoldt, J., Hillenbrand, C.-D., Klages, J. P., Bohaty, S. M., et al.
2223 (2021). Evidence for a Highly Dynamic West Antarctic Ice Sheet During the Pliocene. *Geophysical*
2224 *Research Letters*, 48(14), e2021GL093103. <https://doi.org/10.1029/2021GL093103>
2225 Gohl, K., Uenzelmann-Neben, G., Larter, R. D., Hillenbrand, C. D., Hochmuth, K., Kalberg, T., et al. (2013).
2226 Seismic stratigraphic record of the Amundsen Sea Embayment shelf from pre-glacial to recent times:
2227 Evidence for a dynamic West Antarctic ice sheet. *Marine Geology*, 344, 115-131.
2228 <https://doi.org/10.1016/j.margeo.2013.06.011>
2229 Golynsky, A., Chiappini, M., Damaske, D., Ferraccioli, F., Finn, C., Ghidella, M., et al. (Cartographer). (2001).
2230 ADMAP – Magnetic anomaly map of the Antarctic, 1: 10 000 000 scale map
2231 Golynsky, A., Chiappini, M., Damaske, D., Ferraccioli, F., Finn, C. A., Ishihara, T., et al. (2006). ADMAP — A
2232 Digital Magnetic Anomaly Map of the Antarctic. In D. K. Fütterer, D. Damaske, G. Kleinschmidt, H.
2233 Miller, & F. Tessensohn (Eds.), *Antarctica: Contributions to Global Earth Sciences* (pp. 109-116).
2234 Berlin, Heidelberg: Springer Berlin Heidelberg. https://doi.org/10.1007/3-540-32934-X_12
2235 Golynsky, A. V., Ferraccioli, F., Hong, J. K., Golynsky, D. A., von Frese, R. R. B., Young, D. A., et al. (2018). New
2236 Magnetic Anomaly Map of the Antarctic. *Geophysical Research Letters*, 45(13), 6437-6449.
2237 <https://doi.org/10.1029/2018gl078153>
2238 Golynsky, D. A., & Golynsky, A. V. (2007). Gaussberg rift - illusion or reality? In A. K. Cooper & C. R. Raymond
2239 (Eds.), *Antarctica: A Keystone in a Changing World--Online Proceedings of the 10th ISAES*: USGS
2240 Open-File Report 2007-1047, Extended Abstract 168, 5 p.
2241 Gong, D., Fan, X., Li, Y., Li, B., Zhang, N., Gromig, R., et al. (2019). Coring of antarctic subglacial sediments.
2242 *Journal of Marine Science and Engineering*, 7(6). <https://doi.org/10.3390/jmse7060194>
2243 Gooch, B. T., Young, D. A., & Blankenship, D. D. (2016). Potential groundwater and heterogeneous heat
2244 source contributions to ice sheet dynamics in critical submarine basins of East Antarctica.
2245 *Geochemistry, Geophysics, Geosystems*, 17(2), 395-409. <https://doi.org/10.1002/2015gc006117>

2246 Goodge, J. W. (2020). Geological and tectonic evolution of the Transantarctic Mountains, from ancient
2247 craton to recent enigma. *Gondwana Research*, 80, 50-122. <https://doi.org/10.1016/j.gr.2019.11.001>

2248 Goodge, J. W., Severinghaus, J. P., Johnson, J., Tosi, D., & Bay, R. (2021). Deep ice drilling, bedrock coring and
2249 dust logging with the Rapid Access Ice Drill (RAID) at Minna Bluff, Antarctica. *Annals of Glaciology*.
2250 <https://doi.org/10.1017/aog.2021.13>

2251 Granot, R., & Dymant, J. (2018). Late Cenozoic unification of East and West Antarctica. *Nature*
2252 *Communications*, 9(1), 3189. <https://doi.org/10.1038/s41467-018-05270-w>

2253 Grikurov, G., Leitchenkov, G., Kamenev, E. N., Mikhalsky, E., Golynsky, A., Masolov, V. N., & Laiba, A. A.
2254 (2003). Antarctic tectonic and minerogenic provinces. *Arctic and Antarctic, Russian Academy of*
2255 *Sciences*, 2, 26-47.

2256 Grima, C., Koch, I., Greenbaum, J. S., Soderlund, K. M., Blankenship, D. D., Young, D. A., et al. (2019). Surface
2257 and basal boundary conditions at the Southern McMurdo and Ross Ice Shelves, Antarctica. *Journal of*
2258 *Glaciology*, 65(252), 675-688. <https://doi.org/10.1017/jog.2019.44>

2259 Gulick, S. P. S., Shevenell, A. E., Montelli, A., Fernandez, R., Smith, C., Warny, S., et al. (2017). Initiation and
2260 long-term instability of the East Antarctic Ice Sheet. *Nature*, 552(7684), 225-229.
2261 <https://doi.org/10.1038/nature25026>

2262 Gustafson, C. D., Key, K., Siegfried, M. R., Winberry, J. P., Fricker, H. A., Venturelli, R. A., & Michaud, A. B.
2263 (2022). A dynamic saline groundwater system mapped beneath an Antarctic ice stream. *Science*,
2264 376(6593), 640-644. <https://doi.org/10.1126/science.abm3301>

2265 Haeger, C., & Kaban, M. K. (2019). Decompensative Gravity Anomalies Reveal the Structure of the Upper
2266 Crust of Antarctica. *Pure and Applied Geophysics*, 176(10), 4401-4414.
2267 <https://doi.org/10.1007/s00024-019-02212-5>

2268 Halberstadt, A. R. W., Simkins, L. M., Anderson, J. B., Prothro, L. O., & Bart, P. J. (2018). Characteristics of the
2269 deforming bed: Till properties on the deglaciated Antarctic continental shelf. *Journal of Glaciology*,
2270 64(248), 1014-1027. <https://doi.org/10.1017/jog.2018.92>

2271 Hale, R., Miller, H., Gogineni, S., Yan, J. B., Rodriguez-Morales, F., Leuschen, C., et al. (2016, 10-15 July 2016).
2272 *Multi-channel ultra-wideband radar sounder and imager*. Paper presented at the 2016 IEEE
2273 International Geoscience and Remote Sensing Symposium (IGARSS).
2274 <https://doi.org/10.1109/igarss.2016.7729545>

2275 Hambrey, M. J., & McKelvey, B. (2000). Major Neogene fluctuations of the East Antarctic ice sheet:
2276 Stratigraphic evidence from the Lambert Glacier region. *Geology*, 28(10), 887-890.
2277 [https://doi.org/10.1130/0091-7613\(2000\)28<887:MNFOTE>2.0.CO;2](https://doi.org/10.1130/0091-7613(2000)28<887:MNFOTE>2.0.CO;2)

2278 Harry, D. L., Anoka, J. L., & Jha, S. (2018). Geodynamic models of the West Antarctic Rift System: Implications
2279 for the mantle thermal state. *Geosphere*, 14(6), 2407-2429. <https://doi.org/10.1130/ges01594.1>

2280 Hathway, B. (2000). Continental rift to back-arc basin: Jurassic-Cretaceous stratigraphical and structural
2281 evolution of the Larsen Basin, Antarctic Peninsula. *Journal of the Geological Society*, 157(2), 417-432.
2282 <https://doi.org/10.1144/jgs.157.2.417>

2283 Haynes, M. S., Chapin, E., & Schroeder, D. M. (2018). Geometric Power Fall-Off in Radar Sounding. *IEEE*
2284 *Transactions on Geoscience and Remote Sensing*, 56(11), 6571-6585.
2285 <https://doi.org/10.1109/tgrs.2018.2840511>

2286 Hazzard, J. A. N., Richards, F. D., Goes, S. D. B., & Roberts, G. G. (2023). Probabilistic Assessment of Antarctic
2287 Thermomechanical Structure: Impacts on Ice Sheet Stability. *Journal of Geophysical Research: Solid*
2288 *Earth*, 128(5), e2023JB026653. <https://doi.org/10.1029/2023JB026653>

2289 Heliere, F., Lin, C., Corr, H., & Vaughan, D. (2007). Radio Echo Sounding of Pine Island Glacier, West
2290 Antarctica: Aperture Synthesis Processing and Analysis of Feasibility From Space. *IEEE Transactions*
2291 *on Geoscience and Remote Sensing*, 45(8), 2573-2582. <https://doi.org/10.1109/tgrs.2007.897433>

2292 Hill, G. J. (2020). On the Use of Electromagnetics for Earth Imaging of the Polar Regions. *Surveys in*
2293 *Geophysics*, 41(1), 5-45. <https://doi.org/10.1007/s10712-019-09570-8>

2294 Hillenbrand, C. D., Bentley, M. J., Stoll Dorf, T. D., Hein, A. S., Kuhn, G., Graham, A. G. C., et al. (2014).
2295 Reconstruction of changes in the Weddell Sea sector of the Antarctic Ice Sheet since the Last Glacial

2296 Maximum. *Quaternary Science Reviews*, 100, 111-136.
2297 <https://doi.org/10.1016/j.quascirev.2013.07.020>
2298 Hirt, C., Rexer, M., Scheinert, M., Pail, R., Claessens, S., & Holmes, S. (2016). A new degree-2190 (10 km
2299 resolution) gravity field model for Antarctica developed from GRACE, GOCE and Bedmap2 data.
2300 *Journal of Geodesy*, 90(2), 105-127. <https://doi.org/10.1007/s00190-015-0857-6>
2301 Hochmuth, K., & Gohl, K. (2019). Seaward growth of Antarctic continental shelves since establishment of a
2302 continent-wide ice sheet: Patterns and mechanisms. *Palaeogeography, Palaeoclimatology,*
2303 *Palaeoecology*, 520, 44-54. <https://doi.org/10.1016/j.palaeo.2019.01.025>
2304 Hochmuth, K., Gohl, K., Leitchenkov, G., Sauermilch, I., Whittaker, J. M., Uenzelmann-Neben, G., et al.
2305 (2020). The Evolving Paleobathymetry of the Circum-Antarctic Southern Ocean Since 34 Ma: A Key to
2306 Understanding Past Cryosphere-Ocean Developments. *Geochemistry, Geophysics, Geosystems*,
2307 21(8), e2020GC009122. <https://doi.org/10.1029/2020GC009122>
2308 Hochmuth, K., Whittaker, J. M., Sauermilch, I., Klocker, A., Gohl, K., & LaCasce, J. H. (2022). Southern Ocean
2309 biogenic blooms freezing-in Oligocene colder climates. *Nature Communications*, 13(1), 6785.
2310 <https://doi.org/10.1038/s41467-022-34623-9>
2311 Hodgson, D. A., Bentley, M. J., Smith, J. A., Klepacki, J., Makinson, K., Smith, A. M., et al. (2016). Technologies
2312 for retrieving sediment cores in Antarctic subglacial settings. *Philosophical Transactions of the Royal*
2313 *Society A: Mathematical, Physical and Engineering Sciences*, 374(2059).
2314 <https://doi.org/10.1098/rsta.2015.0056>
2315 Holschuh, N., Christianson, K., Paden, J., Alley, R. B., & Anandakrishnan, S. (2020). Linking postglacial
2316 landscapes to glacier dynamics using swath radar at Thwaites Glacier, Antarctica. *Geology*, 48(3),
2317 268-272. <https://doi.org/10.1130/g46772.1>
2318 Hooyer, T. S., Cohen, D., & Iverson, N. R. (2012). Control of glacial quarrying by bedrock joints.
2319 *Geomorphology*, 153-154, 91-101. <https://doi.org/10.1016/j.geomorph.2012.02.012>
2320 Horgan, H., Naish, T., Bannister, S., Balfour, N., & Wilson, G. (2005). Seismic stratigraphy of the Plio-
2321 Pleistocene Ross Island flexural moat-fill: A prognosis for ANDRILL Program drilling beneath
2322 McMurdo-Ross Ice Shelf. *Global and Planetary Change*, 45(1-3 SPEC. ISS.), 83-97.
2323 <https://doi.org/10.1016/j.gloplacha.2004.09.014>
2324 Horgan, H. J., Van Haastrecht, L., Alley, R. B., Anandakrishnan, S., Beem, L. H., Christianson, K., et al. (2021).
2325 Grounding zone subglacial properties from calibrated active-source seismic methods. *Cryosphere*,
2326 15(4), 1863-1880. <https://doi.org/10.5194/tc-15-1863-2021>
2327 Huang, X., & Jokat, W. (2016). Sedimentation and potential venting on the rifted continental margin of
2328 Dronning Maud Land. *Marine Geophysical Research*, 37. [https://doi.org/10.1007/s11001-016-9296-](https://doi.org/10.1007/s11001-016-9296-x)
2329 [x](https://doi.org/10.1007/s11001-016-9296-x)
2330 Huerta, A. D., & Harry, D. L. (2007). The transition from diffuse to focused extension: Modeled evolution of
2331 the West Antarctic Rift system. *Earth and Planetary Science Letters*, 255(1), 133-147.
2332 <https://doi.org/10.1016/j.epsl.2006.12.011>
2333 Hunter, M. A., & Cantrill, D. J. (2006). A new stratigraphy for the Latady Basin, Antarctic Peninsula: Part 2,
2334 Latady Group and basin evolution. *Geological Magazine*, 143(6), 797-819.
2335 <https://doi.org/10.1017/S0016756806002603>
2336 Hunter, R. J., Johnson, A. C., & Aleshkova, N. D. (1996). Aeromagnetic data from the southern Weddell Sea
2337 embayment and adjacent areas: Synthesis and interpretation. *Geological Society Special Publication*,
2338 108, 143-154. <https://doi.org/10.1144/GSL.SP.1996.108.01.10>
2339 Isanina, E., Krupnova, N., Popov, S., Masolov, V., & Lukin, V. (2009). Deep structure of the Vostok Basin, East
2340 Antarctica as deduced from seismological observations. *Geotectonics*, 43, 221-225.
2341 <https://doi.org/10.1134/S0016852109030042>
2342 Isbell, J. L., Koch, Z. J., Szablewski, G. M., & Lenaker, P. A. (2008). Permian glacial deposits in the
2343 Transantarctic Mountains, Antarctica. In *Special Paper of the Geological Society of America* (Vol. 441,
2344 pp. 59-70). [https://doi.org/10.1130/2008.2441\(04\)](https://doi.org/10.1130/2008.2441(04))
2345 Jamieson, S. S., Sugden, D. E., & Hulton, N. R. (2010). The evolution of the subglacial landscape of Antarctica.
2346 *Earth and Planetary Science Letters*, 293(1-2), 1-27. <https://doi.org/10.1016/j.epsl.2010.02.012>

2347 Jamieson, S. S. R., Ross, N., Greenbaum, J. S., Young, D. A., Aitken, A. R. A., Roberts, J. L., et al. (2016). An
2348 extensive subglacial lake and canyon system in Princess Elizabeth Land, East Antarctica. *Geology*,
2349 44(2), 87-90. <https://doi.org/10.1130/g37220.1>

2350 Jamieson, S. S. R., Stokes, C. R., Ross, N., Rippin, D. M., Bingham, R. G., Wilson, D. S., et al. (2014). The glacial
2351 geomorphology of the Antarctic ice sheet bed. *Antarctic Science*, 26(6), 724-741.
2352 <https://doi.org/10.1017/s0954102014000212>

2353 Jensen, T. E., & Forsberg, R. (2018). Helicopter Test of a Strapdown Airborne Gravimetry System. *Sensors*
2354 (*Basel, Switzerland*), 18(9), 3121. <https://doi.org/10.3390/s18093121>

2355 Johnston, L., Wilson, G., Gorman, A., Henrys, S., Horgan, H., Clark, R., & Naish, T. (2008). Cenozoic basin
2356 evolution beneath the southern McMurdo Ice Shelf, Antarctica. *Global and Planetary Change*, 62,
2357 61-76. <https://doi.org/10.1016/j.gloplacha.2007.11.004>

2358 Jokat, W., Altenbernd, T., Eagles, G., & Geissler, W. H. (2021). The early drift of the Indian plate. *Sci Rep*,
2359 11(1), 10796. <https://doi.org/10.1038/s41598-021-90172-z>

2360 Jokat, W., & Herter, U. (2016). Jurassic failed rift system below the Filchner-Ronne-Shelf, Antarctica: New
2361 evidence from geophysical data. *Tectonophysics*, 688, 65-83.
2362 <https://doi.org/10.1016/j.tecto.2016.09.018>

2363 Jokat, W., Nogi, Y., & Leinweber, V. (2010). New aeromagnetic data from the western Enderby Basin and
2364 consequences for Antarctic-India break-up. *Geophysical Research Letters*, 37(21).
2365 <https://doi.org/10.1029/2010GL045117>

2366 Jones, P., Johnson, A., Frese, R. R. v., & Corr, H. F. J. (2002). Detecting rift basins in the Evans Ice Stream
2367 region of West Antarctica using airborne gravity data. *Tectonophysics*, 347, 25-41.
2368 [https://doi.org/10.1016/S0040-1951\(01\)00236-0](https://doi.org/10.1016/S0040-1951(01)00236-0)

2369 Jordan, T. A., & Becker, D. (2018). Investigating the distribution of magmatism at the onset of Gondwana
2370 breakup with novel strapdown gravity and aeromagnetic data. *Physics of the Earth and Planetary*
2371 *Interiors*, 282, 77-88. <https://doi.org/10.1016/j.pepi.2018.07.007>

2372 Jordan, T. A., Ferraccioli, F., Armadillo, E., & Bozzo, E. (2013). Crustal architecture of the Wilkes Subglacial
2373 Basin in East Antarctica, as revealed from airborne gravity data. *Tectonophysics*, 585, 196-206.
2374 <https://doi.org/10.1016/j.tecto.2012.06.041>

2375 Jordan, T. A., Ferraccioli, F., Corr, H., Graham, A., Armadillo, E., & Bozzo, E. (2010). Hypothesis for mega-
2376 outburst flooding from a palaeo-subglacial lake beneath the East Antarctic Ice Sheet. *Terra Nova*,
2377 22(4), 283-289. <https://doi.org/10.1111/j.1365-3121.2010.00944.x>

2378 Jordan, T. A., Ferraccioli, F., & Forsberg, R. (2022). An embayment in the East Antarctic basement constrains
2379 the shape of the Rodinian continental margin. *Communications Earth & Environment*, 3(1), 52.
2380 <https://doi.org/10.1038/s43247-022-00375-z>

2381 Jordan, T. A., Ferraccioli, F., & Leat, P. T. (2017). New geophysical compilations link crustal block motion to
2382 Jurassic extension and strike-slip faulting in the Weddell Sea Rift System of West Antarctica.
2383 *Gondwana Research*, 42, 29-48. <https://doi.org/10.1016/j.gr.2016.09.009>

2384 Jordan, T. A., Ferraccioli, F., Ross, N., Corr, H. F. J., Leat, P. T., Bingham, R. G., et al. (2013). Inland extent of
2385 the Weddell Sea Rift imaged by new aerogeophysical data. *Tectonophysics*, 585, 137-160.
2386 <https://doi.org/10.1016/j.tecto.2012.09.010>

2387 Jordan, T. A., Ferraccioli, F., Vaughan, D. G., Holt, J. W., Corr, H., Blankenship, D. D., & Diehl, T. M. (2010).
2388 Aerogravity evidence for major crustal thinning under the Pine Island Glacier region (West
2389 Antarctica). *Bulletin of the Geological Society of America*, 122(5-6), 714-726.
2390 <https://doi.org/10.1130/b26417.1>

2391 Jordan, T. A., Riley, T. R., & Siddoway, C. S. (2020). The geological history and evolution of West Antarctica.
2392 *Nature Reviews Earth & Environment*, 1(2), 117-133. <https://doi.org/10.1038/s43017-019-0013-6>

2393 Jordan, T. M., Cooper, M. A., Schroeder, D. M., Williams, C. N., Paden, J. D., Siegert, M. J., & Bamber, J. L.
2394 (2017). Self-affine subglacial roughness: consequences for radar scattering and basal water
2395 discrimination in northern Greenland. *The Cryosphere*, 11(3), 1247-1264.
2396 <https://doi.org/10.5194/tc-11-1247-2017>

2397 Karner, G. D., Studinger, M., & Bell, R. E. (2005). Gravity anomalies of sedimentary basins and their
2398 mechanical implications: Application to the Ross Sea basins, West Antarctica. *Earth and Planetary*
2399 *Science Letters*, 235(3-4), 577-596. <https://doi.org/10.1016/j.epsl.2005.04.016>

2400 Kennicutt, M. C., Bromwich, D., Liggett, D., Njåstad, B., Peck, L., Rintoul, S. R., et al. (2019). Sustained
2401 Antarctic Research: A 21st Century Imperative. *One Earth*, 1(1), 95-113.
2402 <https://doi.org/10.1016/j.oneear.2019.08.014>

2403 Key, K., & Siegfried, M. R. (2017). The feasibility of imaging subglacial hydrology beneath ice streams with
2404 ground-based electromagnetics. *Journal of Glaciology*, 63(241), 755-771.
2405 <https://doi.org/10.1017/jog.2017.36>

2406 Kim, S., De Santis, L., Hong, J. K., Cottlerle, D., Petronio, L., Colizza, E., et al. (2018). Seismic stratigraphy of
2407 the Central Basin in northwestern Ross Sea slope and rise, Antarctica: Clues to the late Cenozoic ice-
2408 sheet dynamics and bottom-current activity. *Marine Geology*, 395, 363-379.
2409 <https://doi.org/10.1016/j.margeo.2017.10.013>

2410 Kjær, K. H., Larsen, N. K., Binder, T., Bjørk, A. A., Eisen, O., Fahnestock, M. A., et al. (2018). A large impact
2411 crater beneath Hiawatha Glacier in northwest Greenland. *Sci Adv*, 4(11), eaar8173.
2412 <https://doi.org/10.1126/sciadv.aar8173>

2413 König, M., & Jokat, W. (2006). The Mesozoic breakup of the Weddell Sea. *Journal of Geophysical Research:*
2414 *Solid Earth*, 111(12). <https://doi.org/10.1029/2006JB004035>

2415 Kovesi, P. (1999). Image Features from Phase Congruency. *VIDERE*, 1(3), 2-26.

2416 Krabbendam, M., & Glasser, N. F. (2011). Glacial erosion and bedrock properties in NW Scotland: Abrasion
2417 and plucking, hardness and joint spacing. *Geomorphology*, 130(3), 374-383.
2418 <https://doi.org/10.1016/j.geomorph.2011.04.022>

2419 Kristoffersen, Y., Hofstede, C., Diez, A., Blenkner, R., Lambrecht, A., Mayer, C., & Eisen, O. (2014).
2420 Reassembling Gondwana: A new high quality constraint from vibroseis exploration of the sub-ice
2421 shelf geology of the East Antarctic continental margin. *Journal of Geophysical Research: Solid Earth*,
2422 119(12), 9171-9182. <https://doi.org/10.1002/2014jb011479>

2423 Krohne, N., Lisker, F., Kleinschmidt, G., Klügel, A., LÄufer, A., Estrada, S., & Spiegel, C. (2016). The Shackleton
2424 Range (East Antarctica): an alien block at the rim of Gondwana? *Geological Magazine*, 155(4), 841-
2425 864. <https://doi.org/10.1017/S0016756816001011>

2426 Kuhl, T., Gibson, C., Johnson, J., Boeckmann, G., Moravec, E., & Slawny, K. (2021). Agile Sub-Ice Geological
2427 (ASIG) Drill development and Pirrit Hills field project. *Annals of Glaciology*, 62(84), 53-66.
2428 <https://doi.org/10.1017/aog.2020.59>

2429 Kulesa, B. (2007). A Critical Review of the Low-Frequency Electrical Properties of Ice Sheets and Glaciers.
2430 *Journal of Environmental Engineering Geophysics*, 12, 23-36. <https://doi.org/10.2113/jeeg12.1.23>

2431 Kulesa, B., Hubbard, B., & Brown, G. H. (2006). Time-lapse imaging of subglacial drainage conditions using
2432 three-dimensional inversion of borehole electrical resistivity data. *Journal of Glaciology*, 52(176), 49-
2433 57. <https://doi.org/10.3189/172756506781828854>

2434 Kulesa, B., Key, K., Thompson, S., & Siegert, M. (2019). *Heat and groundwater transport between the*
2435 *Antarctic Ice Sheet and subglacial sedimentary basins from electromagnetic geophysical*
2436 *measurements*. Paper presented at the SEG Technical Program Expanded Abstracts
2437 <https://doi.org/10.1190/segam2019-3215566.1>

2438 Kulhanek, D. K., Levy, R. H., Clowes, C. D., Prebble, J. G., Rodelli, D., Jovane, L., et al. (2019). Revised
2439 chronostratigraphy of DSDP Site 270 and late Oligocene to early Miocene paleoecology of the Ross
2440 Sea sector of Antarctica. *Global and Planetary Change*, 178, 46-64.
2441 <https://doi.org/10.1016/j.gloplacha.2019.04.002>

2442 Kvas, A., Brockmann, J. M., Krauss, S., Schubert, T., Gruber, T., Meyer, U., et al. (2021). GOCO06s – a satellite-
2443 only global gravity field model. *Earth Syst. Sci. Data*, 13(1), 99-118. <https://doi.org/10.5194/essd-13-99-2021>

2444

2445 Lane, T. P., Roberts, D. H., Rea, B. R., Ó Cofaigh, C., & Vieli, A. (2015). Controls on bedrock bedform
2446 development beneath the Uummannaq Ice Stream onset zone, West Greenland. *Geomorphology*,
2447 231, 301-313. <https://doi.org/10.1016/j.geomorph.2014.12.019>

2448 Lawrence, J. F., Wiens, D. A., Nyblade, A. A., Anandakrishnan, S., Shore, P. J., & Voigt, D. (2006). Rayleigh
2449 wave phase velocity analysis of the Ross Sea, Transantarctic Mountains, and East Antarctica from a
2450 temporary seismograph array. *Journal of Geophysical Research: Solid Earth*, 111(B6).
2451 <https://doi.org/10.1029/2005JB003812>

2452 Le Brocq, A. M., Ross, N., Griggs, J. A., Bingham, R. G., Corr, H. F. J., Ferraccioli, F., et al. (2013). Evidence from
2453 ice shelves for channelized meltwater flow beneath the Antarctic Ice Sheet. *Nature Geosci*, 6(11),
2454 945-948. <https://doi.org/10.1038/ngeo1977>

2455 Leitchenkov, G. L., Antonov, A. V., Luneov, P. I., & Lipenkov, V. Y. (2016). Geology and environments of
2456 subglacial Lake Vostok. *Philosophical Transactions of the Royal Society A: Mathematical, Physical and*
2457 *Engineering Sciences*, 374(2059). <https://doi.org/10.1098/rsta.2014.0302>

2458 Leitchenkov, G. L., & Kudryavtzev, G. A. (1997). Structure and Origin of the Earth's Crust in the Weddell Sea
2459 Embayment (beneath the Front of the Filchner and Ronne Ice Shelves) from Deep Seismic Sounding
2460 data. *Polarforschung*, 67(3), 143-154.

2461 Levy, R., Harwood, D., Florindo, F., Sangiorgi, F., Tripathi, R., Eynatten, H. v., et al. (2016). Antarctic ice sheet
2462 sensitivity to atmospheric CO₂ variations in the early to mid-Miocene. *Proceedings of the National*
2463 *Academy of Sciences*, 113(13), 3453-3458. <https://doi.org/10.1073/pnas.1516030113>

2464 Li, L., Aitken, A. R. A., Lindsay, M. D., & Kulesa, B. (2022). Sedimentary basins reduce stability of Antarctic ice
2465 streams through groundwater feedbacks. *Nature Geoscience*, 15(8), 645-650.
2466 <https://doi.org/10.1038/s41561-022-00992-5>

2467 Lin, F.-C., Schmandt, B., & Tsai, V. C. (2012). Joint inversion of Rayleigh wave phase velocity and ellipticity
2468 using USArray: Constraining velocity and density structure in the upper crust. *Geophysical Research*
2469 *Letters*, 39(12). <http://dx.doi.org/10.1029/2012GL052196>

2470 Lindeque, A., Gohl, K., Henrys, S., Wobbe, F., & Davy, B. (2016). Seismic stratigraphy along the Amundsen Sea
2471 to Ross Sea continental rise: A cross-regional record of pre-glacial to glacial processes of the West
2472 Antarctic margin. *Palaeogeography, Palaeoclimatology, Palaeoecology*, 443, 183-202.
2473 <https://doi.org/10.1016/j.palaeo.2015.11.017>

2474 Lindeque, A., Gohl, K., Wobbe, F., & Uenzelmann-Neben, G. (2016). Preglacial to glacial sediment thickness
2475 grids for the Southern Pacific Margin of West Antarctica. *Geochemistry, Geophysics, Geosystems*,
2476 17(10), 4276-4285. <https://doi.org/10.1002/2016GC006401>

2477 Lindeque, A., Martos Martin, Y. M., Gohl, K., & Maldonado, A. (2013). Deep-sea pre-glacial to glacial
2478 sedimentation in the Weddell Sea and southern Scotia Sea from a cross-basin seismic transect.
2479 *Marine Geology*, 336, 61-83. <https://doi.org/10.1016/j.margeo.2012.11.004>

2480 Lisker, F., Wilson, C. J. L., & Gibson, H. J. (2007). Thermal history of the Vestfold Hills (East Antarctica)
2481 between Lambert rifting and Gondwana break-up, evidence from apatite fission track data. *Antarctic*
2482 *Science*, 19(1), 97-106. <https://doi.org/10.1017/S0954102007000144>

2483 Livingstone, S. J., Li, Y., Rutishauser, A., Sanderson, R. J., Winter, K., Mikucki, J. A., et al. (2022). Subglacial
2484 lakes and their changing role in a warming climate. *Nature Reviews Earth & Environment*, 3(2), 106-
2485 124. <https://doi.org/10.1038/s43017-021-00246-9>

2486 Lloyd, A. J., Wiens, D. A., Nyblade, A. A., Anandakrishnan, S., Aster, R. C., Huerta, A. D., et al. (2015). A
2487 seismic transect across West Antarctica: Evidence for mantle thermal anomalies beneath the Bentley
2488 Subglacial Trench and the Marie Byrd Land Dome. *Journal of Geophysical Research: Solid Earth*,
2489 120(12), 8439-8460. <https://doi.org/10.1002/2015jb012455>

2490 Lloyd, A. J., Wiens, D. A., Zhu, H., Tromp, J., Nyblade, A. A., Aster, R. C., et al. (2020). Seismic Structure of the
2491 Antarctic Upper Mantle Imaged with Adjoint Tomography. *Journal of Geophysical Research: Solid*
2492 *Earth*, 125(3). <https://doi.org/10.1029/2019JB017823>

2493 Löising, M., & Ebbing, J. (2021). Predicting Geothermal Heat Flow in Antarctica With a Machine Learning
2494 Approach. *Journal of Geophysical Research: Solid Earth*, 126(6), e2020JB021499.
2495 <https://doi.org/10.1029/2020JB021499>

2496 Lowry, D. P., Golledge, N. R., Bertler, N. A. N., Jones, R. S., McKay, R., & Stutz, J. (2020). Geologic controls on
2497 ice sheet sensitivity to deglacial climate forcing in the Ross Embayment, Antarctica. *Quaternary*
2498 *Science Advances*, 1, 100002. <https://doi.org/10.1016/j.qsa.2020.100002>

2499 Luyendyk, B. P., Sorlien, C. C., Wilson, D. S., Bartek, L. R., & Siddoway, C. S. (2001). Structural and tectonic
2500 evolution of the Ross Sea rift in the Cape Colbeck region, Eastern Ross Sea, Antarctica. *Tectonics*,
2501 20(6), 933-958. <https://doi.org/10.1029/2000TC001260>

2502 Lythe, M. B., & Vaughan, D. G. (2001). BEDMAP: A new ice thickness and subglacial topographic model of
2503 Antarctica. *Journal of Geophysical Research: Solid Earth*, 106(B6), 11335-11351.
2504 <https://doi.org/10.1029/2000jb900449>

2505 MacGregor, J. A., Boisvert, L. N., Medley, B., Petty, A. A., Harbeck, J. P., Bell, R. E., et al. (2021). The Scientific
2506 Legacy of NASA's Operation IceBridge. *Reviews of Geophysics*, 59(2).
2507 <https://doi.org/10.1029/2020rg000712>

2508 MacKie, E. J., Schroeder, D. M., Caers, J., Siegfried, M. R., & Scheidt, C. (2020). Antarctic Topographic
2509 Realizations and Geostatistical Modeling Used to Map Subglacial Lakes. *Journal of Geophysical*
2510 *Research: Earth Surface*, 125(3), e2019JF005420. <https://doi.org/10.1029/2019JF005420>

2511 MacKie, E. J., Schroeder, D. M., Zuo, C., Yin, Z., & Caers, J. (2021). Stochastic modeling of subglacial
2512 topography exposes uncertainty in water routing at Jakobshavn Glacier. *Journal of Glaciology*,
2513 67(261), 75-83. <https://doi.org/10.1017/jog.2020.84>

2514 Maggi, M., Cianfarra, P., & Salvini, F. (2016). Erosion by tectonic carving in the Concordia Subglacial Fault
2515 Zone, East Antarctica. *Earth and Planetary Science Letters*, 433, 99-108.
2516 <https://doi.org/10.1016/j.epsl.2015.10.045>

2517 Maldonado, A., Bohoyo, F., Galindo-Zaldívar, J., Hernández-Molina, J., Jabaloy, A., Lobo, F. J., et al. (2006).
2518 Ocean basins near the Scotia-Antarctic plate boundary; influence of tectonics and paleoceanography
2519 on the Cenozoic deposits. *Marine Geophysical Researches*, 27(2), 83-107.
2520 <https://doi.org/10.1007/s11001-006-9003-4>

2521 Maldonado, A., Larter, R. D., & Aldaya, F. (1994). Forearc tectonic evolution of the South Shetland margin,
2522 Antarctic Peninsula. *Tectonics*, 13(6), 1345-1370. <https://doi.org/10.1029/94TC01352>

2523 Maritati, A., Aitken, A. R. A., Young, D. A., Roberts, J. L., Blankenship, D. D., & Siegert, M. J. (2016). The
2524 tectonic development and erosion of the Knox Subglacial Sedimentary Basin, East Antarctica.
2525 *Geophysical Research Letters*, 43(20), 10,728-710,737. <https://doi.org/10.1002/2016gl071063>

2526 Maritati, A., Danišik, M., Halpin, J. A., Whittaker, J. M., & Aitken, A. R. A. (2020). Pangea Rifting Shaped the
2527 East Antarctic Landscape. *Tectonics*, 39(8), e2020TC006180. <https://doi.org/10.1029/2020TC006180>

2528 Maritati, A., Halpin, J. A., Whittaker, J. M., & Daczko, N. R. (2019). Fingerprinting Proterozoic Bedrock in
2529 Interior Wilkes Land, East Antarctica. *Scientific Reports*, 9(1). <https://doi.org/10.1038/s41598-019-46612-y>

2530

2531 Maritati, A., Halpin, J. A., Whittaker, J. M., Daczko, N. R., & Wainman, C. C. (2021). Provenance of Upper
2532 Jurassic–Lower Cretaceous strata in the Mentelle Basin, southwestern Australia, reveals a trans-
2533 Gondwanan fluvial pathway. *Gondwana Research*, 93, 128-141.
2534 <https://doi.org/10.1016/j.gr.2020.12.032>

2535 Marschalek, J. W., Zurli, L., Talarico, F., van de Fliedert, T., Vermeesch, P., Carter, A., et al. (2021). A large West
2536 Antarctic Ice Sheet explains early Neogene sea-level amplitude. *Nature*, 600(7889), 450-455.
2537 <https://doi.org/10.1038/s41586-021-04148-0>

2538 Marschall, H. R., Hawkesworth, C. J., & Leat, P. T. (2013). Mesoproterozoic subduction under the eastern
2539 edge of the Kalahari-Grunehogna Craton preceding Rodinia assembly: The Ritscherflya detrital zircon
2540 record, Ahlmannryggen (Dronning Maud Land, Antarctica). *Precambrian Research*, 236, 31-45.
2541 <https://doi.org/10.1016/j.precamres.2013.07.006>

2542 Matsuka, K. (2011). Pitfalls in radar diagnosis of ice-sheet bed conditions: Lessons from englacial
2543 attenuation models. *Geophysical Research Letters*, 38(5). <https://doi.org/10.1029/2010GL046205>

2544 Mawson, D. (1928). Unsolved Problems of Antarctic Exploration and Research. *American Geographical*
2545 *Society Special Publication*, 7, 253-266.

2546 Mawson, D. (1940). *Sedimentary Rocks, Australasian Antarctic Expedition, 1911-1914, Sci. Rept., Ser. A,*
2547 *Geol., vol. 4, pt. 11, pp. 347-367.* Retrieved from
2548 McCormack, F. S., Roberts, J. L., Dow, C. F., Stål, T., Halpin, J. A., Reading, A. M., & Siegert, M. J. (2022). Fine-
2549 Scale Geothermal Heat Flow in Antarctica Can Increase Simulated Subglacial Melt Estimates.
2550 *Geophysical Research Letters*, 49(15), e2022GL098539. <https://doi.org/10.1029/2022GL098539>
2551 McKay, R., Naish, T., Carter, L., Riesselman, C., Dunbar, R., Sjunneskog, C., et al. (2012). Antarctic and
2552 Southern Ocean influences on Late Pliocene global cooling. *Proceedings of the National Academy of*
2553 *Sciences of the United States of America*, 109(17), 6423-6428.
2554 <https://doi.org/10.1073/pnas.1112248109>
2555 McKay, R., Naish, T., Powell, R., Barrett, P., Scherer, R., Talarico, F., et al. (2012). Pleistocene variability of
2556 Antarctic Ice Sheet extent in the Ross Embayment. *Quaternary Science Reviews*, 34, 93-112.
2557 <https://doi.org/10.1016/j.quascirev.2011.12.012>
2558 McKay, R. M., Barrett, P. J., Levy, R. S., Naish, T. R., Golledge, N. R., & Pyne, A. (2016). Antarctic Cenozoic
2559 climate history from sedimentary records: ANDRILL and beyond. *Philosophical Transactions of the*
2560 *Royal Society A: Mathematical, Physical and Engineering Sciences*, 374(2059).
2561 <https://doi.org/10.1098/rsta.2014.0301>
2562 McLean, M. A., Rawling, T. J., Betts, P. G., Phillips, G., & Wilson, C. J. L. (2008). Three-dimensional inversion
2563 modelling of a Neoproterozoic basin in the southern Prince Charles Mountains, East Antarctica.
2564 *Tectonophysics*, 456(3-4), 180-193. <https://doi.org/10.1016/j.tecto.2008.04.023>
2565 McLean, M. A., Wilson, C. J. L., Boger, S. D., Betts, P. G., Rawling, T. J., & Damaske, D. (2009). Basement
2566 interpretations from airborne magnetic and gravity data over the Lambert rift region of east
2567 Antarctica. *Journal of Geophysical Research B: Solid Earth*, 114(6).
2568 <https://doi.org/10.1029/2008JB005650>
2569 McLoughlin, S., & Drinnan, A. N. (1997). Revised stratigraphy of the Permian Bainmedart Coal Measures,
2570 northern Prince Charles Mountains, East Antarctica. *Geological Magazine*, 134(3), 335-353.
2571 <https://doi.org/10.1017/S0016756897006870>
2572 McMahan, K. L., & Lackie, M. A. (2006). Seismic reflection studies of the Amery Ice Shelf, East Antarctica:
2573 delineating meteoric and marine ice. *Geophysical Journal International*, 166(2), 757-766.
2574 <https://doi.org/10.1111/j.1365-246X.2006.03043.x>
2575 Mieth, M., & Jokat, W. (2014). New aeromagnetic view of the geological fabric of southern Dronning Maud
2576 Land and Coats Land, East Antarctica. *Gondwana Research*, 25(1), 358-367.
2577 <https://doi.org/10.1016/j.gr.2013.04.003>
2578 Mikhalsky, E. V., Tkacheva, D. A., Skublov, S. G., Leitchenkov, G. L., Rodionov, N. V., Kapitonov, I. N., &
2579 Kunakkuzin, E. L. (2020). Low-grade Sandow Group metasediments of the Denman Glacier area (East
2580 Antarctica): Chemical composition, age and provenance from U–Pb detrital zircon data, with some
2581 palaeotectonic implications. *Polar Science*, 26, 100587. <https://doi.org/10.1016/j.polar.2020.100587>
2582 Mishra, D. C., Chandra Sekhar, D. V., Venkata Raju, D. C., & Vijaya Kumar, V. (1999). Crustal structure based
2583 on gravity-magnetic modelling constrained from seismic studies under Lambert Rift, Antarctica and
2584 Godavari and Mahanadi rifts, India and their interrelationship. *Earth and Planetary Science Letters*,
2585 172(3-4), 287-300. [https://doi.org/10.1016/S0012-821X\(99\)00212-5](https://doi.org/10.1016/S0012-821X(99)00212-5)
2586 Montelli, A., Gulick, S. P. S., Fernandez, R., Frederick, B. C., Shevenell, A. E., Leventer, A., & Blankenship, D. D.
2587 (2019). Seismic stratigraphy of the Sabrina Coast shelf, East Antarctica: Early history of dynamic
2588 meltwater-rich glaciations. *GSA Bulletin*, 132(3-4), 545-561. <https://doi.org/10.1130/b35100.1>
2589 Morlighem, M. (2020). *MEaSURES BedMachine Antarctica, Version 2.*
2590 <https://doi.org/10.5067/E1QL9HFQ7A8M>
2591 Morlighem, M., Rignot, E., Binder, T., Blankenship, D., Drews, R., Eagles, G., et al. (2020). Deep glacial troughs
2592 and stabilizing ridges unveiled beneath the margins of the Antarctic ice sheet. *Nature Geoscience*,
2593 13(2), 132-137. <https://doi.org/10.1038/s41561-019-0510-8>
2594 Mouginit, J., Rignot, E., & Scheuchl, B. (2019). Continent-Wide, Interferometric SAR Phase, Mapping of
2595 Antarctic Ice Velocity. *Geophysical Research Letters*, 46(16), 9710-9718.
2596 <https://doi.org/10.1029/2019gl083826>

2597 Mulder, J. A., Halpin, J. A., Daczko, N. R., Orth, K., Meffre, S., Thompson, J. M., & Morrissey, L. J. (2019). A
2598 Multiproxy provenance approach to uncovering the assembly of East Gondwana in Antarctica.
2599 *Geology*, 47(7), 645-649. <https://doi.org/10.1130/g45952.1>

2600 Müller, R. D., Zahirovic, S., Williams, S. E., Cannon, J., Seton, M., Bower, D. J., et al. (2019). A Global Plate
2601 Model Including Lithospheric Deformation Along Major Rifts and Orogens Since the Triassic.
2602 *Tectonics*, 38(6), 1884-1907. <https://doi.org/10.1029/2018TC005462>

2603 Muto, A., Alley, R. B., Parizek, B. R., & Anandakrishnan, S. (2019). Bed-type variability and till (dis)continuity
2604 beneath Thwaites Glacier, West Antarctica. *Annals of Glaciology*, 60(80), 82-90.
2605 <https://doi.org/10.1017/aog.2019.32>

2606 Muto, A., Anandakrishnan, S., Alley, R. B., Horgan, H. J., Parizek, B. R., Koellner, S., et al. (2019). Relating bed
2607 character and subglacial morphology using seismic data from Thwaites Glacier, West Antarctica.
2608 *Earth and Planetary Science Letters*, 507, 199-206. <https://doi.org/10.1016/j.epsl.2018.12.008>

2609 Muto, A., Peters, L. E., Gohl, K., Sasgen, I., Alley, R. B., Anandakrishnan, S., & Riverman, K. L. (2016).
2610 Subglacial bathymetry and sediment distribution beneath Pine Island Glacier ice shelf modeled using
2611 aerogravity and in situ geophysical data: New results. *Earth and Planetary Science Letters*, 433, 63-
2612 75. <https://doi.org/10.1016/j.epsl.2015.10.037>

2613 Naish, T., Powell, R., Levy, R., Wilson, G., Scherer, R., Talarico, F., et al. (2009). Obliquity-paced Pliocene West
2614 Antarctic ice sheet oscillations. *Nature*, 458(7236), 322-328. <https://doi.org/10.1038/nature07867>

2615 Naylor, S., Dean, K., & Siegert, M. (2008). The IGY and the ice sheet: surveying Antarctica. *Journal of*
2616 *Historical Geography*, 34(4), 574-595. <https://doi.org/10.1016/j.jhg.2008.07.001>

2617 Noble, T. L., Rohling, E. J., Aitken, A. R. A., Bostock, H. C., Chase, Z., Gomez, N., et al. (2020). The Sensitivity of
2618 the Antarctic Ice Sheet to a Changing Climate: Past, Present, and Future. *Reviews of Geophysics*,
2619 58(4), e2019RG000663. <https://doi.org/10.1029/2019RG000663>

2620 Olesen, A., Ferraccioli, F., Forsberg, R., Jordan, T., Matsuoka, K., Zakrajsek, A., & Ghidella, M. (2020).
2621 *Processed line aerogravity data over the Recovery Lakes region and interior Dronning Maud Land,*
2622 *East Antarctica (2013) [Data set]. UK Polar Data Centre, Natural Environment Research Council, UK*
2623 *Research & Innovation.* <https://doi.org/10.5285/28E3B21F-BF4B-46A6-8559-F69D69C63A48>

2624 Olierook, H. K. H., Jourdan, F., Merle, R. E., Timms, N. E., Kuznir, N., & Muhling, J. R. (2016). Bunbury Basalt:
2625 Gondwana breakup products or earliest vestiges of the Kerguelen mantle plume? *Earth and*
2626 *Planetary Science Letters*, 440, 20-32. <https://doi.org/10.1016/j.epsl.2016.02.008>

2627 Paden, J., Akins, T., Dunson, D., Allen, C., & Gogineni, P. (2010). Ice-sheet bed 3-D tomography. *Journal of*
2628 *Glaciology*, 56(195), 3-11. <https://doi.org/10.3189/002214310791190811>

2629 Pappa, F., Ebbing, J., & Ferraccioli, F. (2019). Moho Depths of Antarctica: Comparison of Seismic, Gravity, and
2630 Isostatic Results. *Geochemistry, Geophysics, Geosystems*, 20(3), 1629-1645.
2631 <https://doi.org/10.1029/2018GC008111>

2632 Pappa, F., Ebbing, J., Ferraccioli, F., & van der Wal, W. (2019). Modeling Satellite Gravity Gradient Data to
2633 Derive Density, Temperature, and Viscosity Structure of the Antarctic Lithosphere. *Journal of*
2634 *Geophysical Research: Solid Earth*, 124(11), 12053-12076. <https://doi.org/10.1029/2019jb017997>

2635 Paxman, G. J. G., Gasson, E. G. W., Jamieson, S. S. R., Bentley, M. J., & Ferraccioli, F. (2020). Long-Term
2636 Increase in Antarctic Ice Sheet Vulnerability Driven by Bed Topography Evolution. *Geophysical*
2637 *Research Letters*, 47(20), e2020GL090003. <https://doi.org/10.1029/2020GL090003>

2638 Paxman, G. J. G., Jamieson, S. S. R., Ferraccioli, F., Bentley, M. J., Forsberg, R., Ross, N., et al. (2017). Uplift
2639 and tilting of the Shackleton Range in East Antarctica driven by glacial erosion and normal faulting.
2640 *Journal of Geophysical Research: Solid Earth*, 122(3), 2390-2408.
2641 <https://doi.org/10.1002/2016JB013841>

2642 Paxman, G. J. G., Jamieson, S. S. R., Ferraccioli, F., Jordan, T. A., Bentley, M. J., Ross, N., et al. (2019).
2643 Subglacial Geology and Geomorphology of the Pensacola-Pole Basin, East Antarctica. *Geochemistry,*
2644 *Geophysics, Geosystems*, 20(6), 2786-2807. <https://doi.org/10.1029/2018gc008126>

2645 Paxman, G. J. G., Jamieson, S. S. R., Hochmuth, K., Gohl, K., Bentley, M. J., Leitchenkov, G., & Ferraccioli, F.
2646 (2019). Reconstructions of Antarctic topography since the Eocene–Oligocene boundary.

2647 *Palaeogeography, Palaeoclimatology, Palaeoecology*, 535, 109346.
2648 <https://doi.org/10.1016/j.palaeo.2019.109346>

2649 Pérez, L. F., Santis, L. D., McKay, R. M., Larter, R. D., Ash, J., Bart, P. J., et al. (2021). Early and middle Miocene
2650 ice sheet dynamics in the Ross Sea: Results from integrated core-log-seismic interpretation. *GSA*
2651 *Bulletin*, 134(1-2), 348-370. <https://doi.org/10.1130/b35814.1>

2652 Person, M., Bense, V., Cohen, D., & Banerjee, A. (2012). Models of ice-sheet hydrogeologic interactions: A
2653 review. *Geofluids*, 12(1), 58-78. <https://doi.org/10.1111/j.1468-8123.2011.00360.x>

2654 Person, M., McIntosh, J., Bense, V., & Remenda, V. H. (2007). Pleistocene hydrology of North America: The
2655 role of ice sheets in reorganizing groundwater flow systems. *Reviews of Geophysics*, 45(3).
2656 <https://doi.org/10.1029/2006rg000206>

2657 Peters, L. E., Anandkrishnan, S., Alley, R. B., Winberry, J. P., Voigt, D. E., Smith, A. M., & Morse, D. L. (2006).
2658 Subglacial sediments as a control on the onset and location of two Siple Coast ice streams, West
2659 Antarctica. *Journal of Geophysical Research: Solid Earth*, 111(1).
2660 <https://doi.org/10.1029/2005jb003766>

2661 Peters, M. E., Blankenship, D. D., Carter, S. P., Kempf, S. D., Young, D. A., & Holt, J. W. (2007). Along-Track
2662 Focusing of Airborne Radar Sounding Data From West Antarctica for Improving Basal Reflection
2663 Analysis and Layer Detection. *IEEE Transactions on Geoscience and Remote Sensing*, 45(9), 2725-
2664 2736. <https://doi.org/10.1109/tgrs.2007.897416>

2665 Phillips, G., & Läufer, A. L. (2009). Brittle deformation relating to the Carboniferous–Cretaceous evolution of
2666 the Lambert Graben, East Antarctica: A precursor for Cenozoic relief development in an intraplate
2667 and glaciated region. *Tectonophysics*, 471(3–4), 216-224.
2668 <http://dx.doi.org/10.1016/j.tecto.2009.02.012>

2669 Pollard, D., & DeConto, R. M. (2020). Continuous simulations over the last 40 million years with a coupled
2670 Antarctic ice sheet-sediment model. *Palaeogeography, Palaeoclimatology, Palaeoecology*, 537,
2671 109374. <https://doi.org/10.1016/j.palaeo.2019.109374>

2672 Pourpoint, M., Wiens, D., Shen, W., Aster, R. C., Nyblade, A., & Wilson, T. J. (2019). *Constraints on shallow*
2673 *subglacial structure beneath Thwaites Glacier from joint inversion of receiver function and surface*
2674 *wave data. abstract #NS11B-0632. Paper presented at the AGU Fall Meeting 2019 Abstracts*
2675 <https://ui.adsabs.harvard.edu/abs/2019AGUFMNS11B0632P>.

2676 Pyle, M. L., Wiens, D. A., Nyblade, A. A., & Anandkrishnan, S. (2010). Crustal structure of the Transantarctic
2677 Mountains near the Ross Sea from ambient seismic noise tomography. *Journal of Geophysical*
2678 *Research: Solid Earth*, 115(11). <https://doi.org/10.1029/2009jb007081>

2679 Reid, A. B. (1980). Aeromagnetic survey design. *GEOPHYSICS*, 45(5), 973-976.
2680 <https://doi.org/10.1190/1.1441102>

2681 Reid, A. B., Allsop, J. M., Granser, H., Millett, A. J., & Somerton, I. W. (1990). Magnetic interpretation in three
2682 dimensions using Euler deconvolution. *GEOPHYSICS*, 55(1), 80-91.
2683 <https://doi.org/10.1190/1.1442774>

2684 Riedel, S., Jacobs, J., & Jokat, W. (2013). Interpretation of new regional aeromagnetic data over Dronning
2685 Maud Land (East Antarctica). *Tectonophysics*, 585, 161-171.
2686 <https://doi.org/10.1016/j.tecto.2012.10.011>

2687 Riedel, S., Jokat, W., & Steinhage, D. (2012). Mapping tectonic provinces with airborne gravity and radar data
2688 in Dronning Maud Land, East Antarctica. *Geophysical Journal International*, 189(1), 414-427.
2689 <https://doi.org/10.1111/j.1365-246X.2012.05363.x>

2690 Riley, T. R., Flowerdew, M. J., & Whitehouse, M. J. (2012). Chrono- and lithostratigraphy of a Mesozoic-
2691 Tertiary fore- to intra-arc basin: Adelaide Island, Antarctic Peninsula. *Geological Magazine*, 149(5),
2692 768-782. <https://doi.org/10.1017/S0016756811001002>

2693 Riley, T. R., Jordan, T. A., Leat, P. T., Curtis, M. L., & Millar, I. L. (2020). Magmatism of the Weddell Sea rift
2694 system in Antarctica: Implications for the age and mechanism of rifting and early stage Gondwana
2695 breakup. *Gondwana Research*, 79, 185-196. <https://doi.org/10.1016/j.gr.2019.09.014>

2696 Rippin, D. M., Bingham, R. G., Jordan, T. A., Wright, A. P., Ross, N., Corr, H. F. J., et al. (2014). Basal roughness
2697 of the Institute and Möller Ice Streams, West Antarctica: Process determination and landscape
2698 interpretation. *Geomorphology*, 214, 139-147. <https://doi.org/10.1016/j.geomorph.2014.01.021>
2699 Robin, G. d. Q. (1958). Glaciology III: Seismic Shooting and Related Investigations. *Norwegian–British–
2700 Swedish Antarctic Expedition, 1949–52, Scientific Results*, 5.
2701 Rogenhagen, J., Jokat, W., Hinz, K., & Kristoffersen, Y. (2004). Improved seismic stratigraphy of the Mesozoic
2702 Weddell Sea. *Marine Geophysical Research*, 25(3-4), 265-282. [https://doi.org/10.1007/s11001-005-
2704 1335-y](https://doi.org/10.1007/s11001-005-
2703 1335-y)
2705 Rolland, Y., Bernet, M., van der Beek, P., Gautheron, C., Duclaux, G., Bascou, J., et al. (2019). Late Paleozoic
2706 Ice Age glaciers shaped East Antarctica landscape. *Earth and Planetary Science Letters*, 506, 123-133.
2707 <https://doi.org/10.1016/j.epsl.2018.10.044>
2708 Rosier, S. H. R., Hofstede, C., Brisbourne, A. M., Hattermann, T., Nicholls, K. W., Davis, P. E. D., et al. (2018). A
2709 New Bathymetry for the Southeastern Filchner-Ronne Ice Shelf: Implications for Modern
2710 Oceanographic Processes and Glacial History. *Journal of Geophysical Research: Oceans*, 123(7), 4610-
2711 4623. <https://doi.org/10.1029/2018jc013982>
2712 Ruppel, A., Jacobs, J., Eagles, G., Läuffer, A., & Jokat, W. (2018). New geophysical data from a key region in
2713 East Antarctica: Estimates for the spatial extent of the Tonian Oceanic Arc Super Terrane (TOAST).
2714 *Gondwana Research*, 59, 97-107. <https://doi.org/10.1016/j.gr.2018.02.019>
2715 Salvini, F., Brancolini, G., Busetti, M., Storti, F., Mazzarini, F., & Coren, F. (1997). Cenozoic geodynamics of the
2716 Ross Sea region, Antarctica: Crustal extension, intraplate strike-slip faulting, and tectonic
2717 inheritance. *Journal of Geophysical Research B: Solid Earth*, 102(11), 24669-24696.
2718 <https://doi.org/10.1029/97jb01643>
2719 Sanchez, G., Halpin, J. A., Gard, M., Hasterok, D., Stål, T., Raimondo, T., et al. (2021). PetroChron Antarctica:
2720 A Geological Database for Interdisciplinary Use. *Geochemistry, Geophysics, Geosystems*, 22(12).
2721 <https://doi.org/10.1029/2021gc010154>
2722 Sandwell, D. T., Müller, R. D., Smith, W. H. F., Garcia, E., & Francis, R. (2014). New global marine gravity
2723 model from CryoSat-2 and Jason-1 reveals buried tectonic structure. *Science*, 346(6205), 65-67.
2724 <https://doi.org/10.1126/science.1258213>
2725 Sauermlch, I., Whittaker, J. M., Bijl, P. K., Totterdell, J. M., & Jokat, W. (2019). Tectonic, Oceanographic, and
2726 Climatic Controls on the Cretaceous-Cenozoic Sedimentary Record of the Australian-Antarctic Basin.
2727 *Journal of Geophysical Research: Solid Earth*, 124(8), 7699-7724.
2728 <https://doi.org/10.1029/2018JB016683>
2729 Sauli, C., Sorlien, C., Busetti, M., De Santis, L., Geletti, R., Wardell, N., & Luyendyk, B. P. (2021). Neogene
2730 Development of the Terror Rift, Western Ross Sea, Antarctica. *Geochemistry, Geophysics,
2731 Geosystems*, 22(3). <https://doi.org/10.1029/2020GC009076>
2732 Scambos, T. A., Bell, R. E., Alley, R. B., Anandakrishnan, S., Bromwich, D. H., Brunt, K., et al. (2017). How
2733 much, how fast?: A science review and outlook for research on the instability of Antarctica's
2734 Thwaites Glacier in the 21st century. *Global and Planetary Change*, 153, 16-34.
2735 <https://doi.org/10.1016/j.gloplacha.2017.04.008>
2736 Scanlan, K. M., Buhl, D. P., & Blankenship, D. D. (2022). Polarimetric Airborne Radar Sounding as an Approach
2737 to Characterizing Subglacial Röhrlisberger Channels. *IEEE Journal of Selected Topics in Applied Earth
2738 Observations and Remote Sensing*, 15, 4455-4467. <https://doi.org/10.1109/JSTARS.2022.3174473>
2739 Scheinert, M., Ferraccioli, F., Schwabe, J., Bell, R., Studinger, M., Damaske, D., et al. (2016). New Antarctic
2740 gravity anomaly grid for enhanced geodetic and geophysical studies in Antarctica. *Geophysical
2741 Research Letters*, 43(2), 600-610. <https://doi.org/10.1002/2015gl067439>
2742 Scher, H. D., & Martin, E. E. (2006). Timing and climatic consequences of the opening of Drake Passage.
2743 *Science*, 312(5772), 428-430. <https://doi.org/10.1126/science.1120044>
2744 Scher, H. D., Whittaker, J. M., Williams, S. E., Latimer, J. C., Kordesch, W. E. C., & Delaney, M. L. (2015). Onset
2745 of Antarctic Circumpolar Current 30 million years ago as Tasmanian Gateway aligned with westerlies.
Nature, 523(7562), 580-583. <https://doi.org/10.1038/nature14598>

2746 Schoof, C. (2010). Ice-sheet acceleration driven by melt supply variability. *Nature*, 468(7325), 803-806.
2747 <https://doi.org/10.1038/nature09618>

2748 Schroeder, D. M., Bingham, R. G., Blankenship, D. D., Christianson, K., Eisen, O., Flowers, G. E., et al. (2020).
2749 Five decades of radioglaciology. *Annals of Glaciology*, 61(81), 1-13.
2750 <https://doi.org/10.1017/aog.2020.11>

2751 Schroeder, D. M., Blankenship, D. D., Raney, R. K., & Grima, C. (2015). Estimating Subglacial Water Geometry
2752 Using Radar Bed Echo Specularity: Application to Thwaites Glacier, West Antarctica. *IEEE Geoscience
2753 and Remote Sensing Letters*, 12(3), 443-447. <https://doi.org/10.1109/lgrs.2014.2337878>

2754 Schroeder, D. M., Blankenship, D. D., & Young, D. A. (2013). Evidence for a water system transition beneath
2755 Thwaites Glacier, West Antarctica. *Proceedings of the National Academy of Sciences*, 110(30), 12225-
2756 12228. <https://doi.org/10.1073/pnas.1302828110>

2757 Schroeder, D. M., Dowdeswell, J. A., Siegert, M. J., Bingham, R. G., Chu, W., MacKie, E. J., et al. (2019).
2758 Multidecadal observations of the Antarctic ice sheet from restored analog radar records.
2759 *Proceedings of the National Academy of Sciences*, 116(38), 18867-18873.
2760 <https://doi.org/10.1073/pnas.1821646116>

2761 Shapiro, N. M., Campillo, M., Stehly, L., & Ritzwoller, M. H. (2005). High-Resolution Surface-Wave
2762 Tomography from Ambient Seismic Noise. *Science*, 307(5715), 1615-1618.
2763 <https://doi.org/10.1126/science.1108339>

2764 Shen, W., Wiens, D., Stern, T., Anandakrishnan, S., Aster, R., Dalziel, I., et al. (2017). Seismic evidence for
2765 lithospheric foundering beneath the southern Transantarctic Mountains, Antarctica. *Geology*, 46.
2766 <https://doi.org/10.1130/G39555.1>

2767 Shen, W., Wiens, D. A., Anandakrishnan, S., Aster, R. C., Gerstoft, P., Bromirski, P. D., et al. (2018). The Crust
2768 and Upper Mantle Structure of Central and West Antarctica From Bayesian Inversion of Rayleigh
2769 Wave and Receiver Functions. *Journal of Geophysical Research: Solid Earth*, 123(9), 7824-7849.
2770 <https://doi.org/10.1029/2017jb015346>

2771 Shepherd, T., Bamber, J. L., & Ferraccioli, F. (2006). Subglacial geology in Coats Land, East Antarctica,
2772 revealed by airborne magnetics and radar sounding. *Earth and Planetary Science Letters*, 244(1),
2773 323-335. <https://doi.org/10.1016/j.epsl.2006.01.068>

2774 Siddoway, C. S. (2008). Tectonics of the West Antarctic Rift System: new light on the history and dynamics of
2775 distributed intracontinental extension. *Antarctica: A keystone in a changing world*, 91-114.
2776 <https://doi.org/10.3133/ofr20071047KP09>

2777 Siddoway, C. S., Baldwin, S. L., Fitzgerald, P. G., Fanning, C. M., & Luyendyk, B. P. (2004). Ross Sea mylonites
2778 and the timing of intracontinental extension within the West Antarctic rift system. *Geology*, 32(1),
2779 57-60. <https://doi.org/10.1130/G20005.1>

2780 Siegert, M., Popov, S., & Studinger, M. (2011). Vostok Subglacial Lake: A Review of Geophysical Data
2781 Regarding Its Discovery and Topographic Setting. *Washington DC American Geophysical Union
2782 Geophysical Monograph Series*, 192, 45-60. <https://doi.org/10.1029/2010GM000934>

2783 Siegert, M. J., Kulesa, B., Bougamont, M., Christoffersen, P., Key, K., Andersen, K. R., et al. (2018). Antarctic
2784 subglacial groundwater: A concept paper on its measurement and potential influence on ice flow.
2785 *Geological Society Special Publication*, 461, 197-213. <https://doi.org/10.1144/sp461.8>

2786 Siegert, M. J., Ross, N., Li, J., Schroeder, D. M., Rippin, D., Ashmore, D., et al. (2016). Subglacial controls on
2787 the flow of Institute Ice Stream, West Antarctica. *Annals of Glaciology*, 57(73), 19-24.
2788 <https://doi.org/10.1017/aog.2016.17>

2789 Siegert, M. J., Taylor, J., & Payne, A. J. (2005). Spectral roughness of subglacial topography and implications
2790 for former ice-sheet dynamics in East Antarctica. *Global and Planetary Change*, 45(1), 249-263.
2791 <https://doi.org/10.1016/j.gloplacha.2004.09.008>

2792 Smellie, J. L., & Collerson, K. D. (2021). Chapter 5.5 Gaussberg: volcanology and petrology. *Volcanism in
2793 Antarctica: 200 Million Years of Subduction, Rifting and Continental Break-up*, 0.
2794 <https://doi.org/10.1144/m55-2018-85>

2795 Smith, A. M. (1997). Basal conditions on Rutford Ice Stream, West Antarctica, from seismic observations.
2796 *Journal of Geophysical Research: Solid Earth*, 102(B1), 543-552. <https://doi.org/10.1029/96JB02933>

2797 Smith, A. M., Jordan, T. A., Ferraccioli, F., & Bingham, R. G. (2013). Influence of subglacial conditions on ice
2798 stream dynamics: Seismic and potential field data from Pine Island Glacier, West Antarctica. *Journal*
2799 *of Geophysical Research: Solid Earth*, 118(4), 1471-1482. <https://doi.org/10.1029/2012jb009582>

2800 Smith, C., Warny, S., Shevenell, A. E., Gulick, S. P. S., & Leventer, A. (2019). New species from the Sabrina
2801 Flora: an early Paleogene pollen and spore assemblage from the Sabrina Coast, East Antarctica.
2802 *Palynology*, 43(4), 650-659. <https://doi.org/10.1080/01916122.2018.1471422>

2803 Smith, E. C., Hattermann, T., Kuhn, G., Gaedicke, C., Berger, S., Drews, R., et al. (2020). Detailed Seismic
2804 Bathymetry Beneath Ekström Ice Shelf, Antarctica: Implications for Glacial History and Ice-Ocean
2805 Interaction. *Geophysical Research Letters*, 47(10), e2019GL086187.
2806 <https://doi.org/10.1029/2019GL086187>

2807 Smith, J. A., Graham, A. G. C., Post, A. L., Hillenbrand, C.-D., Bart, P. J., & Powell, R. D. (2019). The marine
2808 geological imprint of Antarctic ice shelves. *Nature Communications*, 10(1), 5635.
2809 <https://doi.org/10.1038/s41467-019-13496-5>

2810 Song, T., & Cawood, P. A. (2000). Structural styles in the Perth Basin associated with the Mesozoic break-up
2811 of Greater India and Australia. *Tectonophysics*, 317(1-2), 55-72. [https://doi.org/10.1016/S0040-](https://doi.org/10.1016/S0040-1951(99)00273-5)
2812 [1951\(99\)00273-5](https://doi.org/10.1016/S0040-1951(99)00273-5)

2813 Stagg, H., Colwel, J., Direen, N., O'Brien, P., Bernardel, G., Borissova, I., et al. (2004). Geology of the
2814 Continental Margin of Enderby and Mac. Robertson Lands, East Antarctica: Insights from a Regional
2815 Data Set. *Marine Geophysical Researches*, 25, 183-219. [https://doi.org/10.1007/s11001-005-1316-](https://doi.org/10.1007/s11001-005-1316-1)
2816 [1](https://doi.org/10.1007/s11001-005-1316-1)

2817 Stål, T., Reading, A. M., Halpin, J. A., & Whittaker, J. M. (2019). A Multivariate Approach for Mapping
2818 Lithospheric Domain Boundaries in East Antarctica. *Geophysical Research Letters*, 46(17-18), 10404-
2819 10416. <https://doi.org/10.1029/2019GL083453>

2820 Straume, E. O., Gaina, C., Medvedev, S., Hochmuth, K., Gohl, K., Whittaker, J. M., et al. (2019). GlobSed:
2821 Updated Total Sediment Thickness in the World's Oceans. *Geochemistry, Geophysics, Geosystems*,
2822 20(4), 1756-1772. <https://doi.org/10.1029/2018GC008115>

2823 Studinger, M., Bell, R., & Frearson, N. (2008). Comparison of AIRGrav and GT-1A airborne gravimeters for
2824 research applications. *GEOPHYSICS*, 73(6), I51-I61. <https://doi.org/10.1190/1.2969664>

2825 Studinger, M., Bell, R. E., Blankenship, D. D., Finn, C. A., Arko, R. A., Morse, D. L., & Joughin, I. (2001).
2826 Subglacial sediments: A regional geological template for iceflow in West Antarctica. *Geophysical*
2827 *Research Letters*, 28(18), 3493-3496. <https://doi.org/10.1029/2000GL011788>

2828 Studinger, M., Bell, R. E., Buck, W. R., Karner, G. D., & Blankenship, D. D. (2004). Sub-ice geology inland of the
2829 Transantarctic Mountains in light of new aerogeophysical data. *Earth and Planetary Science Letters*,
2830 220(3-4), 391-408. [https://doi.org/10.1016/S0012-821X\(04\)00066-4](https://doi.org/10.1016/S0012-821X(04)00066-4)

2831 Studinger, M., Karner, G. D., Bell, R. E., Levin, V., Raymond, C. A., & A. Tikku, A. (2003). Geophysical models
2832 for the tectonic framework of the Lake Vostok region, East Antarctica. *Earth and Planetary Science*
2833 *Letters*, 216(4), 663-677. [https://doi.org/10.1016/S0012-821X\(03\)00548-X](https://doi.org/10.1016/S0012-821X(03)00548-X)

2834 Swink, M., & Speier, C. (1999). Presenting geographic information: effects of data aggregation, dispersion,
2835 and users' spatial orientation. *Decision sciences*, 30(1), 169-195. [https://doi.org/10.1111/j.1540-](https://doi.org/10.1111/j.1540-5915.1999.tb01605.x)
2836 [5915.1999.tb01605.x](https://doi.org/10.1111/j.1540-5915.1999.tb01605.x)

2837 Tabacco, I. E., Cianfarra, P., Forieri, A., Salvini, F., & Zirizzotti, A. (2006). Physiography and tectonic setting of
2838 the subglacial lake district between Vostok and Belgica subglacial highlands (Antarctica). *Geophysical*
2839 *Journal International*, 165(3), 1029-1040. <https://doi.org/10.1111/j.1365-246X.2006.02954.x>

2840 Talalay, P., Li, X., Zhang, N., Fan, X., Sun, Y., Cao, P., et al. (2021). Antarctic subglacial drilling rig: Part II. Ice
2841 and Bedrock Electromechanical Drill (IBED). *Annals of Glaciology*, 62(84), 12-22.
2842 <https://doi.org/10.1017/aog.2020.38>

2843 Tankersley, M. D., Horgan, H. J., Siddoway, C. S., Caratori Tontini, F., & Tinto, K. J. (2022). Basement
2844 Topography and Sediment Thickness Beneath Antarctica's Ross Ice Shelf. *Geophysical Research*
2845 *Letters*, 49(10), e2021GL097371. <https://doi.org/10.1029/2021GL097371>

2846 Teisberg, T. O., Schroeder, D. M., Broome, A. L., Lurie, F., & Woo, D. (2022, 17-22 July 2022). *Development of*
2847 *a Uav-Borne Pulsed ICE-Penetrating Radar System*. Paper presented at the IGARSS 2022 - 2022 IEEE
2848 International Geoscience and Remote Sensing Symposium.
2849 <https://doi.org/10.1109/IGARSS46834.2022.9883583>

2850 Thomson, S. N., Reiners, P. W., Hemming, S. R., & Gehrels, G. E. (2013). The contribution of glacial erosion to
2851 shaping the hidden landscape of East Antarctica. *Nature Geoscience*, 6(3), 203-207.
2852 <https://doi.org/10.1038/ngeo1722>

2853 Tinto, K. J., Padman, L., Siddoway, C. S., Springer, S. R., Fricker, H. A., Das, I., et al. (2019). Ross Ice Shelf
2854 response to climate driven by the tectonic imprint on seafloor bathymetry. *Nature Geoscience*,
2855 12(6), 441-449. <https://doi.org/10.1038/s41561-019-0370-2>

2856 Tochilin, C. J., Reiners, P. W., Thomson, S. N., Gehrels, G. E., Hemming, S. R., & Pierce, E. L. (2012). Erosional
2857 history of the Prydz Bay sector of East Antarctica from detrital apatite and zircon geo-and
2858 thermochronology multidating. *Geochemistry, Geophysics, Geosystems*, 13(11).
2859 <https://doi.org/10.1029/2012GC004364>

2860 Trey, H., Cooper, A. K., Pellis, G., Della Vedova, B., Cochrane, G., Brancolini, G., & Makris, J. (1999). Transect
2861 across the West Antarctic rift system in the Ross Sea, Antarctica. *Tectonophysics*, 301(1-2), 61-74.
2862 [https://doi.org/10.1016/s0040-1951\(98\)00155-3](https://doi.org/10.1016/s0040-1951(98)00155-3)

2863 Tuckett, P. A., Ely, J. C., Sole, A. J., Livingstone, S. J., Davison, B. J., Melchior van Wessem, J., & Howard, J.
2864 (2019). Rapid accelerations of Antarctic Peninsula outlet glaciers driven by surface melt. *Nature*
2865 *Communications*, 10(1). <https://doi.org/10.1038/s41467-019-12039-2>

2866 Tulaczyk, S. M., & Foley, N. T. (2020). The role of electrical conductivity in radar wave reflection from glacier
2867 beds. *The Cryosphere*, 14(12), 4495-4506. <https://doi.org/10.5194/tc-14-4495-2020>

2868 Turchetti, S., Dean, K., Naylor, S., & Siegert, M. (2008). Accidents and Opportunities: A History of the Radio
2869 Echo-Sounding of Antarctica, 1958-79. *The British Journal for the History of Science*, 41(3), 417-444.
2870 <https://doi.org/10.1017/S0007087408000903>

2871 van de Lagemaat, S. H. A., Swart, M. L. A., Vaes, B., Kosters, M. E., Boschman, L. M., Burton-Johnson, A., et al.
2872 (2021). Subduction initiation in the Scotia Sea region and opening of the Drake Passage: When and
2873 why? *Earth-Science Reviews*, 215, 103551. <https://doi.org/10.1016/j.earscirev.2021.103551>

2874 van Wyk de Vries, M., Bingham, R. G., Hein, A. S., Siegert, M. J., Jamieson, S. S. R., & White, D. A. (2018). A
2875 new volcanic province: an inventory of subglacial volcanoes in West Antarctica. In *Exploration of*
2876 *Subsurface Antarctica: Uncovering Past Changes and Modern Processes* (Vol. 461, pp. 0): The
2877 Geological Society of London. <https://doi.org/10.1144/sp461.7>

2878 Vaughan, D. G., Corr, H. F. J., Smith, A. M., Pritchard, H. D., & Shepherd, A. (2008). Flow-switching and water
2879 piracy between Rutford ice stream and Carlson inlet, West Antarctica. *Journal of Glaciology*, 54(184),
2880 41-48. <https://doi.org/10.3189/002214308784409125>

2881 Vaughan, D. G., Smith, A. M., Nath, P. C., & Meur, E. L. (2003). Acoustic impedance and basal shear stress
2882 beneath four Antarctic ice streams. *Annals of Glaciology*, 36, 225-232.
2883 <https://doi.org/10.3189/172756403781816437>

2884 Voigt, D. E., Peters, L. E., & Anandakrishnan, S. (2013). 'Georods': the development of a four-element
2885 geophone for improved seismic imaging of glaciers and ice sheets. *Annals of Glaciology*, 54(64), 142-
2886 148. <https://doi.org/10.3189/2013AoG64A432>

2887 Wannamaker, P., Hill, G., Stodt, J., Maris, V., Ogawa, Y., Selway, K., et al. (2017). Uplift of the central
2888 Transantarctic Mountains. *Nature Communications*, 8(1), 1588. <https://doi.org/10.1038/s41467-017-01577-2>

2889 Wannamaker, P. E., Stodt, J. A., Pellerin, L., Olsen, S. L., & Hall, D. B. (2004). Structure and thermal regime
2890 beneath the South Pole region, East Antarctica, from magnetotelluric measurements. *Geophysical*
2891 *Journal International*, 157(1), 36-54. <https://doi.org/10.1111/j.1365-246X.2004.02156.x>

2892 Wei, W., Blankenship, D. D., Greenbaum, J. S., Gourmelen, N., Dow, C. F., Richter, T. G., et al. (2020). Getz Ice
2893 Shelf melt enhanced by freshwater discharge from beneath the West Antarctic Ice Sheet. *The*
2894 *Cryosphere*, 14(4), 1399-1408. <https://doi.org/10.5194/tc-14-1399-2020>

2895

- 2896 Wenman, C. P., Harry, D. L., & Jha, S. (2020). Post Middle Miocene Tectonomagmatic and Stratigraphic
2897 Evolution of the Victoria Land Basin, West Antarctica. *Geochemistry, Geophysics, Geosystems*, 21(3).
2898 <https://doi.org/10.1029/2019GC008568>
- 2899 Whitehead, J., Quilty, P., Mckelvey, B. C., & O'Brien, P. (2006). A review of the Cenozoic stratigraphy and
2900 glacial history of the Lambert Graben—Prydz Bay region, East Antarctica. *Antarctic Science*, 18(1),
2901 83-99. <https://doi.org/10.1017/S0954102006000083>
- 2902 Willan, R. C. R. (2003). Provenance of Triassic-Cretaceous sandstones in the Antarctic Peninsula: Implications
2903 for terrane models during Gondwana breakup. *Journal of Sedimentary Research*, 73(6), 1062-1077.
2904 <https://doi.org/10.1306/050103731062>
- 2905 Williams, S. E., Whittaker, J. M., Granot, R., & Müller, D. R. (2013). Early India-Australia spreading history
2906 revealed by newly detected Mesozoic magnetic anomalies in the Perth Abyssal Plain. *Journal of*
2907 *Geophysical Research: Solid Earth*, 118(7), 3275-3284. <https://doi.org/10.1002/jgrb.50239>
- 2908 Williams, S. E., Whittaker, J. M., Halpin, J. A., & Müller, R. D. (2019). Australian-Antarctic breakup and
2909 seafloor spreading: Balancing geological and geophysical constraints. *Earth-Science Reviews*, 188, 41-
2910 58. <https://doi.org/10.1016/j.earscirev.2018.10.011>
- 2911 Wilson, C. G., Bond, C. E., & Shipley, T. F. (2019). How can geologic decision-making under uncertainty be
2912 improved? *Solid Earth*, 10(5), 1469-1488. <https://doi.org/10.5194/se-10-1469-2019>
- 2913 Wilson, D. S., Jamieson, S. S. R., Barrett, P. J., Leitchenkov, G., Gohl, K., & Larter, R. D. (2012). Antarctic
2914 topography at the Eocene-Oligocene boundary. *Palaeogeography, Palaeoclimatology,*
2915 *Palaeoecology*, 335-336, 24-34. <https://doi.org/10.1016/j.palaeo.2011.05.028>
- 2916 Wilson, D. S., & Luyendyk, B. P. (2006). Bedrock platforms within the Ross Embayment, West Antarctica:
2917 Hypotheses for ice sheet history, wave erosion, Cenozoic extension, and thermal subsidence.
2918 *Geochemistry, Geophysics, Geosystems*, 7(12). <https://doi.org/10.1029/2006GC001294>
- 2919 Wilson, G., Damaske, D., Moller, H. D., Tinto, K., & Jordan, T. (2007). The geological evolution of southern
2920 McMurdo Sound - New evidence from a high-resolution aeromagnetic survey. *Geophysical Journal*
2921 *International*, 170(1), 93-100. <https://doi.org/10.1111/j.1365-246X.2007.03395.x>
- 2922 Wilson, T. J. (1999). Cenozoic structural segmentation of the Transantarctic Mountains rift flank in southern
2923 Victoria Land. *Global and Planetary Change*, 23(1-4), 105-127. [https://doi.org/10.1016/S0921-
2924 8181\(99\)00053-3](https://doi.org/10.1016/S0921-8181(99)00053-3)
- 2925 Wright, A. P., Siegert, M. J., Le Brocq, A. M., & Gore, D. B. (2008). High sensitivity of subglacial hydrological
2926 pathways in Antarctica to small ice-sheet changes. *Geophysical Research Letters*, 35(17).
2927 <https://doi.org/10.1029/2008GL034937>
- 2928 Yakymchuk, C., Brown, C. R., Brown, M., Siddoway, C. S., Fanning, C. M., & Korhonen, F. J. (2015). Paleozoic
2929 evolution of western Marie Byrd Land, Antarctica. *Bulletin of the Geological Society of America*,
2930 127(9-10), 1464-1484. <https://doi.org/10.1130/b31136.1>
- 2931 Young, A., Flament, N., Maloney, K., Williams, S., Matthews, K., Zahirovic, S., & Müller, R. D. (2019). Global
2932 kinematics of tectonic plates and subduction zones since the late Paleozoic Era. *Geoscience*
2933 *Frontiers*, 10(3), 989-1013. <https://doi.org/10.1016/j.gsf.2018.05.011>
- 2934 Young, D. A., Blankenship, D. D., & Holt, J. W. (2017a). *Gravity disturbance data over central Marie Byrd*
2935 *Land, West Antarctica (GIMBLE.GGCMG2) U.S. Antarctic Program (USAP) Data Center*
2936 <https://doi.org/10.15784/601003>. <https://doi.org/10.15784/601003>.
- 2937 Young, D. A., Blankenship, D. D., & Holt, J. W. (2017b). *Magnetic anomaly data over central Marie Byrd Land,*
2938 *West Antarctica (GIMBLE.GMGEO2) U.S. Antarctic Program (USAP) Data Center.* doi:
2939 <https://doi.org/10.15784/601002>. <https://doi.org/10.15784/601002>.
- 2940 Young, D. A., Schroeder, D. M., Blankenship, D. D., Kempf, S. D., & Quartini, E. (2016). The distribution of
2941 basal water between Antarctic subglacial lakes from radar sounding. *Philosophical Transactions of*
2942 *the Royal Society A: Mathematical, Physical and Engineering Sciences*, 374(2059).
2943 <https://doi.org/10.1098/rsta.2014.0297>
- 2944 Young, T. J., Schroeder, D. M., Christoffersen, P., Lok, L. B., Nicholls, K. W., Brennan, P. V., et al. (2018).
2945 Resolving the internal and basal geometry of ice masses using imaging phase-sensitive radar. *Journal*
2946 *of Glaciology*, 64(246), 649-660. <https://doi.org/10.1017/jog.2018.54>

- 2947 Zhang, Y., Person, M., Voller, V., Cohen, D., McIntosh, J., & Grapenthin, R. (2018). Hydromechanical Impacts
2948 of Pleistocene Glaciations on Pore Fluid Pressure Evolution, Rock Failure, and Brine Migration Within
2949 Sedimentary Basins and the Crystalline Basement. *Water Resources Research*, 54(10), 7577-7602.
2950 <https://doi.org/10.1029/2017wr022464>
- 2951 Zhou, Z., Wiens, D. A., Shen, W., Aster, R. C., Nyblade, A., & Wilson, T. J. (2022). Radial Anisotropy and
2952 Sediment Thickness of West and Central Antarctica Estimated From Rayleigh and Love Wave
2953 Velocities. *Journal of Geophysical Research: Solid Earth*, 127(3), e2021JB022857.
2954 <https://doi.org/10.1029/2021JB022857>

2955 11 Figure Captions

2956

2957 Figure 1: a) Map of representative data coverage in Antarctica indicating outcropping geology (Cox et al.,
2958 2023) and locations of onshore and offshore drill core sites, onshore passive seismic stations, MT surveys
2959 (Hill, 2020), and active seismic surveys (line centroids) and marine seismic reflection lines. Bedmap3 data
2960 coverage mostly represents the presence of airborne RES data (Frémand, Fretwell, et al., 2022), and not all
2961 surveys measured gravity or magnetic data. A close-up of the data-rich Ross Island area is available in Figure
2962 S1. b) Approaches to detection and characterization of sedimentary basins, including the direct
2963 characterization of rocks from drillcore and outcrop, and indirect characterization from geophysical data. MT
2964 – magnetotelluric, RES – Radio Echo Sounding, UAV- Unmanned Aerial Vehicle, AUV – Autonomous
2965 Underwater Vehicle. Modified from Kennicutt et al. (2019).

2966 Figure 2: Key models and datasets for defining basin distribution in Antarctica including a) model of
2967 sedimentary basin likelihood from machine learning (Li et al., 2022), b) along-track roughness using airborne
2968 RES data compiled from Eisen et al. (2020) and additional data. Along track roughness v was calculated using
2969 a spatial technique as in Eisen et al. (2020), c) bed elevation and d) its large-scale spatial variability defined
2970 as standard deviation in a 30 km by 30 km window; both from BedMachine Antarctica (M. Morlighem, 2020).
2971 e) Airy isostatic residual gravity anomaly and f) spatial variability (standard deviation, 30 km window) of
2972 Bouguer gravity anomaly. Gravity data after AntGG (Scheinert et al., 2016) and additional data (Forsberg et
2973 al., 2018; Kvas et al., 2021; Olesen et al., 2020; G. J. G. Paxman et al., 2019; Sandwell et al., 2014; Tinto et al.,
2974 2019; D. A. Young et al., 2017a) g) magnetic field intensity anomaly and h) its large-scale spatial variability
2975 (standard deviation, 30 km window). Magnetic data after ADMAP-2 (A. V. Golynsky et al., 2018) and
2976 additional data (F. Ferraccioli et al., 2020; Forsberg et al., 2018; G. J. G. Paxman et al., 2019; Tinto et al.,
2977 2019; D. A. Young et al., 2017b). Major sedimentary basin regions used for classification are outlined. CWA –
2978 Central West Antarctica, EW – Ellsworth Whitmore, SC – Siple Coast, CL, TAM – Transantarctic Mountains,
2979 DML-Dronning Maud Land, GSM – Gamburtsev Subglacial Mountains, EML- Enderby-Mac Robertson Land,
2980 PEL – Princess Elizabeth Land, QML – Queen Mary Land, LD – Law Dome.

2981 Figure 3: Classification of geological bed type in Antarctica showing the main classes of Type 1 and Type 2
2982 basins, intra-basin volcanics, and crystalline basement, as well as regions of mixed class. Major sedimentary

2983 basin regions are outlined in grey. The coastline shows both the ice sheet grounding line and the ice shelf
2984 edge. Dashed lines A, B and C indicate locations of annular profiles (Fig 6). PL – Palmer Land, RFIS – Ronne-
2985 Filchner Ice Shelf, BI – Berkner Island, HG – Haag Block, EWM – Ellsworth Whitmore Mountains, PM –
2986 Pensacola Mountains, BSB – Byrd Subglacial Basin, MBL – Marie Byrd Land IB – Iselin Bank, CL – Coats Land,
2987 PPB – Pensacola-Pole Basin, RB – Recovery Basin, RSH – Recovery Subglacial Highlands, JS – Jutulstraumen,
2988 DML-Dronning Maud Land, WRT-West Ragnhild Trough, FSH – Fuji Subglacial Highlands, AIS – Amery Ice
2989 Shelf, SPCM – Southern Prince Charles Mountains, GSM – Gamburtsev Subglacial Mountains, SPB – South
2990 Pole Basin, LV – Lake Vostok, ASB – Aurora Subglacial Basin, VSB – Vincennes Subglacial Basin, WSB – Wilkes
2991 Subglacial Basin. An unannotated version of this figure is available in Figure S2.

2992 Figure 4: Relative effect sizes for selected datasets for a) crystalline basement vs Type 1 basins, b) crystalline
2993 basement vs Type 2 basins, c) Type 1 basins vs Type 2 basins. For each, datasets are ordered by Cohen's
2994 effect size indicating the ability of the dataset to discriminate those classes. The listing on the right highlights
2995 the datasets in rank order. Effect sizes above 0.8 may be considered a large effect, and below 0.5 a small
2996 effect.

2997 Figure 5: Interpreted ages for a) the base of the basin sequence and b) the top of the basin sequence.
2998 Locations of selected age information for volcanic, sedimentary, and metasedimentary rocks are derived
2999 from PetroChron Antarctica (Sanchez et al., 2021), and broadly indicate where basin ages are better
3000 constrained.

3001 Figure 6: Annular profiles of basin structure. a) shows the location of the three profiles A, B and C (see also
3002 Figure 3) at latitudes of 82.5°S, 77.5°S and 72.5°S. b), c) and d) show the profile data for profiles A, B and C
3003 respectively including in the upper panel the basin likelihood model of (Li et al., 2022). The lower panel
3004 shows bed topography (M. Morlighem, 2020) and base-of-basin elevation for several basin thickness model
3005 (Baranov et al., 2021; Haeger & Kaban, 2019; K. Hochmuth et al., 2020; Lindeque, Gohl, Wobbe, et al., 2016;
3006 Straume et al., 2019; Tankersley et al., 2022; Zhou et al., 2022). SPB – South Pole Basin, WSB – Wilkes
3007 Subglacial Basin, VH- Vostok Highlands, TAH – Terre Adelie Highlands TAM – Transantarctic Mountains, EWM
3008 – Ellsworth Whitmore Mountains, PM – Pensacola Mountains, RSH – Recovery Subglacial Highlands, GSM –
3009 Gamburtsev Subglacial Mountains, ASB – Aurora Subglacial Basin, MBL – Marie Byrd Land, LV – Lake Vostok,
3010 BI- Berkner Island, CL – Coats Land, FSH – Fuji Subglacial Highland, SPCM – Southern Prince Charles
3011 Mountains, VSB – Vincennes Subglacial Basin, IB – Iselin Bank, TI – Thurston Island, PL – Palmer Land, JS –
3012 Jutulstraumen, WRT-West Ragnhild Trough, AIS – Amery Ice Shelf.

3013 Figure 7: Sedimentary basins of the Ross Sea and Siple Coast regions, showing basin regions and
3014 reinterpreted basin structures, rift parallel (blue) and transverse (red). Basin faults are reinterpreted from
3015 prior studies (Fred J. Davey et al., 2021; Lindeque, Gohl, Wobbe, et al., 2016; Pérez et al., 2021; Sauli et al.,

3016 2021; M. Studinger et al., 2001; Tankersley et al., 2022; D. S. Wilson et al., 2012; T. J. Wilson, 1999). Also
3017 shown are the interpreted East Antarctica-West Antarctica basement boundary (black) (Tinto et al., 2019),
3018 and the seismically defined extents of thick basin cover (Zhou et al., 2022) (purple). UMB – Upstream
3019 MacAyeal Basin, MB- MacAyeal Basin, TD- Trunk D Basin, ACB – Amundsen Coast Basin, CT- Cray Trough,
3020 SDB- Siple Dome Basin, TR – Terror Rift, VLB – Victoria Land Basin, P3 – Polar 3 Anomaly, RI – Roosevelt
3021 Island, SG – Shackleton Glacier, SMIS – Southern McMurdo Ice Shelf, NG – Nimrod Glacier, BG – Byrd Glacier,
3022 CW – Cape Washington, DG – David Glacier, E- Erebus

3023 Figure 8: Sedimentary basins of the a) Central West Antarctica and b) Antarctic Peninsula Drake and eastern
3024 Weddell Sea regions. Structures in a) are reinterpreted from prior studies (Bell et al., 1998; Bingham et al.,
3025 2012; Haeger & Kaban, 2019; Jordan, Ferraccioli, Ross, et al., 2013; Jordan, Ferraccioli, Vaughan, et al., 2010;
3026 Jordan et al., 2020; M. Studinger et al., 2001) as associated with the WARS (blue) and WSRS (red). PI – Pine
3027 Island Rift Basin, FR – Ferrigno Rift, BSB – Byrd Subglacial Basin, BST – Bentley Subglacial Trough, EWM-
3028 Ellsworth Whitmore Mountains, SR – Sinuous Ridge, PSZ – Pagano Shear Zone, SST – South Shetland Trench,
3029 BB – Bransfield Basin, PB – Powell Basin, JB – Jane Basin, SOS – South Orkney Shelf, TPG – Trinity Peninsula
3030 Group, LMG – LeMay Group, JRB – James Ross Basin.

3031 Figure 9: Sedimentary basins of the Weddell and Weddell Coast regions. Structures are reinterpreted from
3032 prior studies including (Bamber et al., 2006; F. Ferraccioli, Jones, Curtis, Leat, et al., 2005; Jones et al., 2002;
3033 T. A. Jordan et al., 2017; Jordan, Ferraccioli, Ross, et al., 2013; G. J. G. Paxman et al., 2017; G. J. G. Paxman et
3034 al., 2019; Riedel et al., 2012). Blue lines indicate structures parallel with the SWRS, Red lines structures
3035 aligned transverse to the SWRS, parallel to the Pagano Shear Zone. Orange lines indicate structures of other
3036 orientations. Purple lines indicate magnetic trends of the NWRS including the Orion and Explora Anomalies.
3037 ER- Evans Rift, RR- Rutherford Rift, EWM – Ellsworth Whitmore Mountains, WRA – Weddell Rift Anomaly, BIR –
3038 Bungenstock Ice Rise, FB – Foundation Basin, PR Patuxent Range, PM – Pensacola Mountains, AR – Argentina
3039 Range, SR-Shackleton Range, TM – Theron Mountains, U&A – Urfjell and Amelang Groups, PT- Pencksokket
3040 Trough, RSG – Ritscherflya Supergroup, JS – Jutulstraumen, FIS – Fimbul Ice Shelf

3041 Figure 10: Sedimentary basins of the Enderby-Mac. Robertson and Lambert regions. Red structures indicate
3042 structures aligned with the main north-south Lambert Rift trend while purple structures are aligned with the
3043 east-west trend. Blue structures are aligned with Precambrian structures including the Gamburtsev Suture
3044 (F. Ferraccioli et al., 2011), the Ruker anomaly and Proterozoic basins in the southern Prince Charles
3045 Mountains (McLean et al., 2008). Orange lines indicate structures associated with the Fuji Subglacial
3046 Highlands block. SR – Sør Rondane, WRT – West Ragnhild Trough, CRT – Central Ragnhild Trough BLB –
3047 Beaver Lake Basin, FG – Fisher Glacier, MG – Mellor Glacier, LG – Lambert Glacier, ME – Mawson
3048 Escarpment, LSE – Lake Snow Eagle, WIIB – Wilhelm II Basin.

3049 Figure 11: Sedimentary basins of the Vostok, Queen Mary Land, Aurora, and Terre Adelie regions. Purple
3050 lines indicate older structures associated with collisional events (Michael Studinger et al., 2003) while the
3051 blue lines indicate interpreted EARS structures (F. Ferraccioli et al., 2011). Black and Red structures indicate
3052 Paleozoic-Mesozoic structures linked to the Knox, Aurora, Vincennes and Sabrina subglacial basins. Orange
3053 structures indicate structures associated with the Wilkes Subglacial Basin, with slightly different trend.
3054 Structures reinterpreted from prior studies (A. R. A. Aitken et al., 2016; A. R. A. Aitken et al., 2014; Cianfarra
3055 & Salvini, 2016; Maggi et al., 2016; Maritati et al., 2016; Tabacco et al., 2006). LS – Lake Sovetskaya, L90E –
3056 Lake 90°E, LV – Lake Vostok, WIIB – Wilhelm II Basin, SIS – Shackleton Ice Shelf, SG – Sandow Group.

3057 Figure 12: The Transantarctic Mountains and the Wilkes and South Pole subglacial sedimentary basins. Blue
3058 lines indicate major rift structures of the Wilkes and South Pole subglacial basins and red lines major cross-
3059 basin discontinuities. Orange lines indicate structures from other events. Structures reinterpreted from
3060 (Fausto Ferraccioli et al., 2009; Fausto Ferraccioli & Bozzo, 2003; Frederick et al., 2016; Jordan, Ferraccioli,
3061 Armadillo, et al., 2013; T. J. Wilson, 1999). WR – Wisconsin Range, QMR – Queen Maud Range, MR – Miller
3062 Range

3063 Figure 13: Structure of the Antarctic lithosphere showing basins over a) Moho depth (Pappa, Ebbing, &
3064 Ferraccioli, 2019), b) lithosphere-asthenosphere boundary depth (Hazzard et al., 2023), 1 to 6 indicate
3065 lithospheric embayments around the East Antarctic margin c) multidata lineament analysis (Stål et al., 2019)
3066 and d) multiscale gravity edge analysis. All images show the WARS bounding TAM front and East Antarctic
3067 lineament sets in dashed black. Labelling: a to d cross-rift structures in the WARS, 1 to 9 cross-basin
3068 structures in the Beacon Basin, PLL – Palmer Land Lineament, FTL – Filchner Trough Lineament, CLL – Coats
3069 Land Lineament, RL – Ruker Lineament, GS – Gamburtsev Suture, KBL Knox Basin Lineament, AL-Aurora
3070 lineament, HBL – Highland B Lineament, CL – Concordia lineament, ATL-Adventure Trough Lineament, WAL –
3071 Wilkes-Adelie Lineament, MGL – Matusевич Glacier Lineament. WSRS – Weddell Sea Rift System, NG –
3072 Nimrod Glacier, RG – Reedy Glacier, GR – Gunnerus Ridge, FSH – Fuji Subglacial Highlands, WIS – West Ice
3073 Shelf, DML – Dronning Maud Land, VH – Vostok Highland, AB – Aurora Subglacial Basin, SWB – Southern
3074 Wilkes Basin, TAM – Transantarctic Mountains, AP-Antarctic Peninsula, CWA – Central West Antarctica, MBL
3075 – Marie Byrd Land, SC – Siple Coast, EB- Eastern Basin, TR – Terror Rift, SP – South Pole Basin, RSH –
3076 Recovery Subglacial Highlands, SGB – Slessor Glacier Basin, LR – Lambert Rift, GSM- Gamburtsev Subglacial
3077 Mountains. An unannotated version of this figure is available in Fig S3.

3078 Figure 14: Tectonic reconstruction snapshots a) 265 Ma, b) 120 Ma, c) 65 Ma and d) 34 Ma showing the
3079 context of basin formation since Pangea (Müller et al., 2019; A. Young et al., 2019). East Antarctica is held
3080 fixed in this reconstruction which does not include rift block motions not involving ocean spreading. Basins
3081 are shown from their base-of-basin age to their top-of-basin age, with basin age indicating the time elapsed
3082 since the former. Each image also shows the major lithospheric boundaries (see Fig 13). Past plate

3083 trajectories (PPTs) are shown for departing plates for the following time periods a) 280 to 265 Ma 1-
3084 Cimmeria, b) 180 to 120 Ma 1 – South America, 2 – Africa, 3 – Madagascar, 4-Greater India, 5- Australia c) 90
3085 to 65 Ma 1 – South America, 2 – Africa, 3 – Madagascar, 4-Greater India, 5 – Australia, 6 – Zealandia, and d)
3086 64 to 34 Ma, 1 – South America, 2 – Africa, 3 –Indo-Australia 4 – Zealandia/Pacific. TP – Trinity Peninsula, EM
3087 – Ellsworth Mountains (inferred location) PrB – Prydz Bay, GIV - George IV land, KP – Kerguelen Plateau, PAP-
3088 Perth Abyssal Plain, PeB – Perth Basin, DP – Drake Passage, SS – Scotia Sea, AB – Adare Basin TG – Tasman
3089 Gateway. An unannotated version of this figure is available in Fig S4.

3090 Figure 15: a) Paleotopography at the Eocene Oligocene boundary (Guy J. G. Paxman et al., 2019) and b) the
3091 difference with the present day. Negative values indicate surface lowering due to tectonic subsidence and or
3092 glacial erosion.

3093 Figure 16: Influences on ice-sheet dynamics showing basins over a) geothermal heat flux estimated from
3094 geophysical data (Lösing & Ebbing, 2021) b) surface ice sheet velocity derived from InSAR phase mapping
3095 (Mouginot et al., 2019) c) inferred basal friction coefficient derived by inverting for basal conditions using
3096 the Ice sheet and Sea level System Model (Dawson et al., 2022) and d) subglacial hydrology, including
3097 subglacial lakes (Livingstone et al., 2022), and a modern-day drainage network (Le Brocq et al., 2013).
3098 Numbers indicate ice stream systems with sedimentary basins beneath fast flowing ice including 1 – Mercer
3099 and Whillans, 2 – Bindschadler and MacAyeal, 3 – Institute , 4- Academy and Support Force, 5 –
3100 Jutulstraumen, 6 – West and Central Ragnhild, 7 – Cook. Letters indicate ice stream systems with basins
3101 upstream including a – Thwaites and Pine Island, b – Recovery and Slessor, d – Lambert, Mellor and Fisher, d
3102 – Denman and Scott, e – Totten, f – David, Skelton and Byrd. FR – Ferrigno Rift, PIRB – Pine Island Rift Basin,
3103 BIR – Bungenstock Ice Rise, AC – Amundsen Coast Basin, FB – Foundation Basin, SPB – South Pole Basin, AVB
3104 – Aurora-Vincennes Basin, SWB – Southern Wilkes Basin, NWB – Northern Wilkes Basin, RL- Recovery Lakes,
3105 LV- Lake Vostok, DC – Dome C. An unannotated version of this figure is available in Fig S5.

Figure 1.

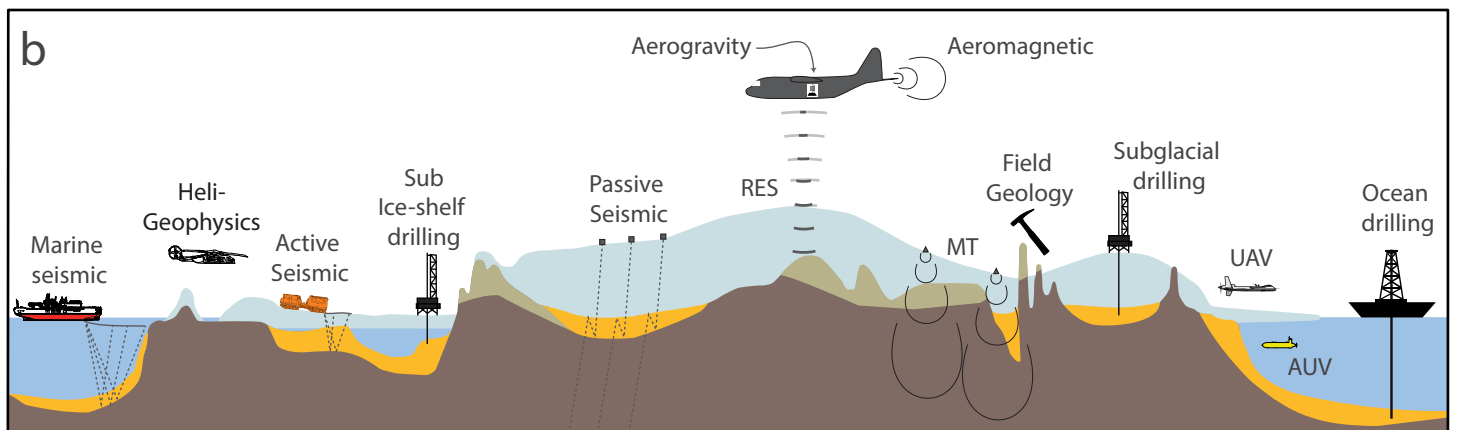
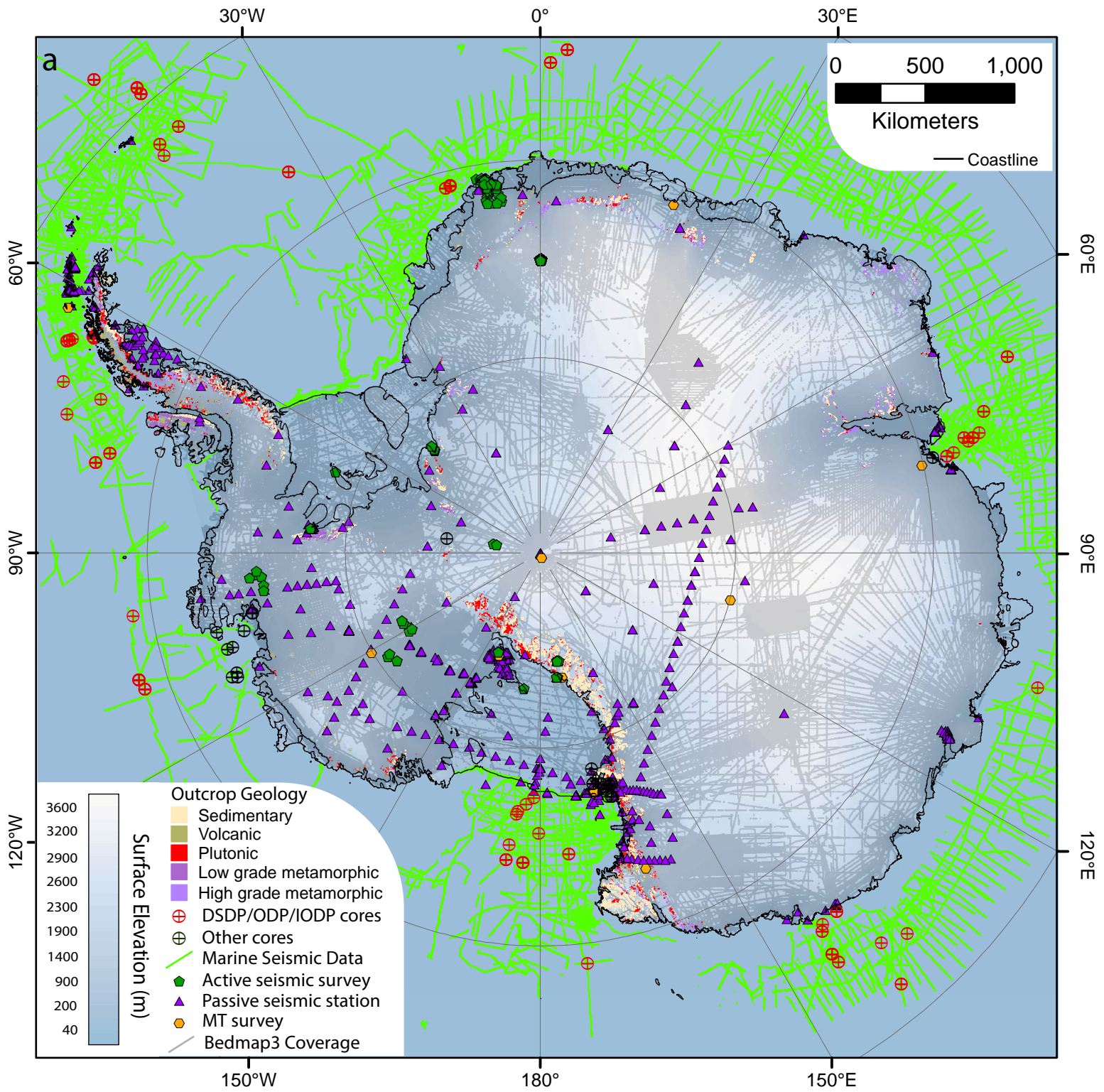


Figure 2.

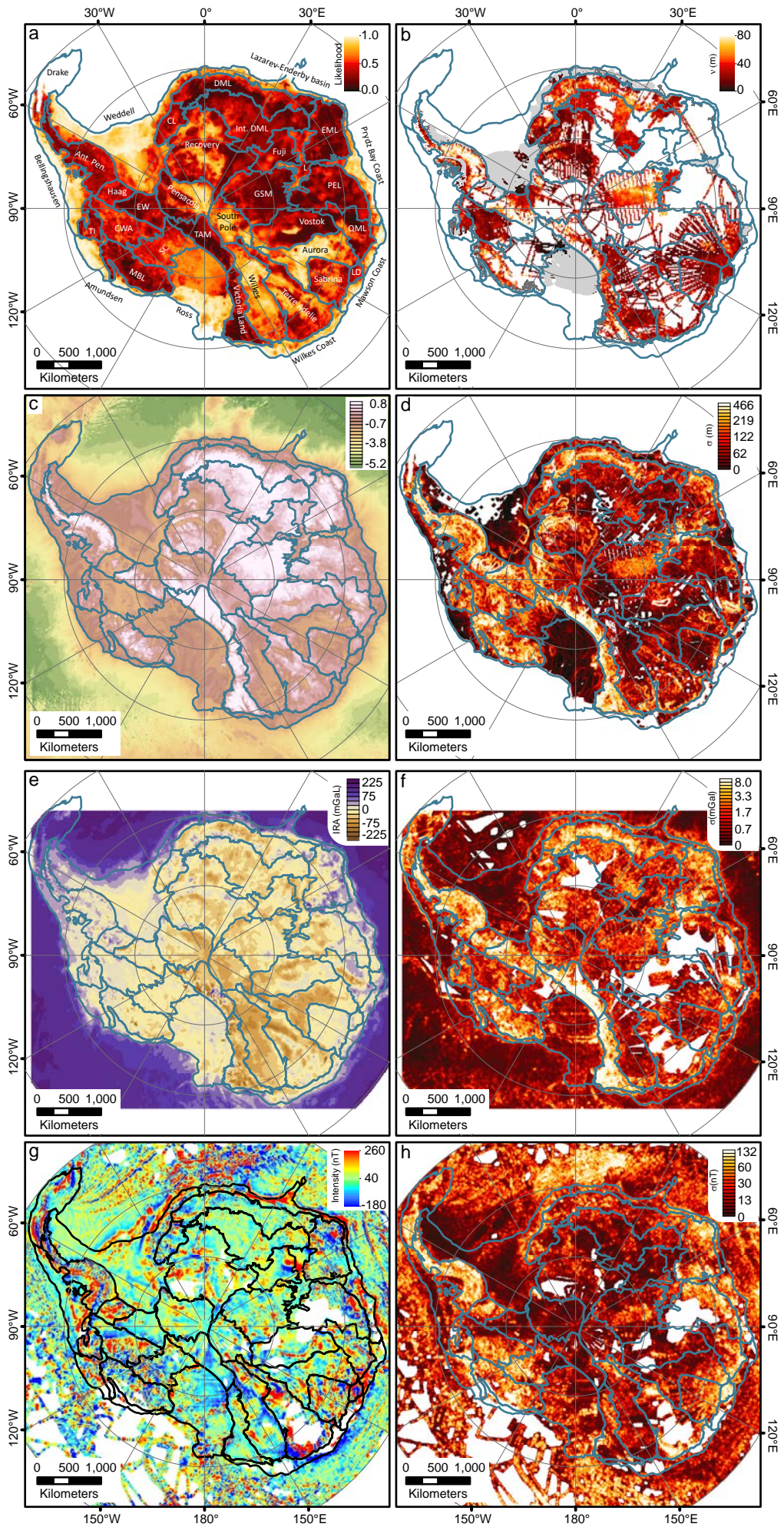


Figure 3.

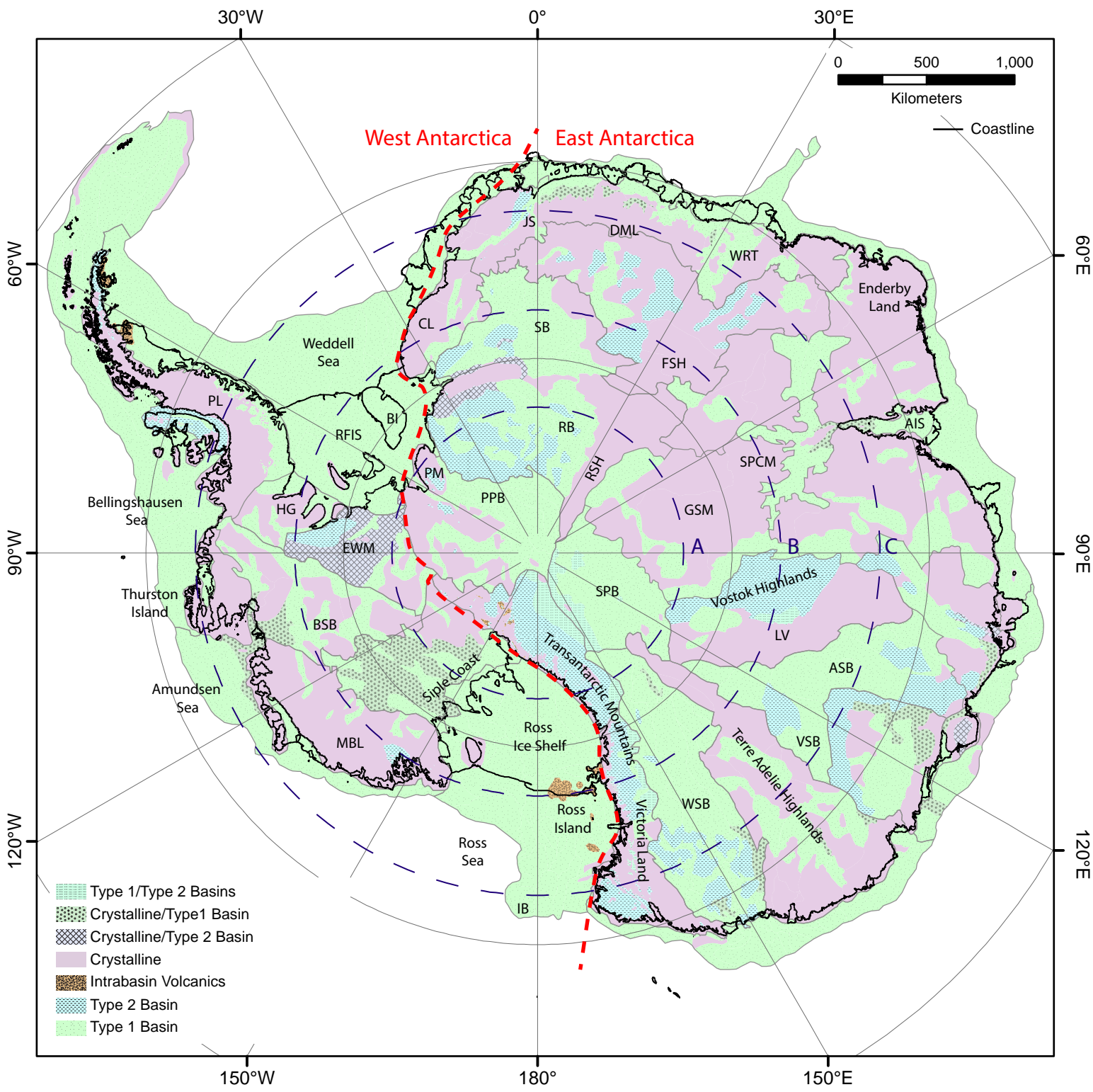


Figure 4.

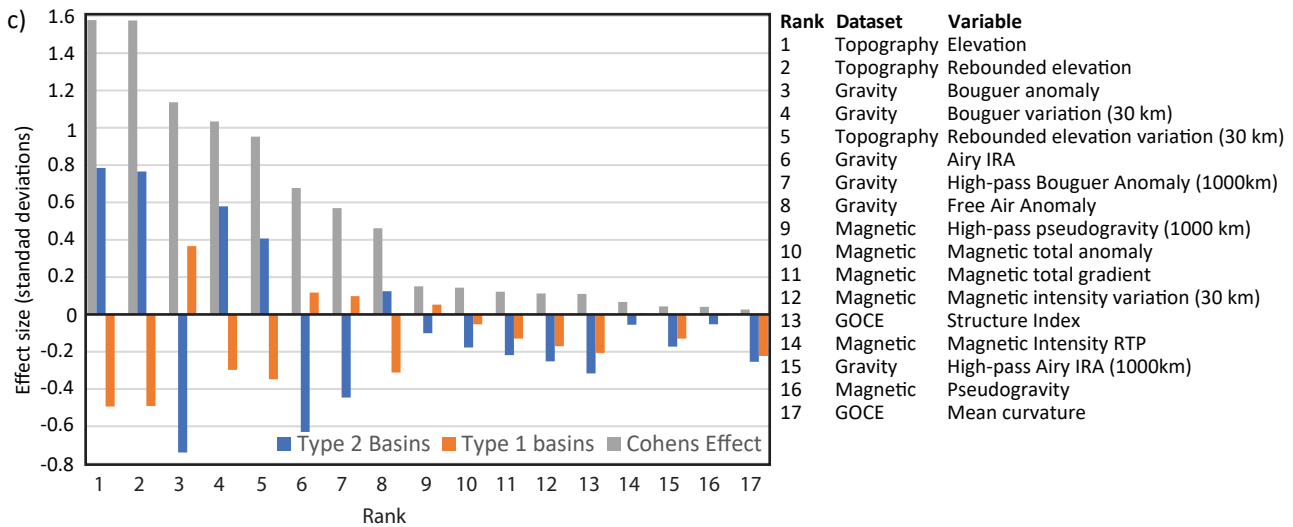
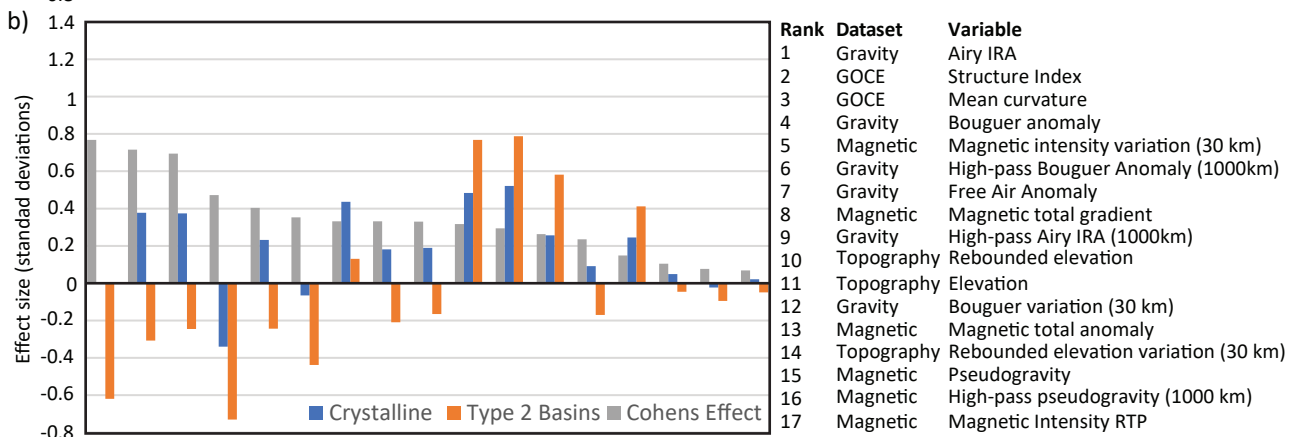
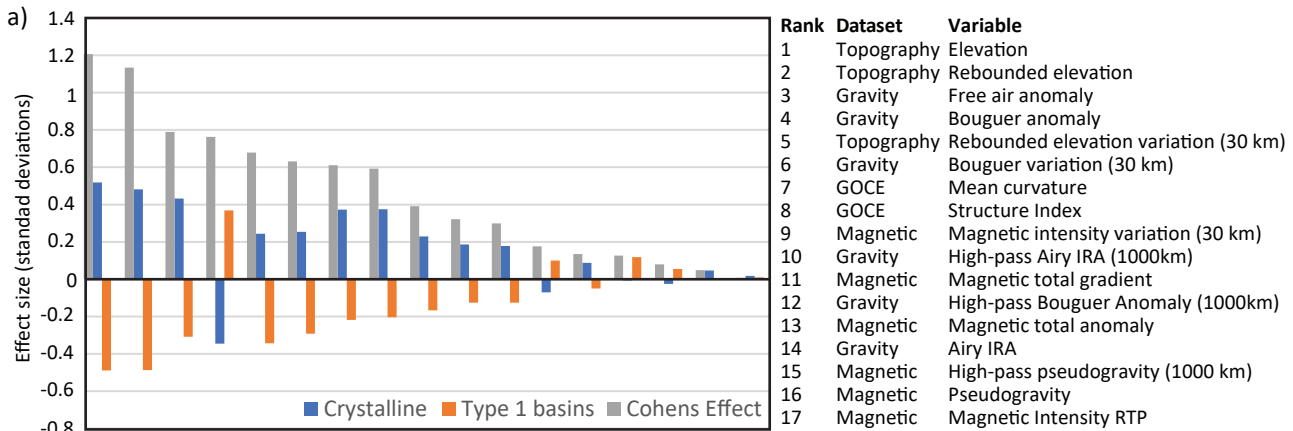


Figure 5.

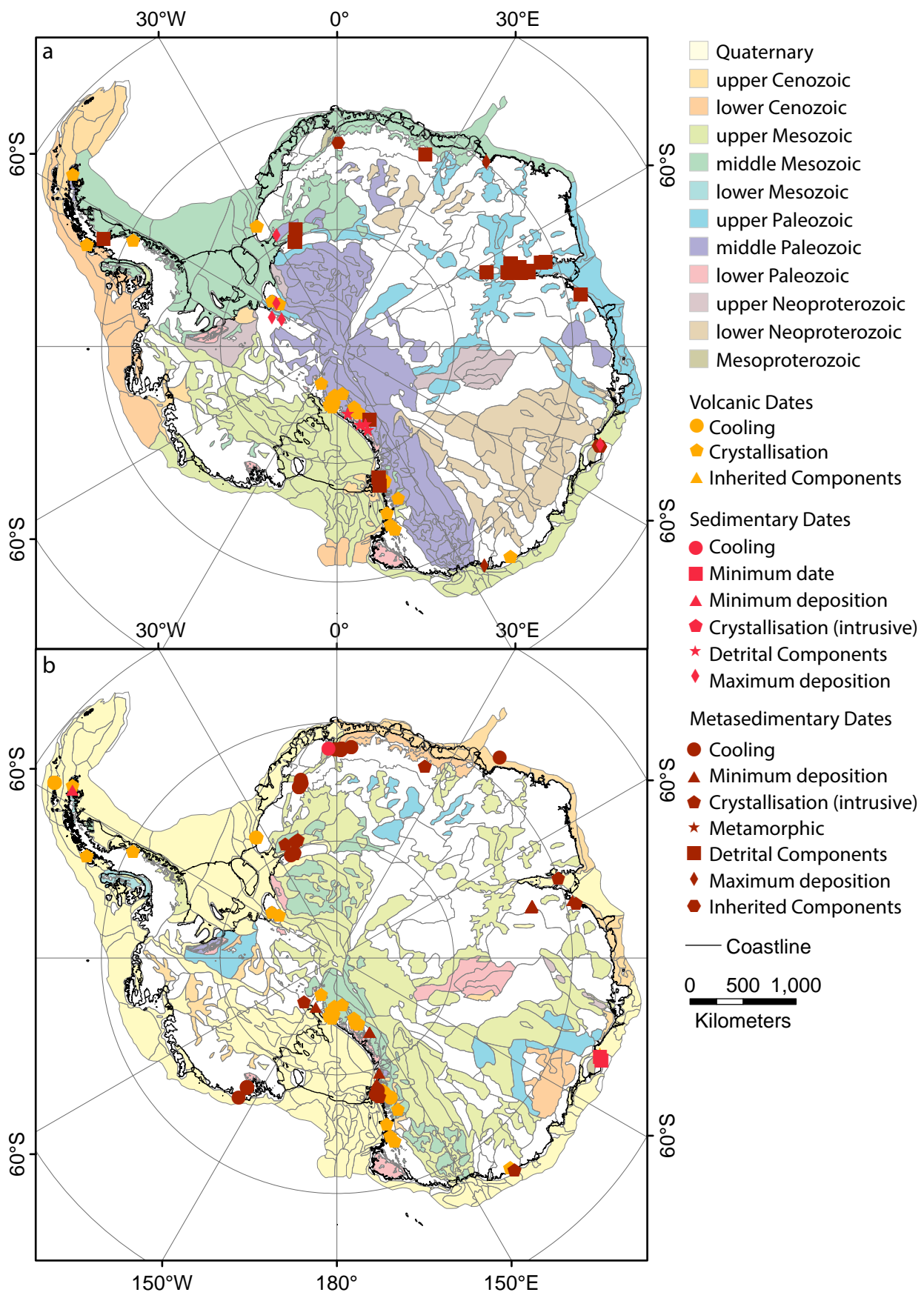
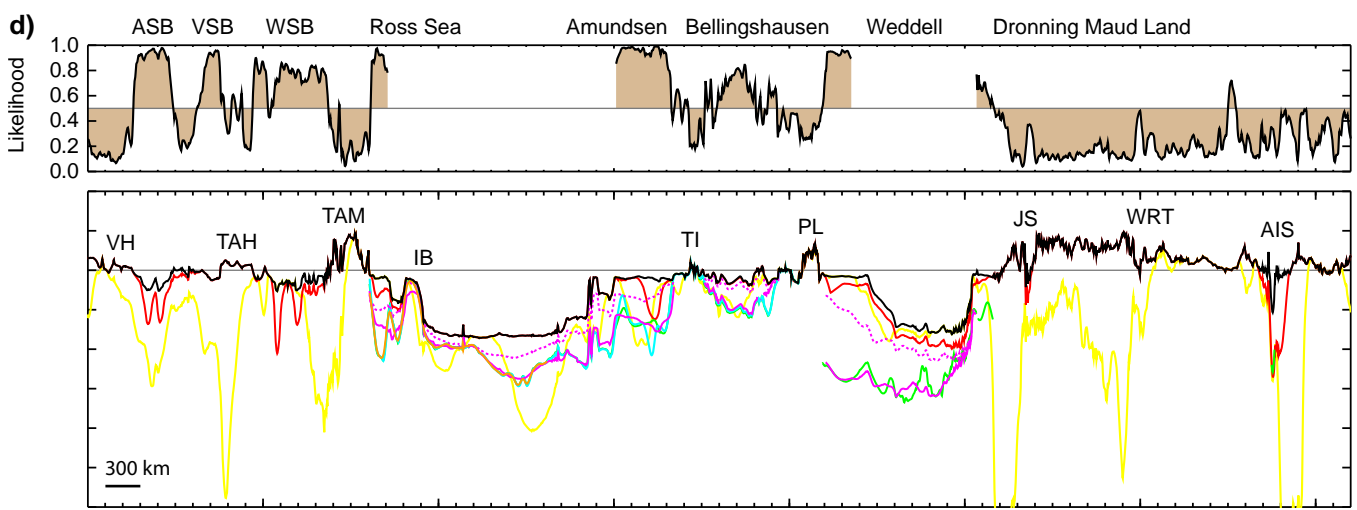
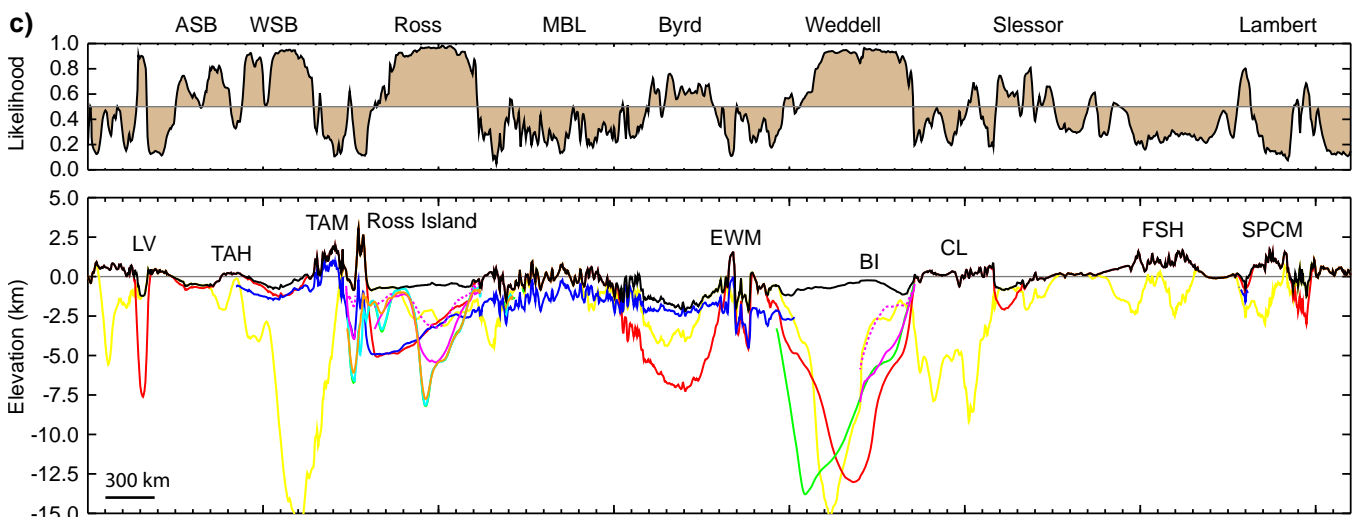
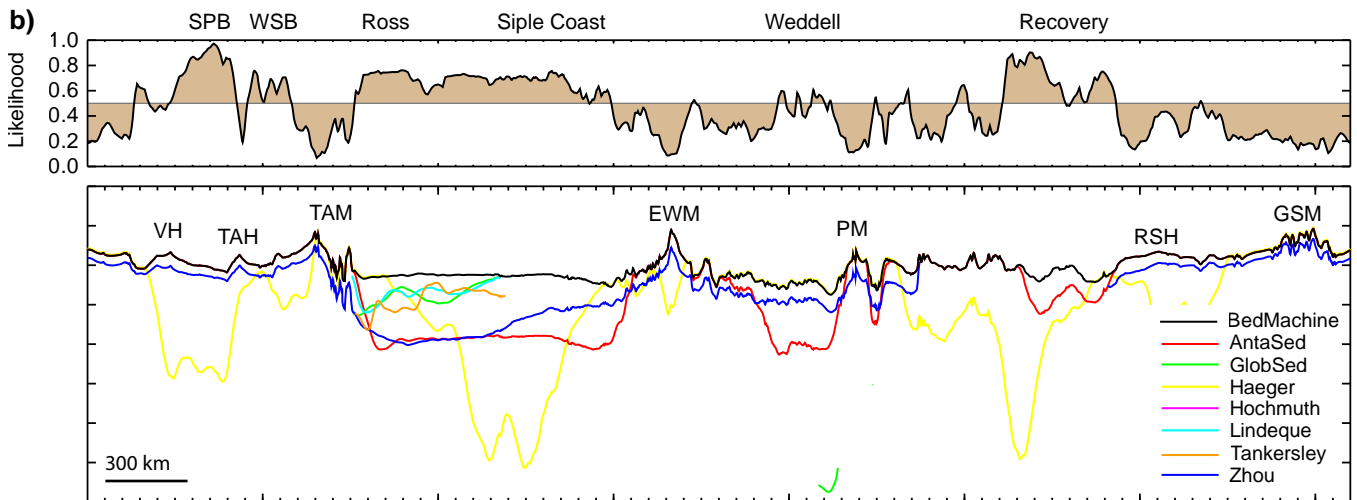
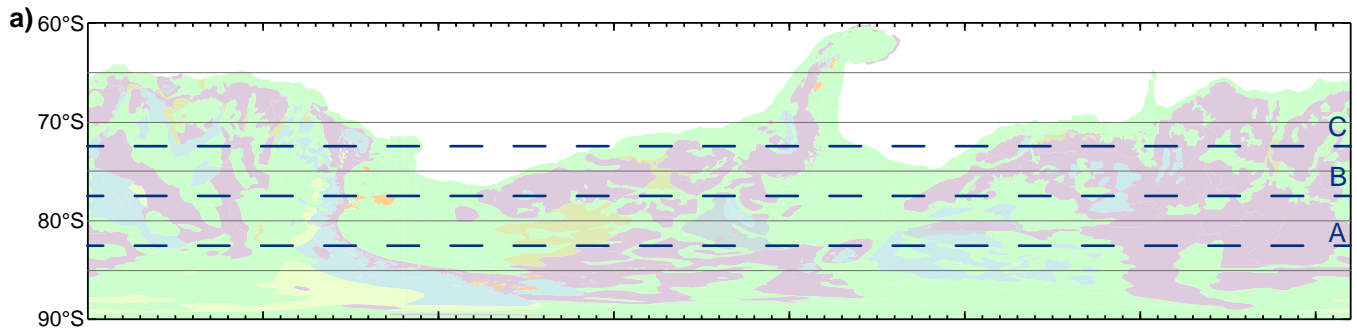


Figure 6.



90°E 135°E 180° 135°W 90°W 45°W 0° 45°E 90°E
Longitude

Figure 7.

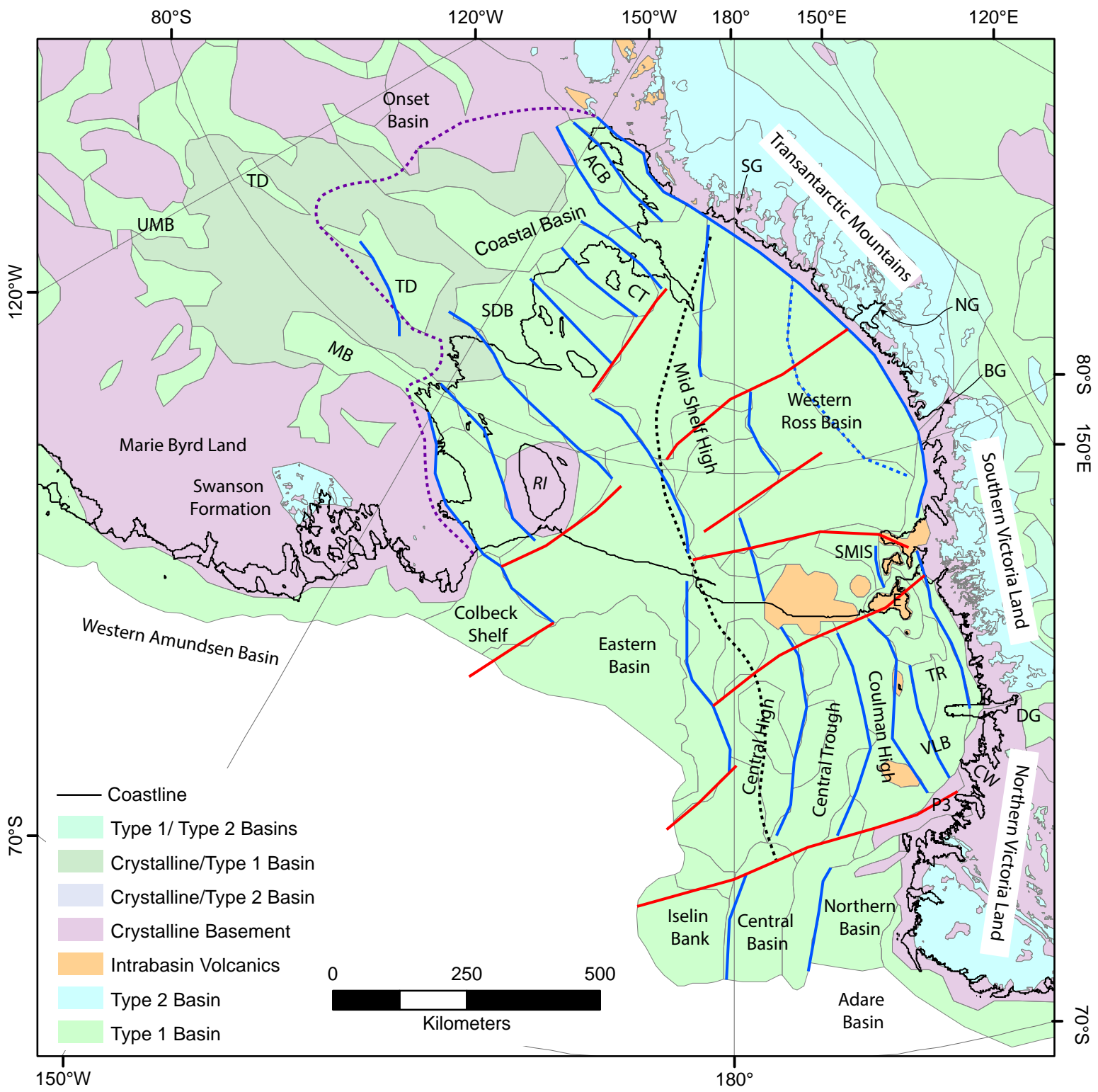


Figure 8.

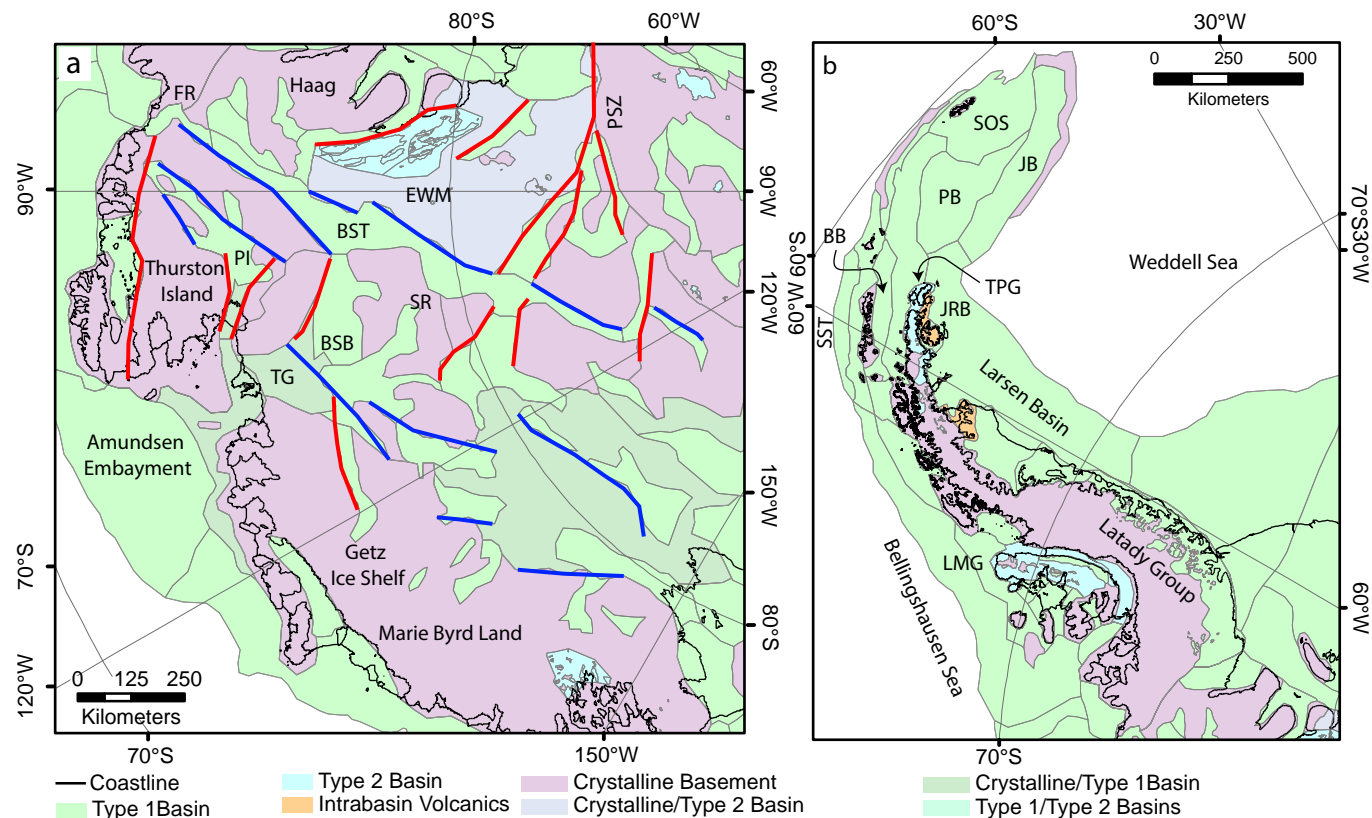


Figure 9.

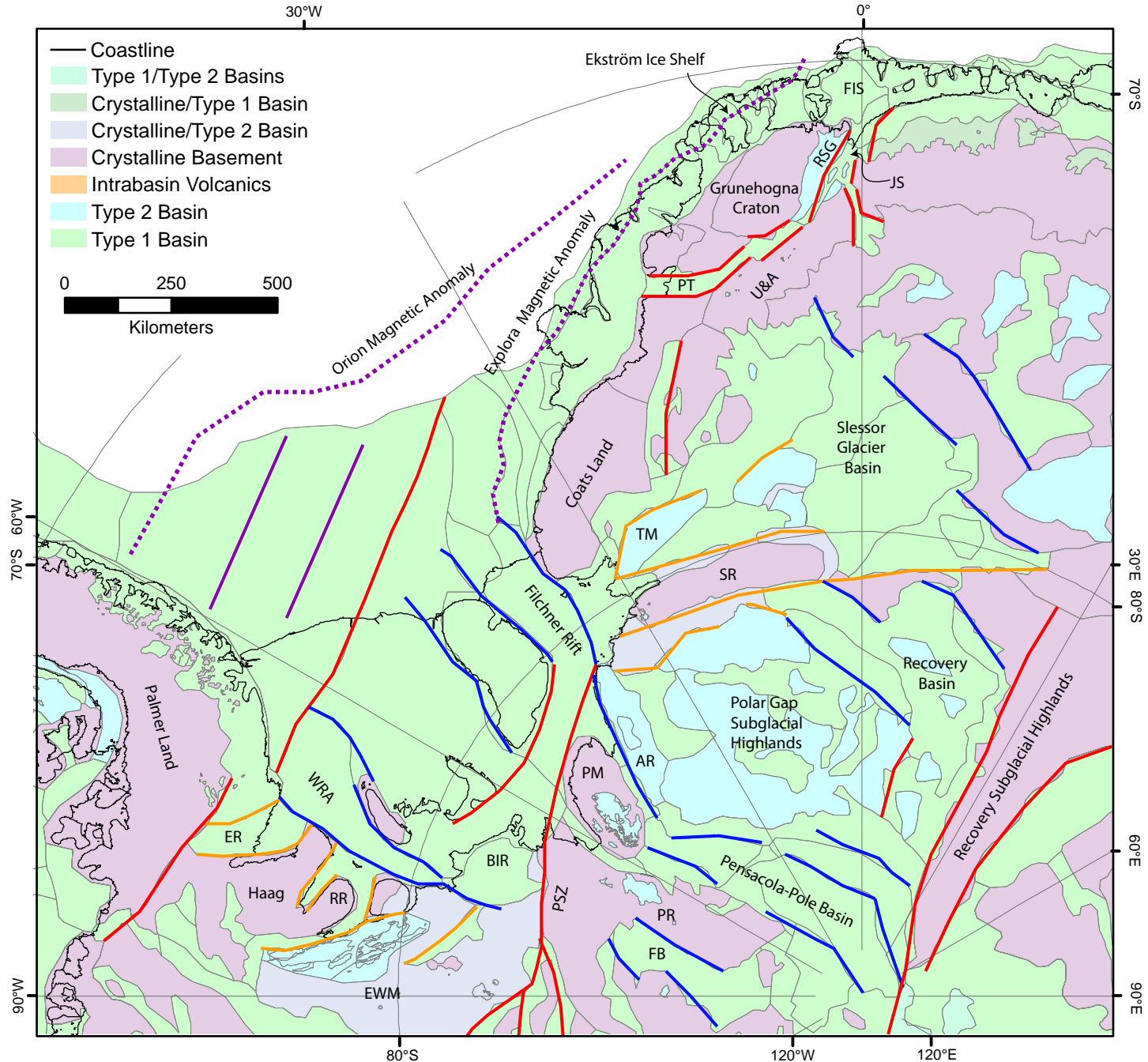


Figure 10.

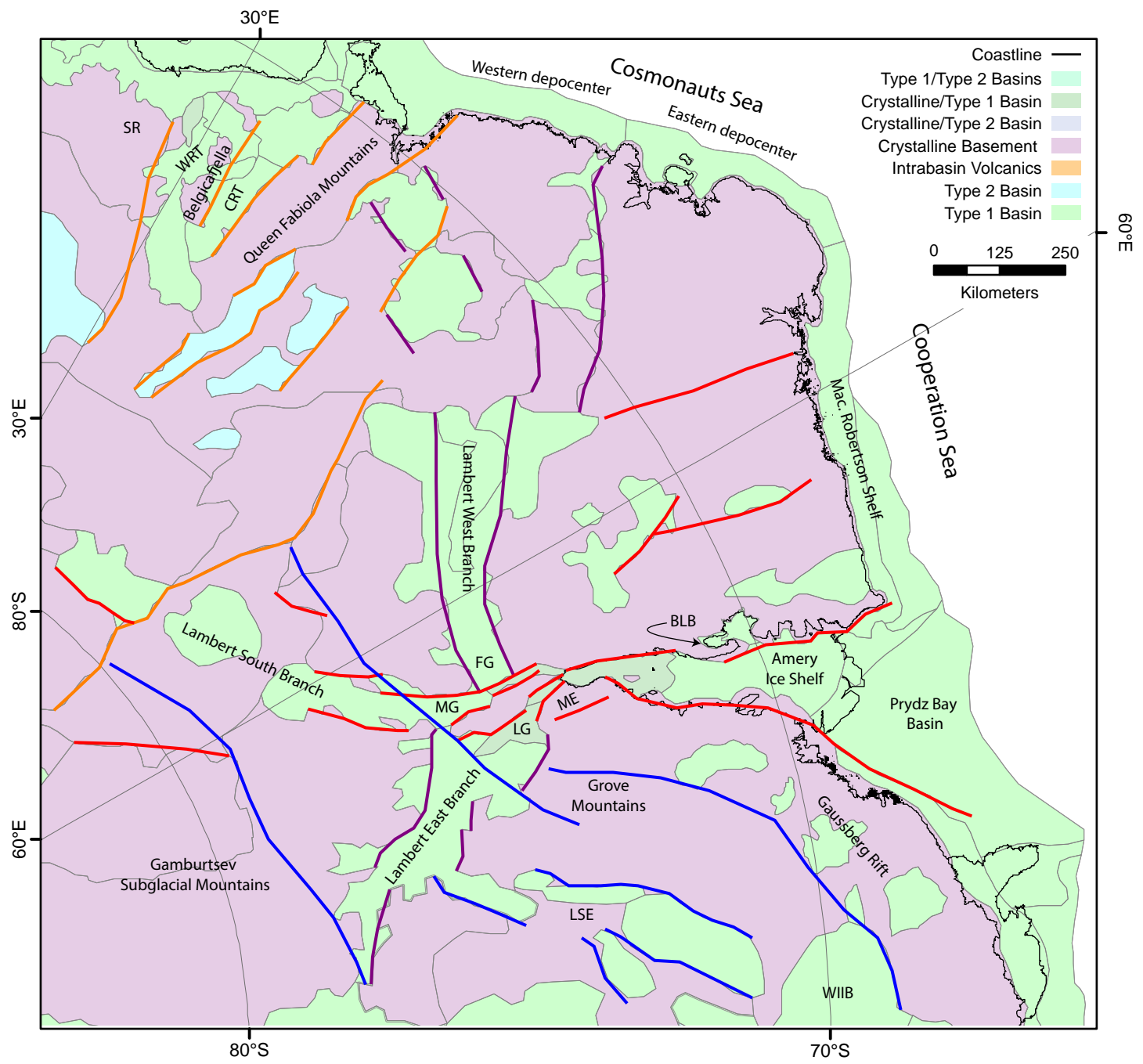


Figure 11.

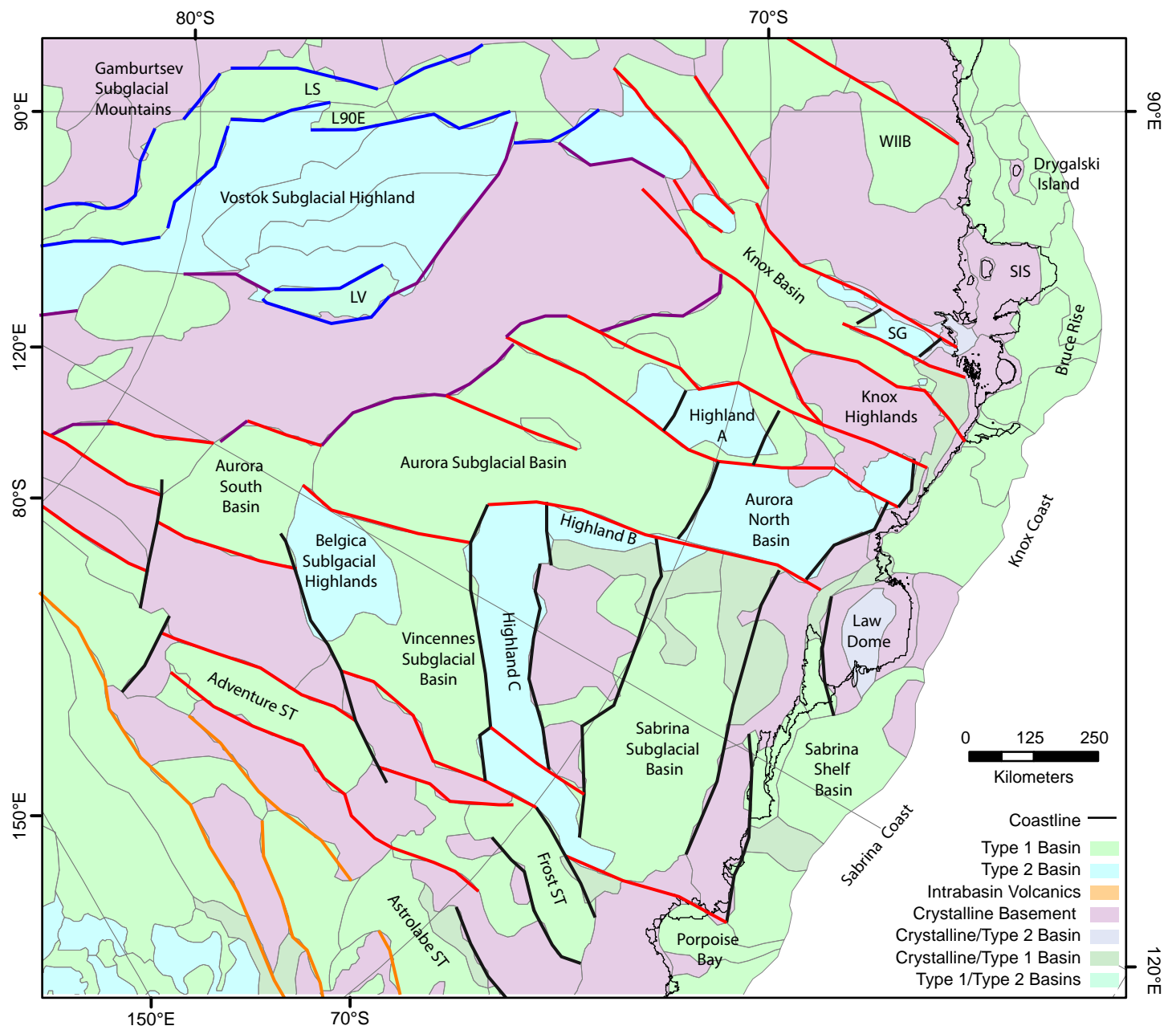


Figure 12.

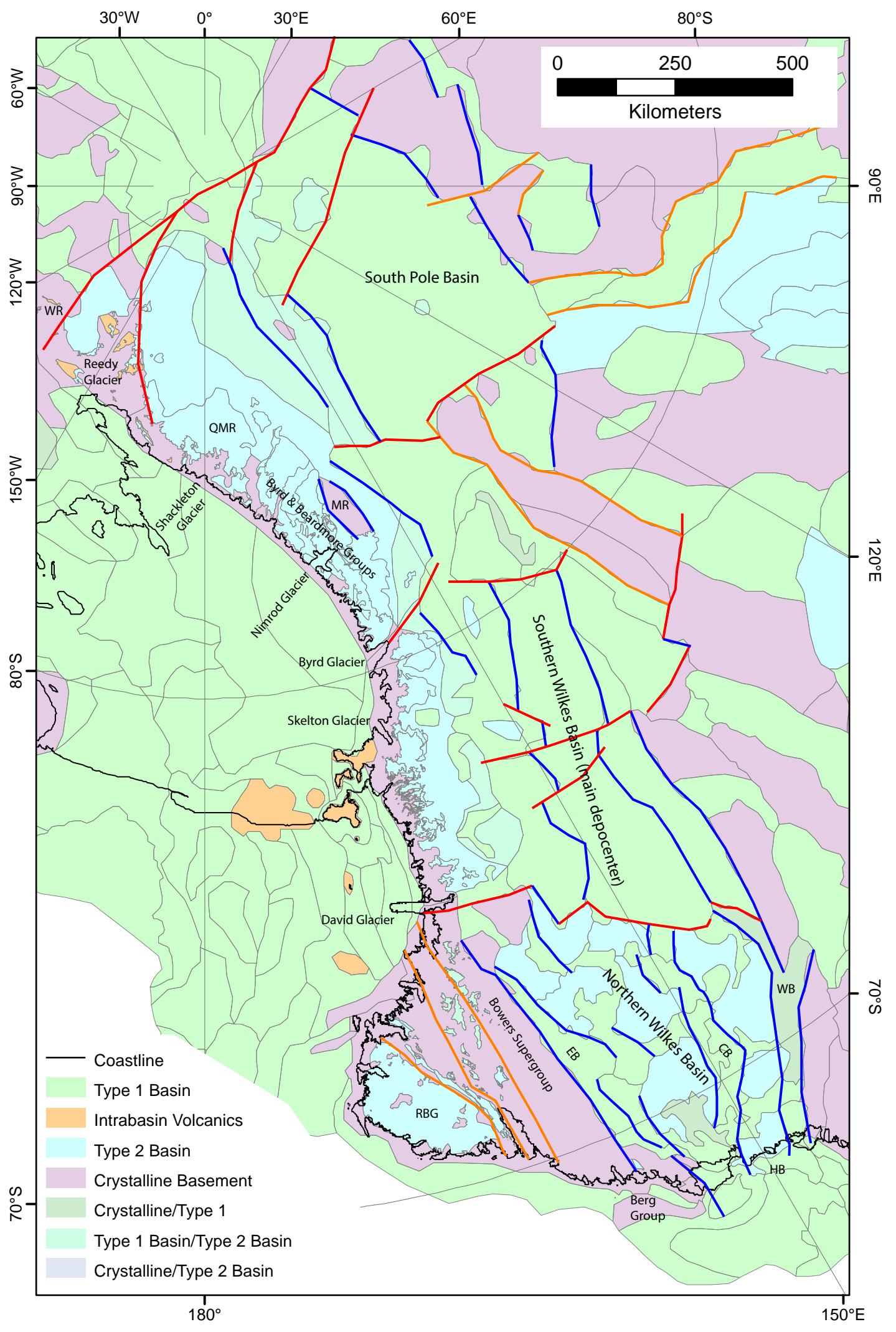
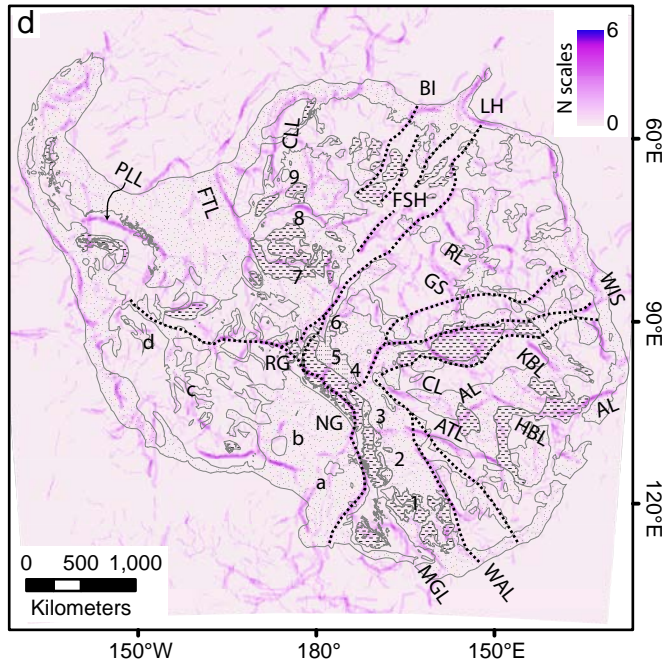
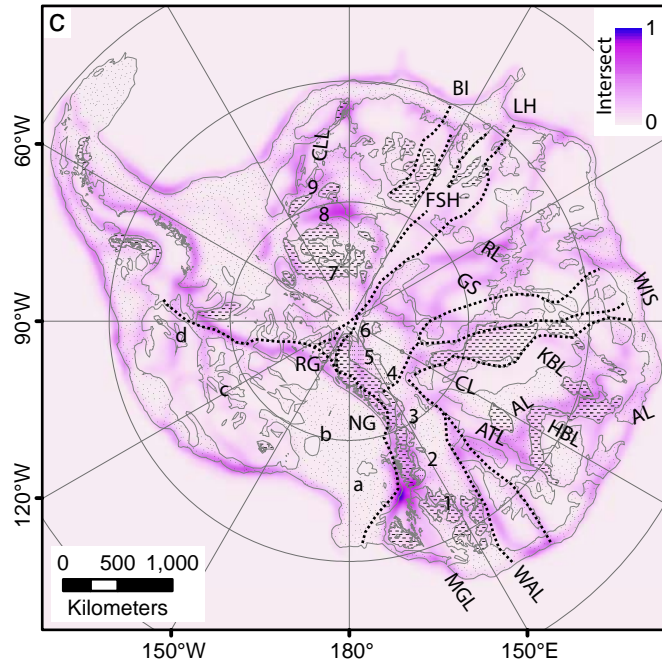
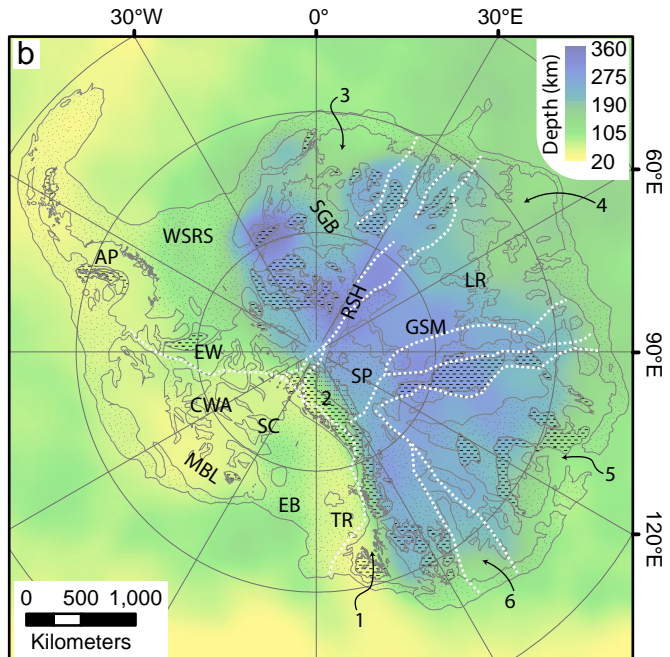
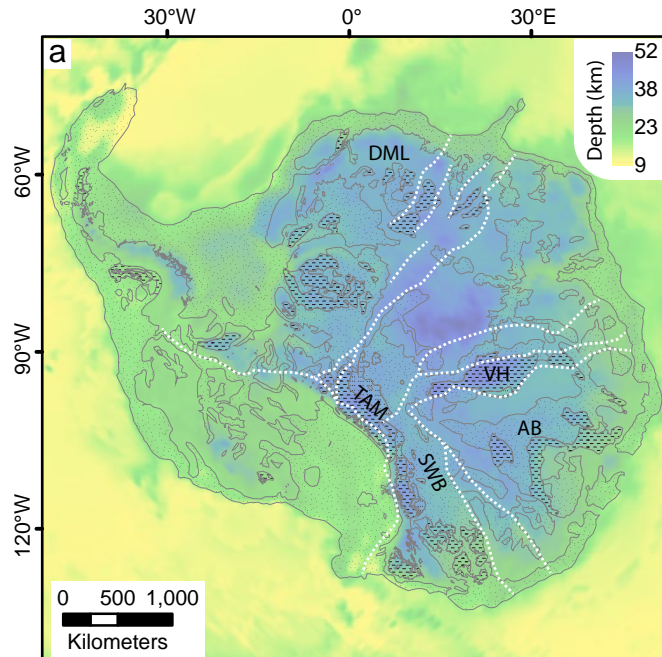


Figure 13.



Type 1 Basin
 Type 2 Basin
 Type 1/Type 2 Basins

Figure 14.

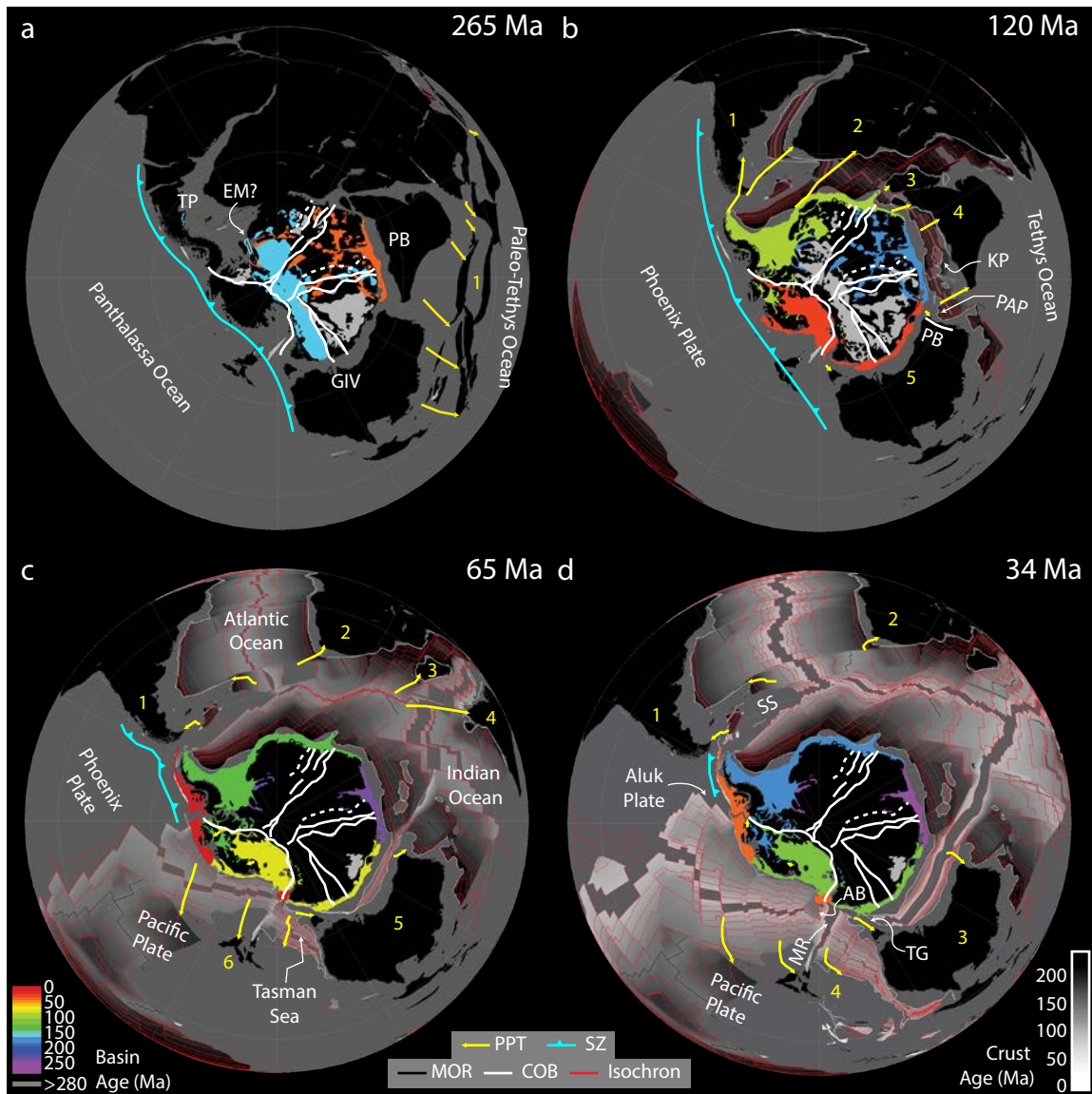


Figure 15.

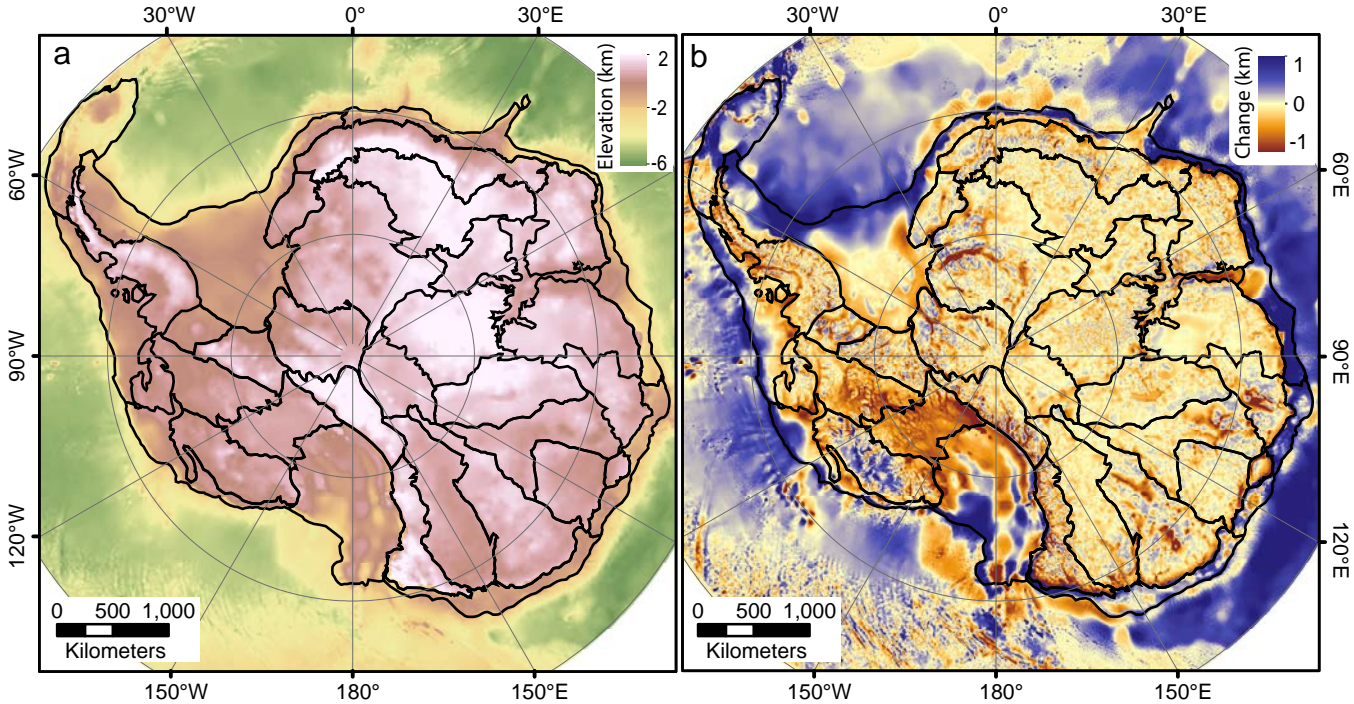


Figure 16.

